JYU DISSERTATIONS 218

Antti Vanhanen

Utilization of Real-time Motion Tracking Methods in Radiotherapy for Prostate Cancer

UNIVERSITY OF JYVÄSKYLÄ
FACULTY OF MATHEMATICS
AND SCIENCE

JYU DISSERTATIONS 218

Antti Vanhanen

Utilization of Real-time Motion Tracking Methods in Radiotherapy for Prostate Cancer

Esitetään Jyväskylän yliopiston matemaattis-luonnontieteellisen tiedekunnan suostumuksella
julkisesti tarkastettavaksi
toukokuun 18. päivänä 2020 kello 12.

Academic dissertation to be publicly discussed, by permission of
the Faculty of Mathematics and Science of the University of Jyväskylä,
on May 18, 2020 at 12 o'clock noon.

JYVÄSKYLÄN YLIOPISTO
UNIVERSITY OF JYVÄSKYLÄ

JYVÄSKYLÄ 2020

Editors
Timo Sajavaara
Department of Physics, University of Jyväskylä
Päivi Vuorio
Open Science Centre, University of Jyväskylä

.

Permanent link to this publication: http://urn.fi/URN:ISBN:978-951-39-8158-7

ISBN 978-951-39-8158-7 (PDF)
URN:ISBN:978-951-39-8158-7
ISSN 2489-9003

ABSTRACT

Vanhanen, Antti
Utilization of real-time motion tracking methods in radiotherapy for prostate cancer
Jyväskylä: University of Jyväskylä, 2020, 73 p.
(JYU Dissertations
ISSN 2489-9003; 218)
ISBN 978-951-39-8158-7 (PDF)

Newly found high fractionation sensitivity of prostate cancer has led to increasing use of stereotactic body radiotherapy (SBRT) in the treatment of prostate cancer. SBRT reduces treatment costs and increases treatment capacity and patient comfort, but due to high fraction doses and few treatment fractions, it requires higher accuracy of the treatment delivery than standard prostate radiotherapy (RT). In addition to standard procedure of interfraction motion correction, also the intrafraction motion correction of the prostate needs to be considered in the localization of the SBRT treatment. For this demand, electromagnetic (EM) localization methods capable of intrafraction motion tracking and treatment adaptation have been developed. In addition to EM methods, rectal immobilization devices (RR), developed for rectal dose sparing, have been suggested to reduce the intrafraction prostate motion. The aim of this thesis was to create a treatment protocol for prostate SBRT utilizing EM methods and RR, in which regard various features of these methods were investigated. These include: the immobilizing effect of the RR (Rectafix, Mimator AB), localization accuracy of two EM systems (RayPilot, Micropos Medical AB, and Calypso, Varian Medical Systems) and dosimetric benefit of continuous motion monitoring based motion correction and beam gating strategy. Results of this thesis indicate that the use of RR in standard clinical setting may increase the intrafraction prostate motion, thus reducing the accuracy of treatment delivery. Localization accuracy of the RayPilot was found being compromised due to the positional instability of the intraprostatic transmitters, whereas the accuracy of the Calypso was comparable to kV imaging of intraprostatic fiducial markers. Dosimetric and motion analyses revealed, that single pre-treatment CBCT-guided treatment localization can lead to clinically relevant target dose deficits, whereas additional pre-treatment motion correction is adequate for most of the patients. However, continuous motion monitoring based correction strategy with beam gating is required to ensure high target dose coverage and to minimize the risk organ doses for all fractions. Currently implemented treatment protocol for prostate SBRT in Tampere University Hospital is based on the findings of this thesis and utilizes continuous motion monitoring based motion correction and beam gating with Calypso.

Keywords: Intrafraction motion, Real-time motion tracking, Motion-including dose reconstruction, Prostate SBRT

Author

Antti Vanhanen
Department of Physics
University of Jyväskylä
Jyväskylä, Finland

Department of Oncology, Unit of Radiotherapy
Tays Cancer Centre
Department of Medical Physics,
Medical Imaging Center
Tampere University Hospital
Tampere, Finland

Supervisors

Chief Physicist, Head of Department Mika Kapanen
Department of Medical Physics,
Medical Imaging Center
Tampere University Hospital
Tampere, Finland

Prof. Markku Kataja
Department of Physics
University of Jyväskylä
Jyväskylä, Finland

Reviewers

Prof. Paul J. Keall
Sydney Medical School
The University of Sydney

Adj. prof., PhD, Chief Physicist Aki Kangasmäki
Docrates Cancer Center
Helsinki, Finland

Opponent

Adj. prof., PhD, Chief Physicist Juha Nikkinen
Department of Oncology and Radiotherapy
Oulu University Hospital
Research Unit of Medical Imaging, Physics and Technology
University of Oulu
Oulu, Finland

PREFACE

The work presented in this thesis was carried out at Department of Oncology, Tampere University Hospital, during the years 2014-2020. The study was financially supported by the Eila Vehmas foundation, Seppo Nieminen Fund of Tampere University Hospital Research Center, the Research funding provided by the Tampere University Hospital and the Faculty of Mathematics and Science of the University of Jyväskylä.

The study originated from an idea to start treating prostate cancer with extremely hypofractionated radiotherapy in Tampere University Hospital. Applying this kind of fractionation scheme to prostate cancer is rather new and international guidelines or consensus on how to implement this kind of treatment safely do not exist. It requires great interest and enthusiasm from medical personnel responsible of patient care to renew conventional treatment methods and implement new ones. In this regard, I want to thank radiation oncologist Tapio Tulijoki, who open-mindedly took the opportunity to start testing different methods to increase the accuracy and safety of the prostate cancer treatment delivery. Without his involvement in the beginning of this project this thesis would never have realized. I also want to thank radiation oncologist Petri Reinikainen who continued in Tapio's footsteps and took the main responsibility of the patients recruited in the study. Special thanks go to the radiation therapists who adapted smoothly to the new treatment techniques implemented within this project.

I am grateful to my supervisor and co-author, Docent Mika Kapanen, Chief Physicist and head of the Medical Physics Department at Tampere University Hospital, for his feedback on the studies related to this thesis. I also want to thank my other supervisor Prof. Markku Kataja for the feedback on the structure of the thesis. I wish to thank my co-authors, Hanna Syrén from Micropos Medical AB for providing details of the RayPilot system and Prof. Per Poulsen from Aarhus University Hospital, whose work with the dose reconstruction algorithm was essential for the realization of one of the studies this thesis is based on. Special thanks go to all colleagues working at the radiotherapy department of the Tampere University Hospital.

I would also like to thank the official reviewers, Prof. Paul Keall and Adj. prof. Aki Kangasmäki for their encouraging comments on this thesis.

Finally, I want to thank my family and friends. I probably drifted towards physics after reading my dad's astronomy books about black holes as a teenager and realizing that we live in an incomprehensibly fascinating world that can be described by physics and mathematics. I am grateful that I could grow in an environment that emphasized the importance of reading books. I am deeply grateful to my wife Emmi for her patience and encouragement during this

process and to our son Alvar whose birth set new order for my priorities. Special thanks go to my childhood and college friends. Our discussions and pondering of everything imaginable have taught me to look at things from different viewpoints and to challenge the usual ways of thinking and conventional norms.

Tampere 21.4.2020
Antti Vanhanen

LIST OF INCLUDED ARTICLES

I Vanhanen A, Kapanen M. The effect of rectal retractor on intrafraction motion of the prostate. Biomed Phys Eng Express 2016;2:035021.

II Vanhanen A, Syrén H, Kapanen M. Localization accuracy of two electromagnetic tracking systems in prostate cancer radiotherapy: a comparison with fiducial marker based kilovoltage imaging. Phys Med 2018;56:10–8.

III Vanhanen A, Poulsen P, Kapanen M. Dosimetric effect of intrafraction motion and different localization strategies in prostate SBRT. Manuscript submitted to Physica Medica on 11th of September 2019.

The author designed the Studies **II** and **III** and participated in the planning of the Study **I**. The author collected the data, performed all data analysis and wrote all articles. The dose reconstruction Matlab code used in Study **III** was written by Per Poulsen.

Articles are referred to by the Roman numerals **I–III** throughout the text.

The thesis also contains some unpublished data.

SYMBOLS AND ABBREVIATIONS

AP	Anterior-posterior
CBCT	Cone beam computed tomography
CP	Center point
CT	Computed tomography
CTV	Clinical target volume
DVH	Dose-volume histogram
Dxx%	Absorbed dose [%] received by at least xx% of the volume
EM	Electromagnetic
ERB	Endorectal balloon
FFF	Flattening filter free
FM	Fiducial marker
FOV	Field-of-view
GI	Gastrointestinal
GU	Genitourinary
KIM	Kilovoltage intrafraction monitoring
kV	Kilovoltage
linac	linear accelerator
LOA	Limits of agreement
LR	Left-right
MLC	Multileaf collimator
MRI	Magnetic resonance imaging
MV	Megavoltage
OAR	Organ at risk
PTV	Planning target volume
QOL	Quality of life
RF	Radiofrequency
RR	Rectal retractor
RT	Radiation therapy
SBRT	Stereotactic body radiotherapy
SD	Standard deviation
SI	Superior-inferior
SIB	Simultaneous integrated boost
SV	Seminal vesicles
TCP	Tumor control probability
TPS	Treatment planning system
US	Ultra-sound
VMAT	Volumetric modulated arc therapy
Vxx%	Volume [%] that received at least xx% of the prescribed dose
2D	Two-dimensional
3D	Three-dimensional
α/β	The ratio of the parameters α and β in the linear-quadratic cell kill model; quantifies the fractionation sensitivity of the tissues

CONTENTS

1 INTRODUCTION

1.1 Hypofractionated radiotherapy of the prostate

In Europe, prostate cancer is the most common cancer in men with estimated number of 450 000 new cases in 2018 (4660 new cases in Finland) [1]. Radiotherapy (RT) is one of the primary modalities for treating prostate cancer and in Tampere University Hospital, definitive prostate cancer treatments made up to 20% of all RT treatments in 2018. Standard regimen in RT of the prostate is conventional treatment fractionation, comprising typically of 2.0 Gy doses per fraction, five fractions per week, to a total dose of 74-80 Gy. Conventional fractionation is based on the assumption of different fractionation sensitivity of the tumor and late radiation effects in surrounding normal tissues. Late radiation effects, typically occurring in slowly proliferating tissues and manifesting 6 months to several years after RT, are usually permanent, sensitive to changes in fraction dose and limit the dose escalation in RT [2]. Using of small fraction doses would eradicate the tumor while giving time for recovery of exposed normal tissues. The reasoning behind the conventional fractionation in prostate RT was contradicted by the findings of high fractionation sensitivity of prostate cancer two decades ago [3], a result that has since been confirmed by several studies [4–6]. Estimates of the fractionation sensitivity for prostate cancer, described by the ratio of α and β parameters in linear-quadratic cell kill model, are lower (α/β = 1.0 - 2.7 Gy [4–6]) than estimates for late rectal reactions ($\alpha/\beta = 5.4 \pm 1.5$ Gy) [7], which suggests that using of larger doses per fraction to a smaller total dose (hypofractionation) could increase the treatment response and decrease the risk of late normal tissue complications (increasing the therapeutic ratio). Hypofractionation in prostate RT is typically categorized into moderate hypofractionation (2.4-3.4 Gy per fraction) and extreme hypofractionation, often called as stereotactic body radiotherapy (SBRT) (≥ 5 Gy per fraction) [8]. Typical total doses are 60-70 Gy in moderate hypofractionation and 35-40 Gy in SBRT of

the prostate. Fewer fractions of hypofractionated treatment schemes increase the patient comfort due to reduced number of hospital visits [8] and reduce the treatment costs [9–11].

Proposed high fractionation sensitivity led to several clinical trials comparing the efficacy and toxicity of conventional and hypofractionated prostate RT [12–16]. Long-term follow-up data has already proved the non-inferiority of moderate hypofractionation to conventional fractionation [12–14]. At the time of writing this thesis, first long-term (5-year) outcomes of a phase 3 trial comparing extremely hypofractionated (42.7 Gy in 7 fractions) and conventionally fractionated prostate RT (78 Gy in 39 fractions) have been published, showing similar efficacy and late gastrointestinal (GI) and genitourinary (GU) toxicity of the treatments, but higher acute toxicity in extremely hypofractionated protocol [15]. Recently published results of another phase 3 trial suggest that SBRT (36.25-40 Gy in five fractions) does not increase either GI or GU acute toxicity compared to moderate hypofractionation (62 Gy in 20 fractions) or conventional fractionation (78 Gy in 39 fractions), but long-term results of the trial are still awaited [16]. The use of SBRT in the treatment of prostate cancer is also supported by recently published pooled analysis of twelve phase 2 prostate SBRT trials comprising of 2142 patients [17] and by the systematic review and meta-analysis of 38 prostate SBRT series comprising more than 6000 patients [18]. Emerging clinical evidence suggests, that the use of hypofractionation, both moderate and SBRT, is likely to increase and could become the new standard in the treatment of prostate cancer.

Although recent studies support the efficacy and safety of the prostate SBRT, also severe GU and GI toxicities have been reported [19–22]. Toxicities are in general associated with high doses to large volumes of rectum and rectum wall [19, 22–24] and bladder and bladder wall [25, 26]. Risk of normal tissue overdosage and target underdosage is higher in SBRT than with conventional treatment regimen, due to high fraction doses and reduced number of fractions and more attention should be paid on accurate treatment delivery and sparing of normal tissues.

1.2 Inter- and intrafraction motion of the prostate

Planning of radiotherapy treatment is based on static patient anatomy and position information, acquired using computed tomography (CT) and/or magnetic resonance imaging (MRI). Thus, the main factors affecting the accuracy of treatment delivery is patient movement, inaccurate patient positioning and organ motion during the treatment [27, 28]. Motion is generally categorized into changes in organ position on a day-to-day level (interfraction motion) and organ motion during the treatment (intrafraction motion). In prostate RT, interfraction motion is mostly caused by changes in bladder and rectum filling between treatment sessions and the motion can range up to 20 mm [27], while major causes for intrafraction motion are gas movements in the rectum, muscle

relaxation and patient position adjustments during the treatment [29–31]. Intrafraction motion has been characterized as a random walk with increasing isocenter offset with time [32], but in some cases also as stationary physical process [30]. The motion pattern varies greatly among the patients [31, 33, 34] but two general types of the motion can be described: continuous, but slow posteriorly and inferiorly directed drift caused by muscle relaxation and sudden, larger anteriorly and superiorly directed position changes related to gas movement and peristalsis [30, 34]. Intrafraction motion is typically less than 5 mm, but can extend beyond 10-15 mm [31, 34] and occurs mostly in anterior-posterior (AP) and superior-inferior (SI) directions and less in left-right (LR) direction [31, 33–35].

1.3 Image-guidance of prostate radiotherapy

In modern RT, image-guidance is used to correct for the variation in patient and organ position, and to ensure correct localization of the treatment. Radiotherapy treatment machines are typically equipped with kilovoltage (kV) and megavoltage (MV) imaging systems, which enable acquisition of two-dimensional (2D) kV or MV images and three-dimensional (3D) cone beam computed tomography (CBCT) images of the patient in treatment position. Patient position is adjusted based on the superimposed treatment and planning images aligned according to the region of interest, which usually is the target volume. In conventionally fractionated prostate RT, treatment localization is typically done by daily pre-treatment image-guidance, using either orthogonal kV imaging or CBCT. Due to low soft tissue contrast of kV and CBCT images, prostate is not identified (2D images), or is poorly discerned from surrounding soft tissues (CBCT images). Thus, fiducial markers (FM) implanted into the prostate prior to planning CT, are commonly used as a surrogate for prostate position in prostate RT. FMs are typically made of gold or other radio-opaque material, thus discerning well in CT, kV and CBCT images. Typically, three gold seed markers are used and the prostate position relative to the machine isocenter is found by triangulation of the detected FMs. Measured and planned positions are compared and possible shift between the positions is corrected by re-positioning the patient/treatment couch. FM alignment provides more accurate localization than soft tissue alignment with CBCT, which is prone to intra- and inter-observer variation [36–39].

Daily imaging corrects only for interfraction motion and safety margins, applied around the clinical target volume (CTV) to form a planning target volume (PTV), are used to cover intrafraction motion and uncertainties related to target delineation and organ deformation. However, while increasing the likelihood of correct target dose coverage, margins expose adjacent normal tissues to higher doses. In addition, fixed safety margins do not optimally take account of prostate intrafraction motion, which increases with treatment time and varies greatly among the patients and fractions [31–34]. The effect of

treatment localization errors in conventionally fractionated and moderately hypofractionated RT tend to average out due to large number of fractions [40–42] and image-guided interfraction motion correction is generally adequate for these treatment regimens. However, the reduced number of fractions and higher fraction doses in SBRT emphasize the accuracy of treatment delivery, and in addition to interfraction motion correction, the correction of intrafraction motion comes to question. Choi et al [43] found that toxicity related to SBRT treatment was highly sensitive to prostate intrafraction motion and concluded that precise motion correction is essential in prostate SBRT, regardless of the magnitude of the motion. In addition to increased accuracy that intrafraction motion correction provides, it enables also the reduction of safety margins [44, 45] which is desired in prostate SBRT, especially in the light of toxicities presented in literature [19, 21–26].

Intrafraction motion detection is possible with repetitive stereoscopic kV imaging of implanted fiducials during the treatment [46, 47]. Monoscopic imaging solely provides only 2D information and the motion perpendicular to the image detector is undetected [48]. Method to estimate prostate 3D position in real-time by utilizing monoscopic kV imaging of FMs and 3D probability density for the target position [Kilovoltage Intrafraction Monitoring (KIM)], has been developed, tested and used clinically in experimental settings, but is not yet commercially available [49–55]. Imaging based methods do not provide actual position information during the imaging intervals, and thus the sensitivity of using only pre- and post-treatment imaging is not sufficient enough to determine intrafraction motion [56]. Increasing imaging frequency increases the accuracy but with a cost of increased imaging dose. Ultra-sound (US) methods have also been used to monitor the intrafraction motion, but the pressure of the US probe can cause anatomy distortions and displace the prostate [57, 58]. Alternative to imaging and US are electromagnetic (EM) tracking devices, such as Calypso (Varian Medical Systems, Palo Alto, CA, USA) and RayPilot (Micropos Medical AB, Gothenburg, Sweden). Calypso consists of three transponders that are implanted permanently into the prostate and an external array that is used for the localization of the transponders. The RayPilot consists of a wired transmitter which is implanted temporarily into the prostate and a receiver plate, which is used for the transmitter activation and for its localization. Both methods utilize radiofrequency (RF) EM fields to enable the localization and real-time tracking of the prostate in 3D space [59–61]. In addition, EM methods can be used for beam gating and repositioning of the patient, if pre-defined motion tolerances are exceeded during the treatment. Several studies have proven the feasibility of the Calypso in prostate RT [33, 34, 62, 63], but there are less published reports of the RayPilot system, as the method is still quite recently introduced [61]. To fully realize the benefit of continuous motion monitoring, the tracking devices should be able to accurately localize the treatment and re-position the patient during the treatment. Disadvantage of the EM methods is that the ferromagnetic transponders and transmitters cause severe MRI artefacts preventing full utilization of MRI in treatment planning and follow-up [64]. EM tracking devices

are also additional devices to radiotherapy linear accelerators (linac) and cause extra expenses. Therefore, the benefit of these devices should be evaluated against pre-existing treatment localization methods.

Large part of this thesis concentrates on investigation of the feasibility, performance and benefits of EM localization and tracking methods in RT and SBRT of the prostate.

1.4 Rectal dose sparing

The use of reduced safety margins reduce the overlapping volume between PTV and bladder and rectum reducing the dose received by these organs. However, dedicated methods have been developed in order to reduce the dose to the rectal wall. These include biodegradable hydrogel (polyethylene-glycol or hyaluronic acid) spacers and biodegradable balloons implanted between the prostate and the rectum to increase the prostate-rectum separation [65]. Most commonly used spacer gels have been reported to significantly reduce the rectal dose and rectal toxicity [66–68], but injection of the gel is also associated with severe complications [69]. Endorectal balloon (ERB) pushes parts of the rectal wall out of the high-dose region and also reduces the prostate intrafraction motion [70–73], but can cause prostate deformations affecting negatively to the treatment, if positioned incorrectly [74]. Rectal retractors (RR), sometimes called as rectal immobilization devices, were developed to increase the space between rectum and prostate by retraction of the rectum in dorsal direction with a rectal rod [75]. Compared to implantable hydrogels and balloons, this method is cost-effective, non-invasive and unlike gels or implantable balloons, the rectal rod can be repositioned, if necessary. As the RR would immobilize the rectal wall and prevent changes in rectal filling, it has been postulated, that the RR would reduce the intrafraction prostate motion [75]. This idea is backed up by the findings of stabilizing effect of transrectal US probe in prostate RT [76]. Ideally, the use of RR could nullify the need for intrafraction motion tracking and save treatment costs, while simultaneously reducing the rectal dose and the risk of rectal toxicity in prostate SBRT.

The basis of this thesis was the creation of a safe treatment protocol for prostate SBRT in Tampere University Hospital, utilizing electromagnetic real-time localization and tracking, to account for intrafraction prostate motion, and RR to reduce the dose to the rectum. In the first part of the thesis, the effect of the RR on prostate intrafraction motion is investigated by utilizing RayPilot motion tracking. Second part of the thesis investigates the localization accuracy of the RayPilot and Calypso systems in comparison to kV imaging of FMs. Finally, the benefit of continuous motion monitoring based localization and motion correction strategy using Calypso system is investigated in comparison to CBCT and kV imaging based localization methods.

2 AIMS OF THE THESIS

The aim of this thesis was to create a safe treatment protocol for prostate SBRT in Tampere University Hospital, utilizing electromagnetic real-time localization and tracking of the prostate to account for intrafraction prostate motion, and the use of RR to reduce the absorbed dose to the rectum. In this regard, the feasibility, performance and benefits of the EM systems in localization and tracking of the prostate, as well as the effect of RR on intrafraction prostate motion, were investigated. More specifically, the aims were:

1) To evaluate the effect of rectal retractor on prostate intrafraction motion and utilizing of RayPilot in motion tracking of the prostate (Study I).

2) To determine the localization accuracy of electromagnetic localization devices (RayPilot and Calypso) in comparison to orthogonal kV imaging of implanted fiducial markers (Study II).

3) To evaluate the dosimetric benefits of continuous motion monitoring based localization and motion correction strategy in comparison to CBCT and kV imaging based strategies in prostate SBRT (Study III).

3 MATERIALS, METHODS AND CLINICAL PROCEDURES

3.1 Immobilization of rectum and prostate with the RR

In the planning of starting prostate SBRT treatments in Tampere University Hospital, different methods to reduce the irradiated rectal volume were considered. Among them were hydrogel spacers and a RR (Rectafix, Mimator AB, Sweden). The latter was chosen for its simplicity, cost-effectiveness and proposed immobilizing effect on prostate. In the initial phase, the use of the RR was tested in conventionally fractionated and moderately hypofractionated prostate RT. At the same time, the feasibility of a motion tracking system RayPilot was tested by recording of prostate intrafraction motion with and without of the RR in place. The main purpose of the Study I was to investigate the effect of RR on prostate intrafraction motion. This was accomplished by comparing intrafraction motion of the prostate between fractions treated with the RR and without the RR. Ideally, the use of RR would stabilize the prostate and substitute motion tracking devices, saving treatment costs and simplifying the treatment procedure.

3.1.1 Patients and treatment

Twenty-eight patients treated for biopsy-proven prostate adenocarcinoma in Tampere University Hospital between April 2014 and July 2015 were included in the study. They were treated with volumetric modulated arc therapy (VMAT) using two full arcs and 6 MV flattened beams. Treatments were carried out on TrueBeam STx linac (Varian Medical Systems, Palo Alto, CA, USA). Thirteen patients were given a total dose of 60 Gy in 3 Gy fractions to the prostate and fifteen patients received 78 Gy in 2 Gy fractions to the prostate. CTV was prostate alone or prostate and seminal vesicles (SV) and PTV was formed adding 5 mm isotropic margin around the CTV. If SVs were included in the treatment, the dose

to the SVs was 46 Gy in 2.3 Gy fractions delivered using simultaneous integrated boost (SIB) technique in 60/3 Gy fractionation scheme and 56 Gy in 2 Gy fractions in 78/2 Gy fractionation scheme.

3.1.2 Rectal immobilization device

The RR used in the study consists of a cylindrical rectal rod (length 110 mm, diameter 20 mm) and a leg support attached to a base plate (figure 1). The position of the rod is adjustable and position indexes on the rod, its support column and leg support are used for reproducible positioning of the rod. Rectal displacement is achieved by posterior depression of the rectal rod inserted into the patient's rectum. Once the optimal retraction is achieved, the position of the rod is fixed. In this study, the initial positioning of the rod was accomplished at the planning CT and reproduced at the treatment. The position of the RR was verified by CBCT imaging on each fraction it was used. RR was used in first 10/20 and first 15/39 fractions according to the fractionation scheme in question. Two planning CTs were acquired for the planning of RR and non-RR treatments. MRI scan for target delineation was acquired without the RR, as the leg support did not fit inside the MRI scanner.

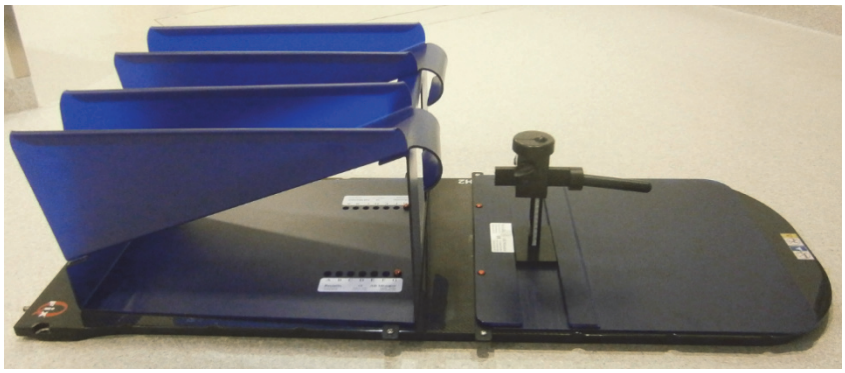

FIGURE 1 Rectal immobilization device "Rectafix" (Mimator AB, Sweden) [I].

3.1.3 Patient setup and treatment localization

Patients were positioned and treated supine, using RR leg support on RR fractions and in-house made knee support with non-RR fractions. After the initial positioning of the patient, CBCT was acquired for the verification of the RR position. CBCT scans were performed also at every other non-RR fraction to check the filling status of rectum and bladder. Treatment localization was performed with orthogonal kV imaging of three gold seed FMs, which were implanted into the prostate prior to planning CT. FMs were implanted transrectally, using endorectal US guidance. The FMs were placed in triangular

pattern, avoiding urethra, centrally to another of the lateral lobes, midway between apex and base of the prostate. Online matching between the kV and planned images were made manually by radiotherapists. The matching was based on two most stable FMs, if any of the markers had migrated noticeable.

3.1.4 RayPilot system and intrafraction motion tracking

Intrafraction prostate motion was tracked and recorded using RayPilot tracking system. The system consists of a wired transmitter, which is implanted into the prostate, and a receiver plate, which is setup on the treatment couch under the patient. Transmitter was implanted transperineally, using endorectal US guidance on a separate session after the FM implantation. Average time between the implantations was three weeks and the transmitter implantation was performed at least one week prior to planning CT scans. Planning CT slice thickness was 0.5-1.0 mm for accurate detection and determination of the transmitter coil center point (CP). The length and the diameter of the cylindrical transmitter are 17 mm and 3 mm, respectively. The actual transmitting part consists of 10 mm long copper coil with a ferrite core, placed 2 mm from the tip of the transmitter. MRI scan for delineation was acquired before transmitter implantation, as the ferromagnetic core of the transmitter would have caused severe artefact to the MRI image. The wired transmitter is activated via a connection to the receiver plate. The transmitter signal is read by an antenna array within the receiver plate and the position of the transmitter relative to the plate is located. The position of the receiver plate is calibrated to the machine isocenter and thus the position of the transmitter relative to the machine isocenter can be determined. The system locates the treatment isocenter position relative to the detected transmitter position based on the coordinates of the isocenter and transmitter in the planning CT. Treatment couch bending due to patient weight is measured and taken into account in the system. The sampling frequency of the system is 30 Hz, which enables real-time motion tracking. The transmitter location is given in AP, SI and LR directions. The system detects also the transmitter pitch (rotation around the LR axis) and yaw (rotation around the AP axis) angles. Operation limits for the transmitter are ±40° pitch and ±5° yaw angles of the transmitter. Localization uncertainty, measured in a laboratory setting by the vendor, was 0.60 ± 0.46 mm [radial mean ± standard deviation (SD)] for the two systems used in the study.

Motion tracking was initiated immediately after the initial positioning of the patient. For fractions with the RR, the tracking was initiated immediately after the RR placement. If the position of the RR needed additional adjustment, the tracking was stopped, reset and restarted after the adjustment, so that the prostate motion trace would not be influenced by irrelevant disturbances. RayPilot was used only for the motion tracking and any treatment interruptions or corrections to the prostate position, based on the observed intrafraction motion, were not made during the treatment. Tracking was stopped after the completed treatment. Motion data was gathered from all RR and non-RR fractions.

3.1.5 Data processing and analysis

Sub-millimeter offset in the initial position of the motion trace, which is a consequence of a finite measurement resolution of the RayPilot, was extracted from the motion data. The effect of instrumental noise and RF disturbances on raw motion data were smoothed by filtering of the data using simple exponential smoothing. Bidirectional filtering and averaging of the data were used to avoid changes in phase response. Noise characteristics of the RayPilot system differ according to measurement direction. Thus, different smoothing factors (α) were used for different translational motion directions. Smoothing factors used were $\alpha=0.15$ for LR and SI and $\alpha=0.1$ for AP direction.

Intrafraction motion was determined by calculating prostate displacement relative to its initial position in AP, SI and LR directions. 3D motion of the prostate was calculated based on the Cartesian motion data. Evaluation of the motion was based on percentile ranges of prostate displacement: mean percentages of tracking time that the prostate was displaced ≥ 1, 2, 3, 4, 5 and 6 mm were calculated over all fractions of all patients (RR and non-RR fractions separately). Evaluation of the 3D motion was also done separately for individual patients. Due to variable duration of the treatment sessions, the calculation of the displacement time percentages was limited up to 10 min of tracking time. The effect of the duration of the tracking time on observed 3D displacements was evaluated by calculating displacement time percentages within 3, 6 and 10 min of tracking time. Directionality of the motion was analyzed by calculating proportions of time of unidirectional prostate displacements within 6 and 10 min of tracking time. To evaluate the time dependency of the motion, percentages of time at 3D displacements were calculated within 1 min intervals of the tracking time, ranging from 0 to 10 min. The effect of RR on prostate intrafraction motion was assessed by the comparison of motion patterns between RR and non-RR fractions.

Differences in the time dependent motion distributions between the fractions using the RR and fractions without it were estimated with Kolmogorov-Smirnov test. Paired Wilcoxon signed-rank test was used to evaluate the difference in percentage times at 3D and unidirectional displacements ≥ 1, 2, 3, 4, 5 and 6 mm within 6 and 10 min tracking time between all RR and non-RR fractions. For patients with small motion, the comparison was made for displacements ≥ 1, 1.5, 2, 2.5, 3 and 3.5 mm. Comparison of 3D motion distributions between the fractions with the RR and fractions without it were made additionally for individual patients.

3.2 Accuracy assessment of the electromagnetic tracking devices

Besides motion tracking, full utilization of real-time motion monitoring devices include treatment localization. In addition to pre-treatment localization, motion management system should be able to locate the treatment adaptively according to the changes in prostate position during the treatment. Adaptive repositioning would enable the use of reduced PTV margins and reducing of normal tissue dose. Reliable localization requires high accuracy. The aim of the Study II was to investigate the localization accuracy of commercially available electromagnetic tracking systems, RayPilot (Micropos Medical AB, Gothenburg, Sweden) and Calypso (Varian Medical Systems, Palo Alto, CA, USA). At the time of the study, previously published results of the localization accuracy of the RayPilot in a clinical setting did not exist. Localization accuracy of the Calypso was investigated for comparison. The accuracy of the EM devices were assessed in comparison to orthogonal kV imaging aligned with FMs, which can be considered as a golden standard in prostate RT localization. Differences between the methods were investigated by comparing kV-imaging based corrective translational couch shifts to couch shifts, or isocenter offsets, suggested by the EM methods.

3.2.1 Calypso system

Calypso (Varian Medical Systems, Palo Alto, CA, USA) localization and motion tracking system was introduced to enable precise localization and continuous tracking of moving targets during RT and surgery [59, 60]. The system is based on alternating current (AC) electromagnetic fields and consists of three transponders implanted into the target (prostate) and antenna array setup above the patient during the treatment. Transponders consists of a copper coil wired around a ferrite core, encapsulated in a cylindrical glass capsule. Length of the transponder is 8.7 mm and two gauges, 14 G (1.85 mm) and 17 G (1.3 mm) are available. Both 14 G and newer 17 G transponders were used in this study. Antenna array contains 4 source and 32 receiver coils. Source coils are used to generate an oscillating EM field which excites transponders at resonant frequencies. When the EM field is switched off, the resonance decays. Transponder 3D positions relative to the array are located based on the transponder decay signal read by the receiver coils of the antenna array. Each transponder have slightly different wiring and thus different resonance frequency, which enables distinction between the transponders. Position of the isocenter relative to transponders is known by the treatment plan and observed transponder positions can be used to localize the treatment isocenter in array coordinate reference frame. The position of the array relative to the treatment machine isocenter is detected with three infrared cameras mounted in the treatment room. The difference between the observed treatment isocenter and machine isocenter positions is used to determine the needed translational (AP, SI and LR) couch adjustments to correct for the isocenter offset. The sampling

frequency of the system is 25 Hz (version 3.0), which enables real-time motion tracking [59, 60]. Based on the phantom measurements of Franz et al, the precision and accuracy of the system is 0.4 ± 0.4 mm and 0.1 ± 0.1 mm, respectively [77]. Basic Calypso procedure prior to treatment includes checking of transponder geometry and treatment localization. Geometry check verifies that the position of the transponders has not changed from the planned position due to migration, or changes in prostate rotation and deformation. In localization part, treatment and machine isocenters are aligned by treatment couch adjustments based on Calypso-detected isocenter displacement (figure 2). Immediately after the localization, motion tracking is started. If prostate motion exceeds pre-defined motion tolerances during the treatment, the beam is gated off automatically. If the prostate displacement will not return within tolerances, treatment couch can be repositioned automatically according to the detected isocenter offset.

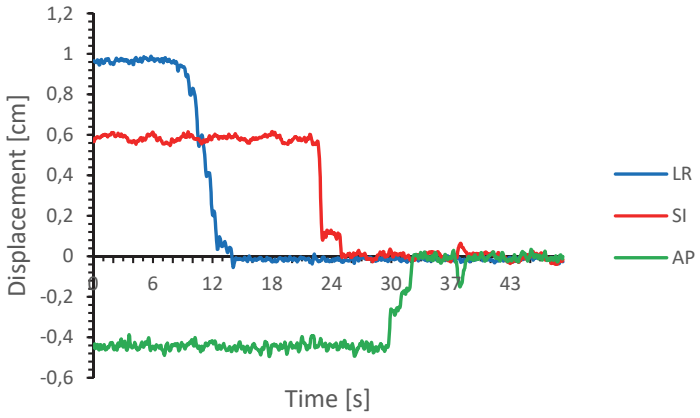

FIGURE 2 Calypso localization. Prostate displacement after patient setup is corrected with Calypso-guided couch adjustments.

3.2.2 Patients and fractionation

RayPilot localization data was gathered from the intrafraction motion data of the Study I of this thesis. Details of the RayPilot patients, fractionation and treatment setup are presented in chapters 3.1.1 and 3.1.3. Calypso localization data was gathered from twenty-six prostate cancer patients treated between January 2016 and December 2017 either using moderate hypofractionation scheme 20 x 3 Gy (n=14) or extreme hypofractionation scheme 5 x 7 Gy or 5 x 7.25 Gy (n=12). For these patients, three Calypso transponders were implanted into the prostate prior to planning CT. Treatment technique was VMAT with two full or two partial arcs using 6 MV beams for moderate hypofractionation and 10 MV flattening filter

free (FFF) beams for extreme hypofractionation. Treatment isocenter was the geometric CP of the three transponders. CTV was the prostate alone. CTV to PTV margins were 3 mm towards the rectum and 5 mm elsewhere.

3.2.3 Treatment localization and data acquisition

Treatment localization of the RayPilot patients was based on orthogonal kV imaging of the implanted FMs. The translational isocenter offsets detected by the kV imaging were corrected with corresponding translational shifts of the treatment couch. In other words, couch shifts depicted isocenter offsets. Prostate motion was tracked with the RayPilot from the initial positioning of the patients and thus the recorded trajectories contained the prostate position data from the kV imaging time points. Details of the imaging procedures and the RayPilot system are written in chapters 3.1.3 and 3.1.4. The RayPilot system is calibrated to the treatment machine isocenter and based on the RayPilot-observed prostate displacement (=isocenter offset), it suggests the desired treatment couch position, in which the displacement would be zero. Difference between the current and desired couch positions depicts the isocenter offset measured by the RayPilot system. These RayPilot suggested couch shifts were recorded from the kV imaging time points for comparison with couch shifts based on kV localization.

For Calypso patients, initial localization was made by shifting treatment couch guided by the Calypso system so that the difference between observed and planned isocenter positions was within ± 0.5 mm in all translational directions. Prostate intrafraction motion was tracked with Calypso subsequent to the initial localization. Calypso localization was verified with orthogonal kV imaging, aligned with Calypso transponders. Possible isocenter offset detected by the kV imaging was corrected by corresponding couch adjustments. Calypso measured isocenter offsets from the kV imaging time points were extracted from the tracking data for comparison with kV imaging based couch corrections.

3.2.4 Stability of the surrogate markers

The localization in all of the methods studied is based on static relative positions between the surrogate markers and the treatment isocenter. Thus, the accuracy of the methods is dependent on the stability of the markers in the prostate. Stability of the gold seed markers and Calypso transponders was investigated by analyzing the distances between each marker and transponder over the treatment course. Distances between the gold seed markers were calculated using marker coordinates obtained from the CBCT data. Intertransponder distances were gathered from Calypso treatment reports. Standard deviation of the intermarker and intertransponder distances was used as a measure of the positional stability. The positional stability of the RayPilot transmitters was assessed by comparing the relative distance between transmitter CP and geometric CP of the gold seed markers during the treatment course. The distance between transmitter CP and the centroid of the markers was calculated from the CP and marker coordinates obtained from the CBCT images acquired at the

treatment. The change in the distance was calculated relative to the initial distance determined from the planning CT.

3.2.5 Bland-Altman analysis

Agreement of the couch shifts or isocenter offsets between the EM methods and kV imaging were estimated using Bland-Altman analysis. In Bland-Altman analysis, differences between the measurements by two methods for the same subject are compared to their mean [78, 79]. Mean difference, calculated over all measurements, is an estimate of possible bias, or systematic error, between the two methods. Limits of agreement (LOA), calculated as mean ± 1.96SD of the differences, define the range in within 95% of the differences are expected to lie. In this study, RayPilot and Calypso measurements of the isocenter offset were compared to simultaneously measured isocenter offset with kV imaging. Differences between each measurement were plotted against their mean and mean difference and SD of the differences, as well as LOA limits, were calculated. Due to the use of small (3-5 mm) CTV-to-PTV margins and submillimeter accuracy of kV imaging [80], differences larger than 2 mm between the EM methods and kV imaging were chosen as clinically unacceptable. The percentage of the differences that were within ± 1 and ± 2 mm was calculated as well. To evaluate the effect of transmitter migration on localization accuracy of the RayPilot system, Bland-Altman analysis was performed for subset of the RayPilot fractions, for which the observed transmitter migration was corrected. Bland-Altman method assumes that the differences are normally distributed. The normality of the difference distributions were analyzed with the Shapiro-Wilks test.

3.3 Evaluation of the dosimetric effect of intrafraction prostate motion

Standard RT treatment machines are not equipped with methods capable of real-time 3D motion tracking and motion correction of the prostate. However, they are equipped with kV and CBCT imaging capabilities and it would be of interest to implement prostate SBRT utilizing these already available imaging methods and strategies familiar from conventionally fractionated prostate RT. On the other hand, the clinical benefit of the added accuracy provided by continuous motion monitoring of the prostate is not known. The clinical effect of different motion correction methods can be approximated by investigating the effect of these strategies on prostate motion and resulting dose distributions. The aim of the Study III was to evaluate the dosimetric effect of different motion correction strategies including pre-treatment imaging based, and continuous motion monitoring based strategies in prostate SBRT. Dosimetric effect of the motion was assessed by reconstructing motion-inclusive dose distributions.

3.3.1 Patients, fractionation and treatment

Twenty-two patients treated between July 2016 and January 2019 were included in the study. They were treated either with 5 x 7 Gy fractions (n=11) or 5 x 7.25 Gy fractions. The CTV was prostate alone and CTV-to-PTV margins were 3 mm towards rectum and 5 mm elsewhere. An MRI scan, acquired prior to transponder implantation, was fused with planning CT for the delineation of the prostate and prostatic urethra. Urethra was delineated as 8 mm cylindrical tube to cover for uncertainties in delineation and deformation of the prostate between imaging sets and treatment fractions. Organs at risk (OAR) were rectum and bladder. The PTV mean dose was normalized to 100% of the prescribed dose and 95% isodose had to cover the whole PTV. Maximum allowed dose within PTV was 105% of the prescribed dose. For patients getting 5 x 7.25 Gy, the prostatic urethra was optimized to a mean dose of 35 Gy while the surrounding PTV was optimized simultaneously to a mean dose of 36.25 Gy. Treatment technique was VMAT with two full or two partial arcs with 10 FFF beams. Treatments were delivered with a TrueaBeam STx (Varian Medical Systems, Palo Alto, CA, USA) linac.

3.3.2 Patient setup, treatment localization and intrafraction motion tracking

Patients were treated supine using in-house made knee support. Patient position was adjusted by aligning room lasers with tattooed skin marks. Initial treatment localization was made with Calypso, after which a CBCT was acquired and aligned to Calypso transponders for checking of bladder and rectum filling status and for confirming that the prostate was not deformed and located within the PTV. Possible isocenter shift detected in the CBCT image was corrected with couch shifts. After the CBCT, the prostate position was further confirmed with orthogonal kV imaging and image alignment using Calypso transponders as fiducials. Possible prostate displacement seen in kV images, induced by the intrafraction motion during the acquiring, image matching and interpretation of the CBCT, was corrected by couch adjustments. For some fractions, also Calypso-guided couch repositioning was used prior to treatment. If the prostate motion exceeded 2 mm posteriorly or 3 mm elsewhere during the treatment, beam was gated off automatically. If the prostate did not return within tolerances, the prostate position was corrected with Calypso-guided adaptive couch repositioning. Motion tracking was initiated immediately after the Calypso localization and ended after the completed treatment. Prostate motion trajectories were recorded and exported for further analysis. Implemented continuous motion monitoring based correction strategy is referenced as "strategy A" hereafter.

3.3.3 Simulation of motion trajectories for alternative motion correction strategies

Pre-treatment imaging based motion correction strategies were simulated by editing Calypso motion trajectories from the delivered treatments. Two strategies were simulated. First, the Calypso based gating events and motion corrections were corrected from the motion data, to simulate a non-gated correction strategy that was based on CBCT and additional kV based correction prior to treatment. This strategy is referenced as "strategy B" hereafter. To simulate a correction strategy that was based only on single pre-treatment CBCT, all couch corrections other than CBCT based were corrected from the motion data. This strategy is referenced as "strategy C" hereafter. Actual and simulated motion trajectories for one fraction are illustrated in figure 3.

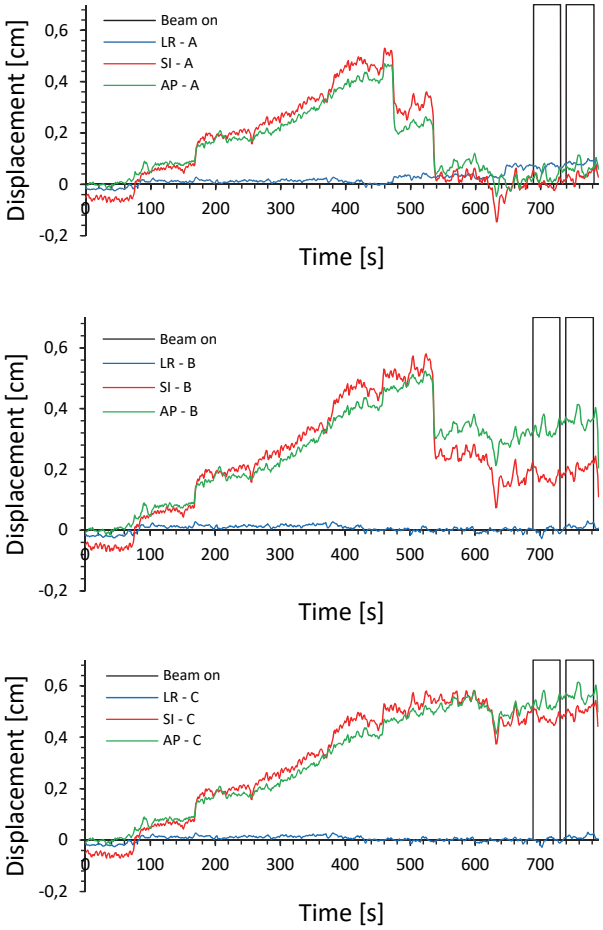

FIGURE 3 Actual (top) and simulated prostate motion trajectories for one fraction. Actual trajectory included two additional motion corrections: first, kV imaging was used to correct for prostate drift during the CBCT. Drifting continued during the kV imaging and residual AP and SI displacements were corrected using Calypso adaptive couch repositioning. In CBCT+kV based trajectory (middle), the Calypso correction was removed. In only CBCT based trajectory (bottom), also the kV imaging based correction was removed. The figure is modified from Study III.

3.3.4 Motion-including dose reconstruction

To evaluate the dosimetric effect of the prostate intrafraction motion in different motion correction strategies, motion-inclusive dose distributions were reconstructed using isocenter shift dose reconstruction method, developed by Poulsen et al [81]. In the method, the treatment plan isocenter is shifted according to the observed 3D motion trajectory during the treatment delivery, and the motion encoded plan is recalculated. The original treatment plans were exported from the treatment planning system (TPS) (Eclipse, versions 13.6 and 15.6, Varian Medical Systems, Palo Alto, CA, USA) for motion encoding. Motion trajectories, extracted from the Calypso logs, were synchronized with the original treatment plans consisting of two VMAT beams. Motion trajectories were divided into 1 mm position bins and for each position bin, sub-beams were constructed from the treatment plan control points to represent the part of the treatment delivery, while the target was located within each position bin. Sub-beam isocenters were shifted by the corresponding target displacements. Motion encoding of the treatment plans was made with in-house MATLAB program (MATLAB R2017b, MathWorks). Motion encoded treatment plans were imported back into the TPS for calculation of motion-inclusive dose distributions. Motion-inclusive dose distributions were reconstructed for each treatment fraction for each patient and for each correction strategy.

3.3.5 Comparison of dose distributions

The dosimetric effect of different motion correction strategies was evaluated by comparing dose-volume histogram (DVH) parameters for target and OAR structures between motion-inclusive and planned dose distributions. DVH parameters for target structures were: PTVD95%, PTVsubCTVD95% (PTV shell volume, obtained by subtracting CTV from the PTV), PTV mean dose, CTVD99%, CTV mean dose, urethra D99%, urethra D2% and urethra mean dose. For patients receiving 7.25 Gy fractions, urethra was optimized to a mean dose of 7 Gy while the surrounding PTV was optimized to 7.25 Gy. For these patients, the urethra was subtracted from the CTV and PTV structures for comparability of DVHs with patients receiving homogeneous 7 Gy dose to the PTV. Analyzed DVH parameters for the OARs were: V50%, V65%, V90% and V100% for the bladder and V50%, V65%, V90%, V96.2% and V100% for the rectum. Comparisons were made for individual fractions, individual patients and different motion correction strategies (DVH parameters averaged over all fractions per strategy). To investigate the potential averaging of the dosimetric errors during the treatment course, running cumulative variation in PTVD95% and CTVD99% between motion-inclusive and planned dose distributions were calculated for individual patients.

3.3.6 Intrafraction motion analysis

Intrafraction motion of the prostate during the beam delivery was analyzed for all correction strategies. Mean 3D, AP, SI and LR displacements, as well as mean of the absolute AP, SI and LR displacements, were calculated for individual fractions and over all fractions per strategy. Percentage time of displacements ≥ 1, 2, 3, 5 and 7 mm in AP, SI and LR directions were calculated over all fractions per strategy as well.

3.3.7 Statistical analysis

Correlation of the prostate motion and dosimetric effects were estimated by calculating Pearson correlation coefficients between motion metrics and dosimetric changes between motion-inclusive and planned values. Motion metrics tested were mean and mean of absolute AP, SI and LR displacements and mean 3D displacement. Wilcoxon signed rank test was used to evaluate the difference between motion-inclusive and planned DVH parameters for target structures (PTV, CTV and urethra). Additionally, DVH parameters from strategies B and C were compared to those of strategy A. The normality of DVH parameter distributions were tested with Kolmogorov-Smirnov test.

4 RESULTS

4.1 The effect of rectal dose sparing device on intrafraction prostate motion

4.1.1 3D motion

Motion data could be successfully gathered from 22 patients out of 28 recruited in the study. In total, 260 RR fractions and 351 non-RR fractions were analyzed. Mean ± SD of the tracking time was 540 ± 150 s and 450 ± 150 s for RR and non-RR fractions, respectively. Proportion of the fractions covering at least 3 min of tracking time was 99.2% (258/260) and 99.7% (350/351) for RR and non-RR fractions, respectively. At least 6 min of tracking time was covered by 95.0% (247/260) and 80.7% (276/351) of RR and non-RR fractions, respectively. Corresponding figures for at least 10 min of tracking time were 22.3% (58/260) and 7.5% (26/351) of the RR and non-RR fractions, respectively. Percentage times of 3D displacements in RR and non-RR fractions, and difference in percentage times between RR and non-RR fractions, within 3, 6 and 10 min of tracking time are shown in figure 4. In general, the observed motion was small but larger when the RR was used. The probability of prostate motion increased with longer tracking time. The difference in 3D motion distributions between RR and non-RR fractions was statistically significant ($p < 0.03$) for all tracking times evaluated. The percentage times of 3D displacements within 10 min of tracking time for individual patients are presented in table 1. For 13 patients the 3D motion was significantly larger ($p < 0.05$) with RR than without it. For two patients the prostate motion was significantly smaller ($p < 0.05$) with RR than without it.

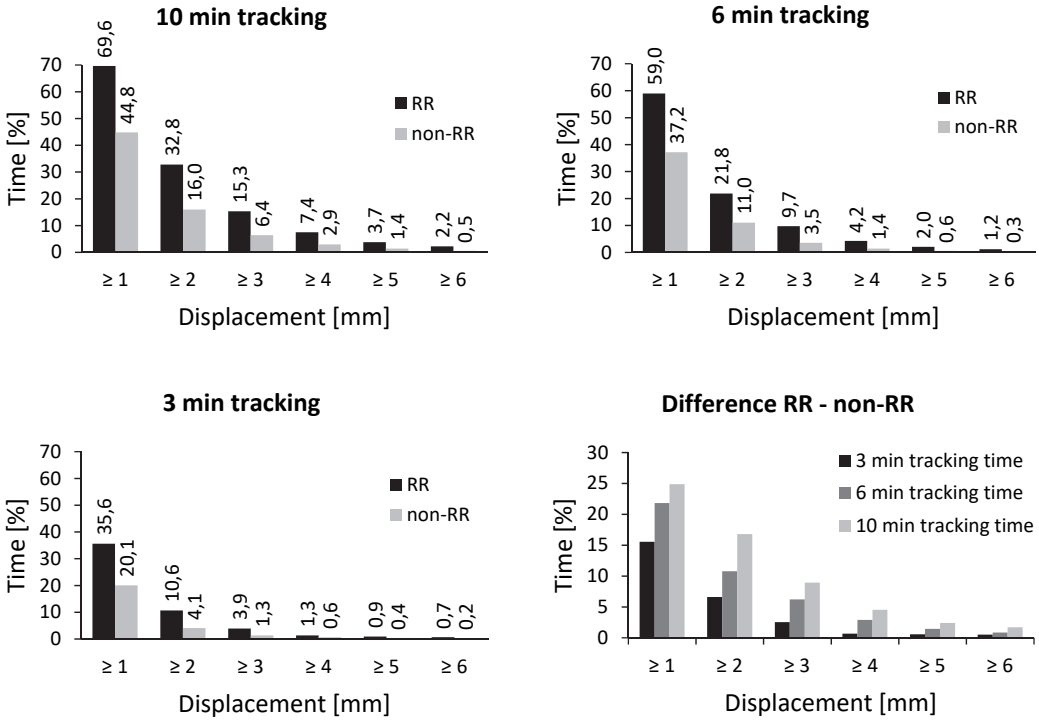

FIGURE 4 Percentage times of 3D prostate displacements within 3, 6 and 10 min of tracking time for RR and non-RR fractions. Also shown is the difference in percentage times between RR and non-RR fractions. Positive values indicate larger motion within the RR fractions. The figure is modified from Study I.

TABLE 1 Proportion of tracking time during which the prostate was displaced in RR and non-RR fractions for each patient [I].

	3D prostate displacement											
	≥ 1 mm		≥ 2 mm		≥ 3 mm		≥ 4 mm		≥ 5 mm		≥ 6 mm	
Patient	RR	non-RR	RR	non-RR	RR	non-RR	RR	non-RR	RR	non-RR	RR	non-RR
1	75.7	44.3	35.0	16.0	17.3	8.8	1.3	6.6	0.0	2.6	0.0	0.5
2	70.8	68.2	36.3	36.4	2.5	13.2	0.0	5.4	0.0	2.8	0.0	0.4
3*	71.6	38.2	38.8	13.0	22.6	2.2	11.1	0.0	6.2	0.0	2.3	0.0
4*	77.4	5.6	53.5	0.0	25.4	0.0	13.8	0.0	11.1	0.0	10.7	0.0
5*	70.2	23.4	21.4	8.8	10.0	0.0	0.9	0.0	0.3	0.0	0.1	0.0
6*	90.1	70.3	67.7	34.8	49.3	9.8	28.3	3.9	16.6	0.2	4.6	0.0
7*	66.9	49.9	44.4	8.7	25.6	2.4	14.9	1.0	6.9	0.3	3.3	0.0
8	69.5	58.2	22.8	24.8	2.1	8.1	0.0	2.9	0.0	0.2	0.0	0.0
9*	65.0	12.0	29.6	0.2	2.2	0.0	0.0	0.0	0.0	0.0	0.0	0.0
10**	66.9	70.4	13.4	27.9	0.0	11.3	0.0	9.7	0.0	4.8	0.0	0.0
11*	57.4	29.1	13.5	1.4	1.0	0.0	0.0	0.0	0.0	0.0	0.0	0.0
12*	57.1	26.1	6.4	1.3	1.0	0.0	0.0	0.0	0.0	0.0	0.0	0.0
13*	88.2	74.8	65.2	43.0	50.5	17.9	28.4	5.7	11.3	3.2	7.6	0.9
14*	85.1	34.2	65.9	7.7	39.5	1.2	21.8	0.2	9.4	0.0	7.1	0.0
15*	59.1	24.5	5.1	0.0	0.4	0.0	0.0	0.0	0.0	0.0	0.0	0.0
16	49.2	40.3	5.0	6.5	0.0	1.0	0.0	0.4	0.0	0.0	0.0	0.0
17	62.2	31.5	7.2	9.5	0.0	3.0	0.0	0.0	0.0	0.0	0.0	0.0
18*	80.4	35.9	39.1	5.7	21.4	4.8	15.7	1.1	8.2	0.0	7.5	0.0
19	73.2	65.9	40.8	37.1	8.5	20.8	0.0	10.7	0.0	4.7	0.0	1.2
20**	46.5	75.5	17.4	41.0	0.5	20.3	0.0	3.9	0.0	1.8	0.0	0.4
21*	87.5	76.4	69.7	49.7	40.9	30.3	22.1	14.9	13.3	7.3	5.7	3.5
22	64.4	46.7	19.3	16.1	4.6	9.2	0.3	8.0	0.0	6.0	0.0	5.0

*$p < 0.05$, RR motion larger than non-RR motion
**$p < 0.05$, non-RR motion larger than RR motion

4.1.2 Direction of the motion

Percentage times of unidirectional prostate displacements within 6 and 10 min of tracking time are presented in figures 5 and 6, respectively. Most of the motion occurred in AP and inferior directions, when the RR was not used, and in inferior and posterior directions, when the RR was used. The use of RR seemed to reduce anterior prostate motion but increase the motion in all other directions, especially in inferior and posterior directions. The difference was statistically significant in inferior and posterior directions ($p < 0.03$) and also in superior direction ($p < 0.03$ for 10 min tracking time and $p < 0.05$ for 6 min tracking time).

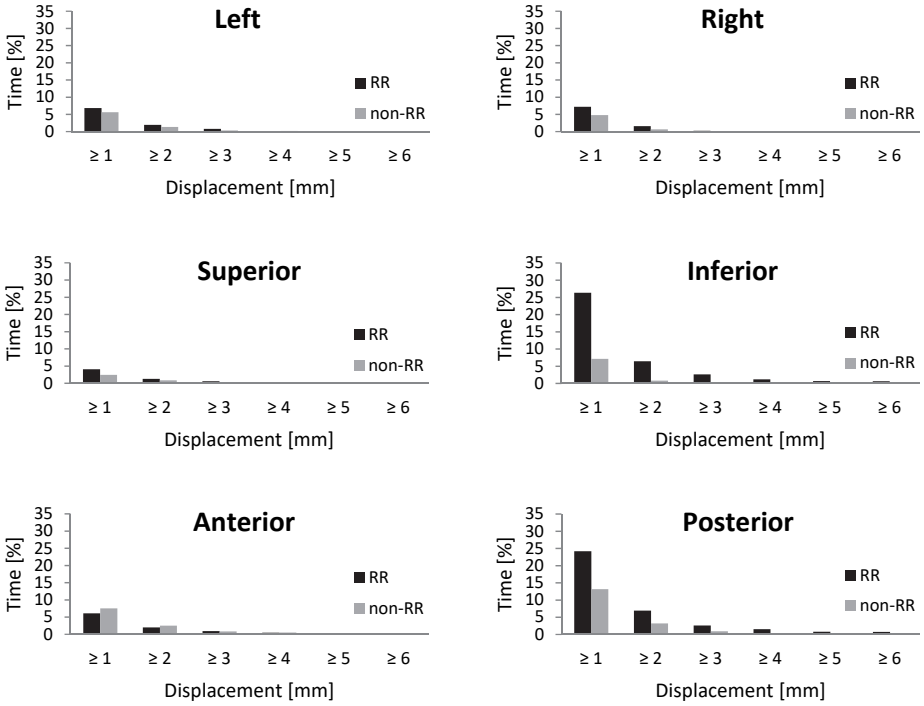

FIGURE 5 Percentages of time when the prostate was displaced in each direction within 6 min of tracking time for RR and non-RR fractions.

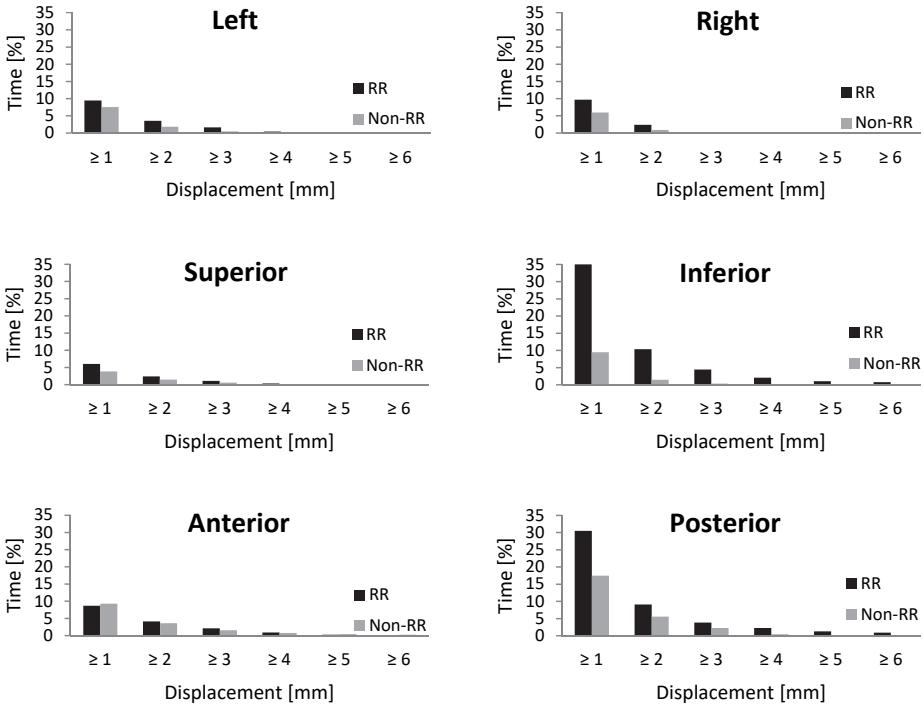

FIGURE 6 Percentages of time when the prostate was displaced in each direction within 10 min of tracking time for RR and non-RR fractions.

4.1.3 Time dependence

Percentage time of prostate 3D displacements ≥ 2, 3, 4, 5 and 6 mm over all RR and non-RR fractions as a function of tracking time are shown in figure 7. The probability of prostate 3D displacement increased linearly as a function of time in both RR and non-RR fractions, though the increase was faster in RR fractions. Percentage time of the 3D displacements correlated strongly with tracking time: Pearson correlation coefficients for 3D displacements ≥ 1, 2, 3, 4, 5 and 6 mm were 0.885, 0.997, 0.982, 0.988, 0.951 and 0.852 for RR-fractions and 0.951, 0.995, 0.942, 0.882, 0.835 and 0.917 for non-RR fractions, respectively. All of the correlations were significant ($p < 0.01$).

Percentage time of unidirectional displacements ≥ 2, 3 and 5 mm are shown in figure 8. Common for all directions except for LR was that the probability of the motion increased with increasing tracking time. LR motion increased until 8-10 min of the tracking time, after which the motion reduced. The probability of the inferior displacement in RR fractions grew especially fast as a function of tracking time. Figure 9 shows the increase in percentage time of inferior prostate displacements ≥ 1 and ≥ 3 mm for RR and non-RR fractions. For RR fractions, the increase in displacements ≥ 1 mm started to plateau after about 6 minutes from the patient setup and start of the motion tracking. The temporal motion patterns between RR and non-RR fractions differed significantly for at least 3 mm inferior displacements ($p \leq 0.015$) and for posterior displacements ≥ 5 mm ($p \leq 0.05$).

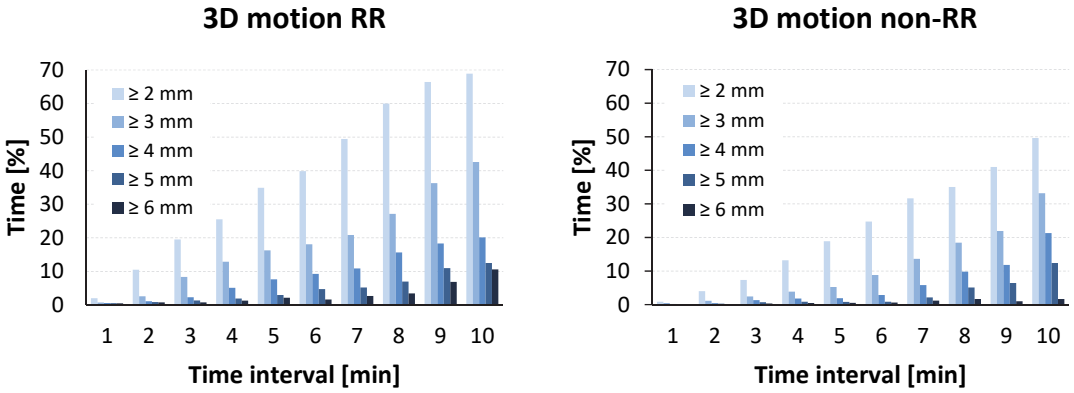

FIGURE 7 Percentage of the time of 3D prostate displacements ≥ 2, 3, 4, 5 and 6 mm within 1 minute intervals as a function of tracking time in RR and non-RR fractions. The figure is modified from Study I.

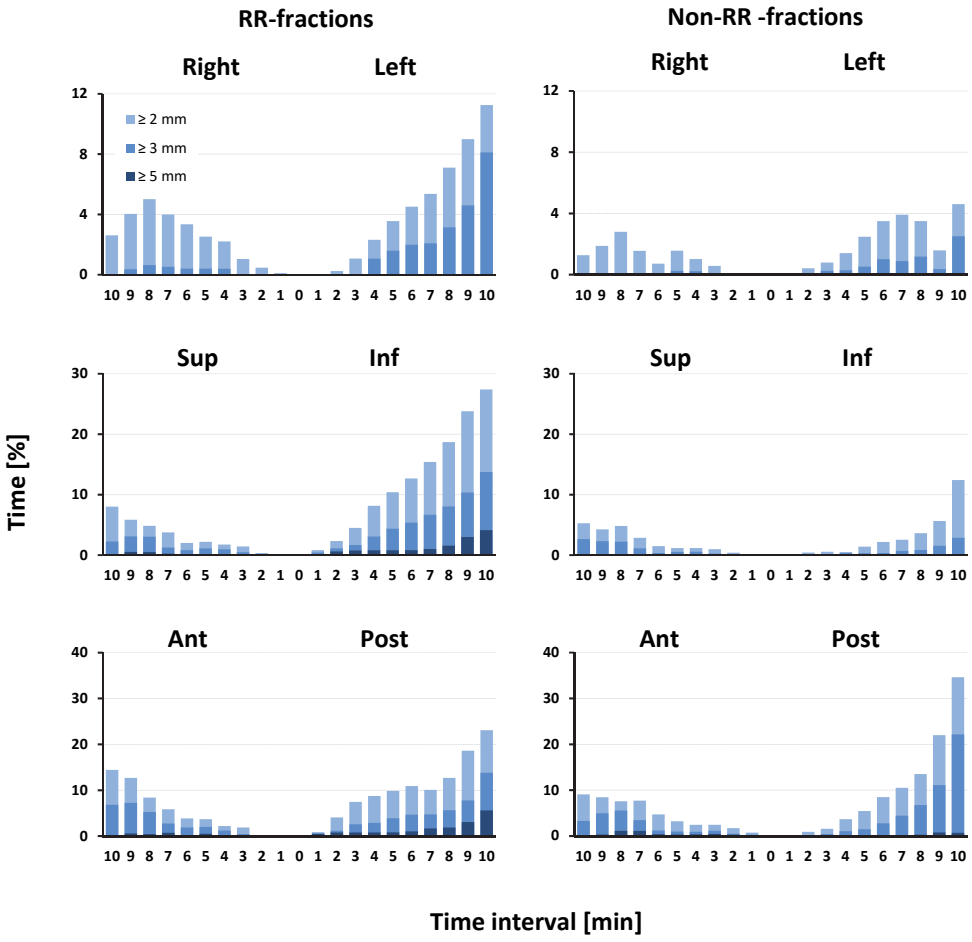

FIGURE 8 Percentage of the time of unidirectional prostate displacements ≥ 2, 3 and 5 mm within 1 minute intervals as a function of tracking time in RR and non-RR fractions [I].

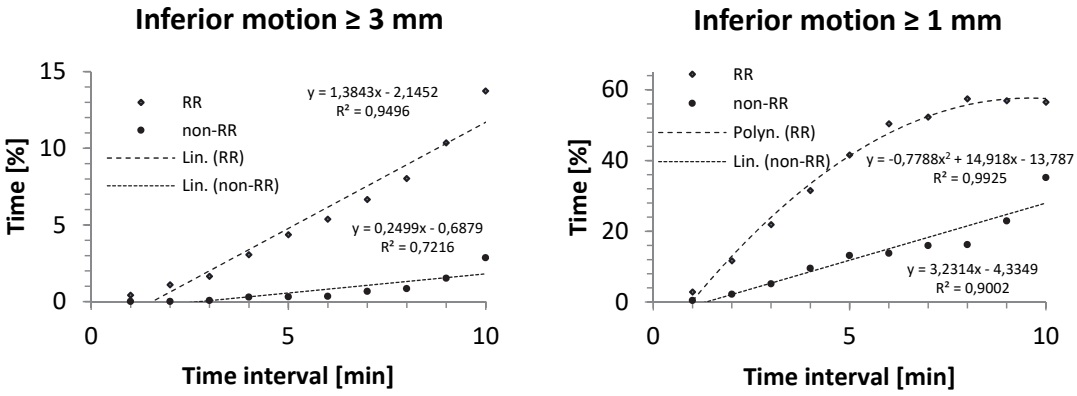

FIGURE 9 Percentage time of inferior prostate displacement ≥ 3 mm and ≥ 1 mm as a function of tracking time for RR and non-RR fractions. Likelihood of the prostate being inferiorly displaced at least 1 and 3 mm increased linearly, except for RR fractions, for which a plateau was seen in displacements ≥ 1 mm. Applied polynomial fit does not reach a plateau mathematically, but fits the data within the inspected time interval range.

4.2 Observed localization accuracy of the electromagnetic tracking devices

4.2.1 Agreement between electromagnetic localization methods and kV imaging

A total of 582 pairs of couch shift values suggested by the RayPilot and kV imaging systems for each translational direction from 582 fractions treated with the RayPilot were included in the Bland-Altman analysis. A total of 335 Calypso fractions were included in the analysis. The number of the paired couch shift data points between Calypso and kV imaging was 353, 700 and 347 for AP, SI and LR directions. For some fractions, kV imaging was repeated, thus giving the opportunity to compare more data points than there were fractions. Apart from AP and LR directions, SI directed displacements could be obtained from both orthogonal kV images, explaining the twofold amount of SI values. Bland-Altman plots of the couch shift differences between the EM systems and kV imaging are presented in figures 10 (RayPilot) and 11 (Calypso). Mean and SD of the differences between the EM methods and kV imaging, as well as LOA values and percentage of differences within ± 1 and ± 2 mm are presented in table 2. Positive values indicate anterior, inferior and left couch shifts and that the kV couch shifts are larger than couch shifts suggested by the RayPilot or the Calypso. Calculated LOA values indicate, that 95% of the differences between RayPilot and kV imaging can be expected to lie within ± 4.3, ± 4.7 and ± 2.1 mm around the mean in AP, SI and LR directions, respectively. Correspondingly, LOA values for Calypso and kV imaging were ± 1.3, ± 1.0 and ± 0.8 mm around the mean in AP, SI and LR directions, respectively. Transmitter migration during the treatment course was investigated for 324 RayPilot fractions. The effect of the transmitter migration on the localization accuracy of the RayPilot was investigated by performing Bland-Altman analysis for a subset of RayPilot fractions, for which the suggested couch values were corrected for the observed migration. The number of fractions analyzed was 317. The results of the Bland-Altman analysis for migration corrected RayPilot fractions are presented in table 3 and Bland-Altman plots in figure 12.

TABLE 2 Couch shift differences between RayPilot and kV imaging, and between Calypso and kV imaging. Positive values in AP-, SI- and LR-axes symbolize couch shifts towards anterior, inferior and left directions. All values are given in mm. Percentages of the differences within ±1 and ±2 mm are also presented. [II]

	AP		SI		LR		3D	
	RayPilot	Calypso	RayPilot	Calypso	RayPilot	Calypso	RayPilot	Calypso
Bias (mean)	0.3	-0.2	-2.2	0.1	-0.0	-0.1	-0.2	-0.1
SD	2.2	0.6	2.4	0.5	1.0	0.4	2.4	0.6
Upper LOA	4.6	1.1	2.5	1.2	2.1	0.8	4.4	1.1
Lower LOA	-4.0	-1.5	-6.8	-0.9	-2.0	-0.9	-4.8	-1.4
≤ 1 mm [%]	32.3	88.7	22.9	93.1	69.4	96.5	35.2	88.8
≤ 2 mm [%]	64.6	98.6	44.0	99.6	94.8	100.0	63.4	99.1

TABLE 3 Couch shift differences between the RayPilot values corrected for migration and values based on kV imaging. All values are given in mm. Percentages of the differences within ±1 and ±2 mm are also presented. The table is modified from Study II.

	AP	SI	LR	3D
Bias (mean)	0.1	-0.7	0.3	-0.2
SD	1.7	1.9	1.2	1.9
Upper LOA	3.4	2.9	2.6	3.4
Lower LOA	-3.2	-4.3	-2.0	-3.8
≤ 1 mm [%]	41.6	44.8	79.2	45.1
≤ 2 mm [%]	78.5	75.7	94.6	77.6

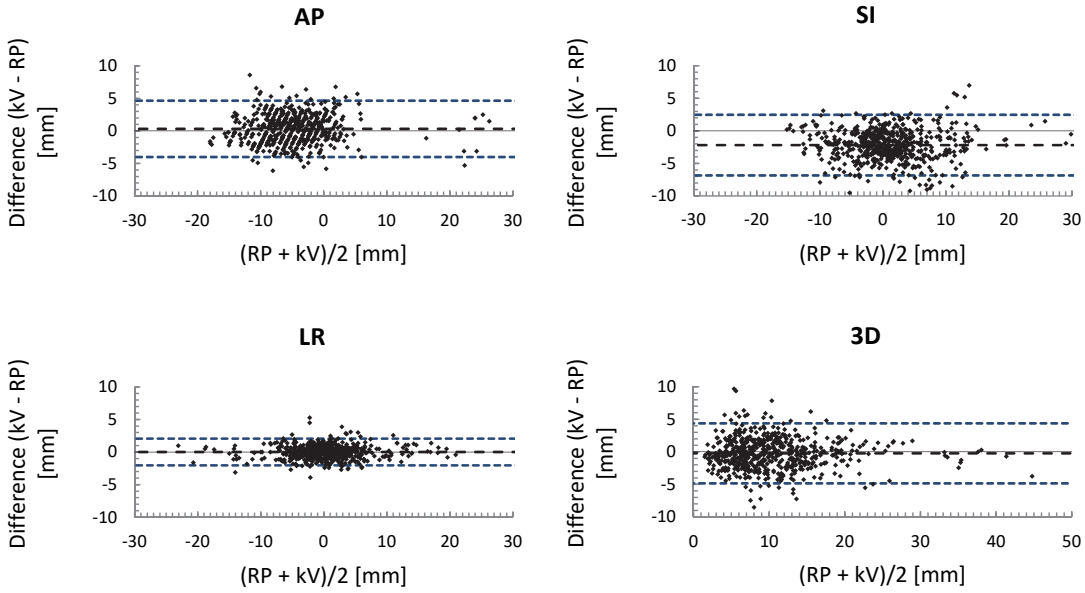

FIGURE 10 Bland-Altman plots of the differences between the couch shifts suggested by the RayPilot and kV imaging. Differences in the couch shifts between the methods are plotted against their average value. Black dashed line represents the mean difference between the methods and blue dashed lines represent the 95% limits of agreement. Black solid line depicts the line of identity. The figure is modified from Study II.

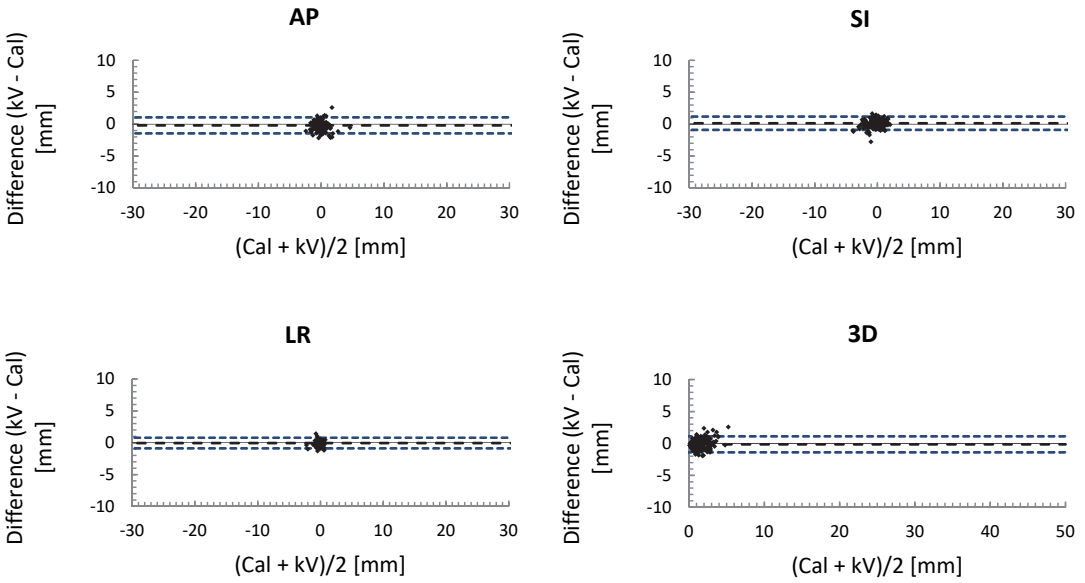

FIGURE 11 Bland-Altman plots of the differences between the couch shifts suggested by the Calypso and kV imaging. Differences in the couch shifts between the methods are plotted against their average value. Black dashed line represents the mean difference between the methods and blue dashed lines represent the 95% limits of agreement. Black solid line depicts the line of identity. Scales of the charts are the same as in figure 10 for comparative purposes. The figure is modified from Study II.

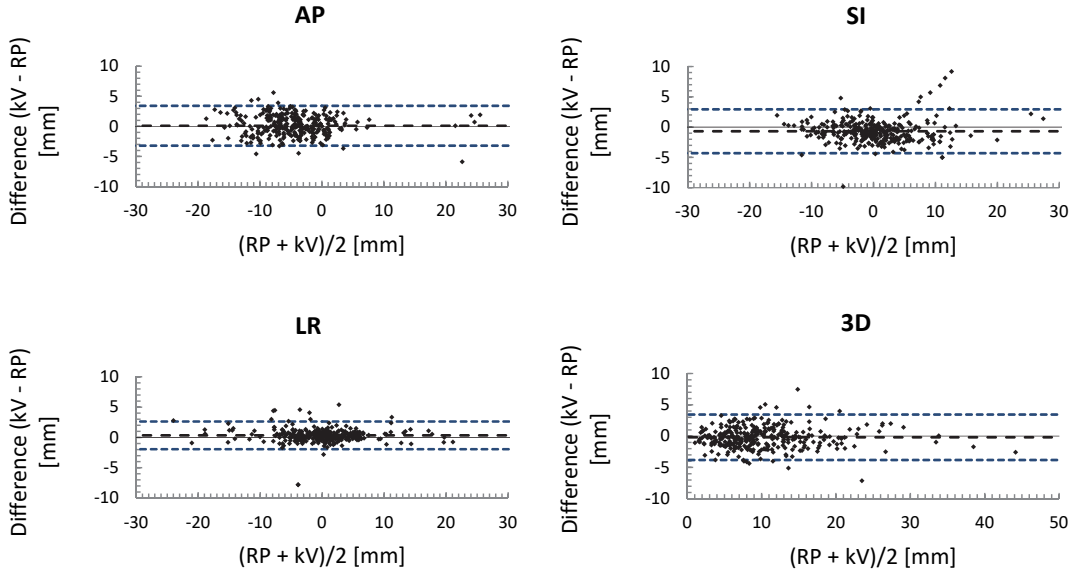

FIGURE 12 Bland-Altman plots representing the differences in couch shifts between migration corrected RayPilot values and kV imaging. Differences in the couch shifts between the methods are plotted against their average value. Black dashed line represents the mean difference between the methods and blue dashed lines represent the 95% limits of agreement. Black solid line depicts the line of identity.

4.2.2 Stability of the surrogate markers

Distances between each gold marker and the distance between transmitter CP and the geometric center point of the three gold seed markers were calculated for 368 instances (324 RayPilot fractions and 44 planning CT images from 22 patients). In general, gold seeds were very stable and the SD of the intermarker distances, averaged over all 22 patients, was 0.5 mm. For one patient, one of the gold seeds had drifted to the implantation canal of the RayPilot transmitter implanted too near to the gold seed, and subsequently migrated caudally 6 mm between the first and the second treatment fraction. For this patient, the migrated marker was ignored and the treatment localization was based on two stable markers. The change in the RayPilot transmitter CP position relative to the geometric CP of the gold seed markers was calculated for 324 fractions. The mean, SD and maximum values of the position change are presented in table 4.

Calypso intertransponder distances were gathered for all 335 fractions from the 26 patients included in the study. The SD of the intertransponder distances, averaged over all fractions, was 0.5 mm indicating good positional stability of the transponders, similar to gold seed markers. However, in three occasions, larger transponder migration was detected: one of the transponders was voided between planning CT and the first treatment fraction due to transponder implantation near to the urethra. For one patient one of the transponders migrated 6 mm caudally between the planning CT and the first treatment fraction and for another patient one transponder migrated 3.8 mm cranially during the treatment course. The voided transponder was ignored in the Calypso

localization plan and the prostate motion tracking and localization was based on the two transponders left. For the patient with 6 mm transponder migration, a new planning CT and treatment plan were prepared. For the third patient with 3.8 mm cranial transponder migration, the treatment localization was performed with kV imaging and alignment of the two stable transponders. Compared to the kV localization based on two transponders, the migration of the transponder decreased the localization accuracy of the Calypso system approximately by 1 mm in SI direction.

TABLE 4 Change in the position of the RayPilot transmitter CP relative to the geometric center point of the three gold seed markers during the treatment course. All values are given in mm. [II]

	AP	SI	LR	3D
Mean	-0.3	-1.8	-0.2	2.8
SD	1.6	2.0	0.8	1.6
Max	-7.3	-7.6	-3.5	9.2

4.3 Dosimetric effect of intrafraction prostate motion for different motion correction strategies

Few of the 110 fractions from 22 patients included in the study could not be reconstructed and the final number of fractions reconstructed was 103 in motion correction strategies A and B, and 102 in strategy C.

4.3.1 Observed and simulated prostate motion during the beam delivery

Mean displacement of the prostate during the beam delivery, averaged over all fractions, and maximum and minimum values of the fraction mean displacements in each motion correction strategy are presented in table 5. Positive values represent anterior, superior and left displacements. Percentage times of AP, SI and LR displacements ≥ 1, 2, 3, 5 and 7 mm within treatment delivery time are presented in table 6.

TABLE 5 Mean intrafraction displacement of the prostate during treatment delivery in each motion correction strategy. Subscript "abs" refers to absolute value. Range describes the observed maximum amplitude of the motion. Maximum and minimum of the mean displacements within a single fraction are shown as well. All values are given in mm. [III]

Strategy		3D	LRabs	SIabs	APabs	LR	SI	AP
A	Mean	1.0	0.4	0.5	0.5	0.0	0.0	0.1
	SD	0.4	0.3	0.4	0.4	0.5	0.7	0.7
	Min	0.3	0.0	0.0	0.0	-1.5	-1.8	-1.3
	Max	2.2	1.5	1.8	1.9	1.1	1.6	1.9
	Range					-2.7,1.8	-4.1,9.8	-2.2,3.1
B	Mean	1.1	0.4	0.5	0.6	0.0	0.0	0.1
	SD	0.6	0.3	0.5	0.6	0.5	0.7	0.8
	Min	0.3	0.0	0.0	0.0	-2.4	-1.9	-1.3
	Max	4.8	2.4	2.3	4.5	1.1	2.3	4.5
	Range					-2.8,1.8	-4.2,11.8	-2.4,9.0
C	Mean	1.7	0.6	0.9	0.9	0.1	0.1	-0.1
	SD	1.1	0.6	0.9	0.9	0.8	1.3	1.3
	Min	0.5	0.0	0.0	0.0	-2.6	-4.6	-4.0
	Max	7.4	3.4	4.9	5.5	3.4	4.9	5.5
	Range					-3.0,4.1	-6.8,12.8	-5.2,7.9

TABLE 6 Percentage time of prostate displacements in translational directions within the treatment delivery time. [III]

	Strategy A			Strategy B			Strategy C		
	LR	SI	AP	LR	SI	AP	LR	SI	AP
≥ 1 mm	5.0	15.9	15.7	5.4	17.8	16.8	14.8	32.5	37.0
≥ 2 mm	0.1	1.1	1.4	1.1	2.6	3.6	3.6	10.4	10.8
≥ 3 mm	0.0	0.0	0.0	0.0	0.3	1.3	1.0	4.8	3.2
≥ 5 mm	0.0	0.0	0.0	0.0	0.0	0.2	0.0	0.6	1.1
≥ 7 mm	0.0	0.0	0.0	0.0	0.0	0.1	0.0	0.0	0.1

4.3.2 The effect of prostate motion on target doses

Mean, SD and maximum differences of the evaluated dose volume parameters between motion-inclusive and planned dose distributions for target structures in each motion correction strategy are presented in table 7. Motion-inclusive mean DVHs of the target structures in each motion correction strategy, along with planned DVHs, are plotted in figure 13. Box-plots of the differences between motion-inclusive and planned CTVD99% and PTVD95% parameters in different motion correction strategies are shown in figure 14. In general, the dosimetric effect of the motion was small but for individual fractions greater dose deficits were seen. The dose deficits were mostly seen in PTVD95% and PTVsubCTVD95%

parameters while the CTV parameters were less affected, indicating that most of the dosimetric effect induced by the motion occurred in the target periphery. It indicates also, that the PTV margins covered most of the motion and that the interplay effect between prostate and multileaf collimator (MLC) motion had less dosimetric impact. Largest dose deficits were seen in strategy C. Maximum dose differences within single fraction were -6.4% (PTV mean), -2.2% (CTV mean), -29.0% (PTVD95%) and -7.1% (CTVD99%). Mean 3D displacement of the prostate for this fraction was 7.4 mm (superior and anterior displacements were 4.9 and 5.5 mm, respectively), while it was 1.0 mm for the actually delivered fraction (figure 3). Corresponding delivered and shifted dose distributions are illustrated in figure 15. Mean ± SD values of the PTV and CTV parameters calculated separately for 5 x 7 Gy and 5 x 7.25 Gy fractionations are presented in table 8. The effect of heterogeneous dose distribution caused by the urethra sparing in plans with 5 x 7.25 Gy fractionation was small on CTV parameters. However, dose deficits in PTV parameters were larger for 5 x 7.25 Gy fractionation, though mainly in strategy C.

All other target DVH parameters than CTV mean dose in strategies A, B and C, and urethra mean dose in strategy C, differed significantly ($p < 0.05$) from the planned values. All other than CTV (D99% and mean dose) and urethra (D2%, D50%, D99% and mean dose) parameters differed significantly between strategies A and B. All other parameters than urethra mean dose differed significantly between strategies A and C. Based on the Kolmogorov-Smirnov test, CTVD99% in strategies A and B and urethra D2% in strategy A were normally distributed. Thus the results of Wilcoxon signed rank test for these parameters may include some uncertainty.

TABLE 7 Mean, SD and maximum percentual differences in target DVH parameters between motion-inclusive and planned dose distributions over all patients and fractions. The table is modified from Study III.

	Strategy A			Strategy B			Strategy C		
	Mean	SD	Max	Mean	SD	Max	Mean	SD	Max
PTVsubCTVD95%	-1.6	1.5	-8.4	-2.0	2.2	-15.4	-5.2	7.2	-45.2
PTVD95%	-0.9	0.8	-4.3	-1.2	1.5	-10.8	-3.1	4.9	-29.0
PTV mean	-0.2	0.2	-1.2	-0.2	0.3	-2.1	-0.5	0.9	-6.4
CTVD99%	-0.3	0.4	-2.5	-0.4	0.6	-3.5	-0.7	1.2	-7.1
CTV mean	0.0	0.2	-0.5	0.0	0.2	-0.5	-0.1	0.3	-2.2
Urethra D2%	0.7	0.8	3.8	0.9	1.1	6.6	1.3	0.9	6.1
Urethra D99%	-1.3	3.4	-20.2	-1.4	3.5	-20.8	-5.7	12.4	-59.6
Urethra mean	0.1	0.3	1.2	0.1	0.4	2.1	0.1	0.8	-2.8

TABLE 8 The mean ± SD of the differences between motion inclusive and planned target DVH parameters for 5 x 7 Gy and 5 x 7.25 Gy fractionated treatments. Urethra sparing in 5 x 7.25 Gy treatments may increase the target dose deficits in the presence of large motion (strategy C). All results are relative to planned values [%]. [III]

	5 x 7 Gy			5 x 7.25 Gy		
	A	B	C	A	B	C
PTVsubCTVD95%	-1.7 ± 1.6	-1.9 ± 1.9	-3.7 ± 5.1	-1.5 ± 1.4	-2.0 ± 2.5	-6.7 ± 8.6
PTVD95%	-0.9 ± 0.8	-1.0 ± 1.0	-2.0 ± 3.3	-0.9 ± 0.8	-1.3 ± 1.9	-4.1 ± 5.9
PTV mean	-0.1 ± 0.3	-0.1 ± 0.2	-0.3 ± 0.5	-0.2 ± 0.2	-0.2 ± 0.4	-0.7 ± 1.2
CTVD99%	-0.4 ± 0.5	-0.4 ± 0.6	-0.6 ± 1.1	-0.2 ± 0.3	-0.3 ± 0.5	-0.7 ± 1.2
CTV mean	0.0 ± 0.2	0.0 ± 0.2	0.0 ± 0.2	0.0 ± 0.2	0.0 ± 0.2	-0.1 ± 0.4

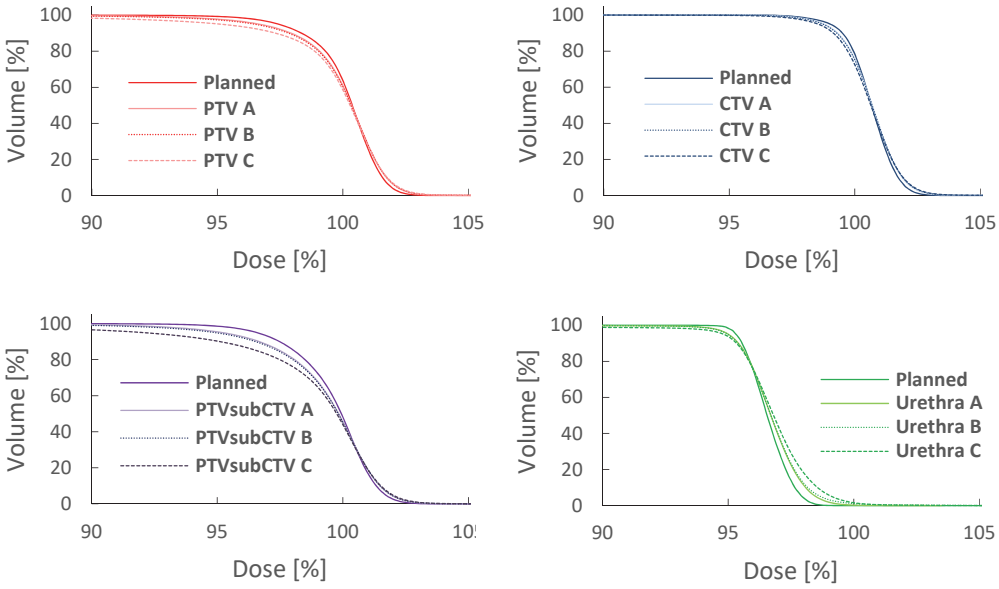

FIGURE 13 The effect of prostate displacement on mean DVHs of the target structures in each motion correction strategy. Planned DVHs are plotted for comparison. The figure is modified from Study III.

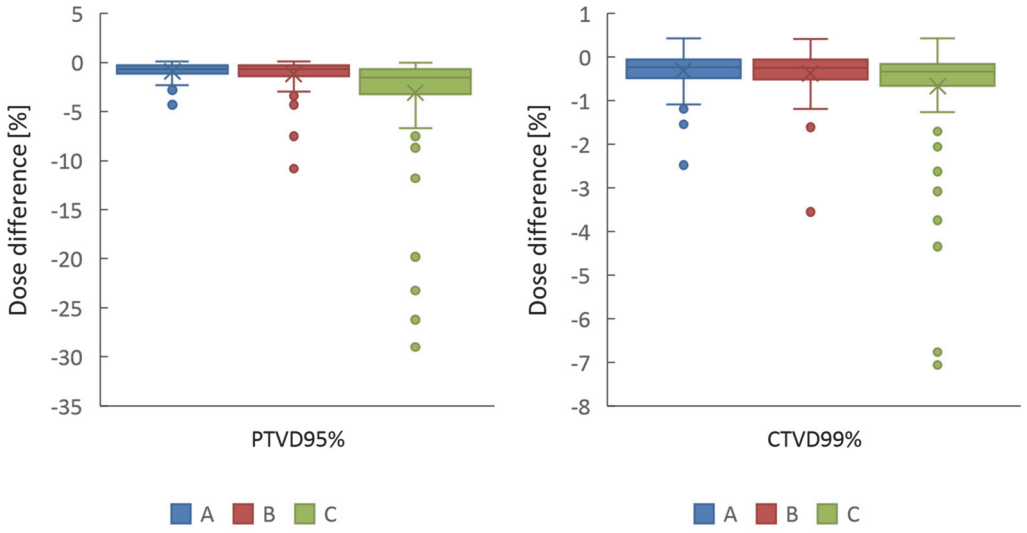

FIGURE 14 The distribution of dose differences of all fractions between motion-inclusive and planned PTVD95% and CTVD99% parameters in motion correction strategies A, B and C. The box limits represent the median and 25th and 75th percentiles. The cross shows the mean value. The whiskers extend up to the largest values that are less than or equal to 1.5 times the interquartile range or down to the smallest values that are larger than 1.5 times the interquartile range. Dots outside the whiskers represent outliers.

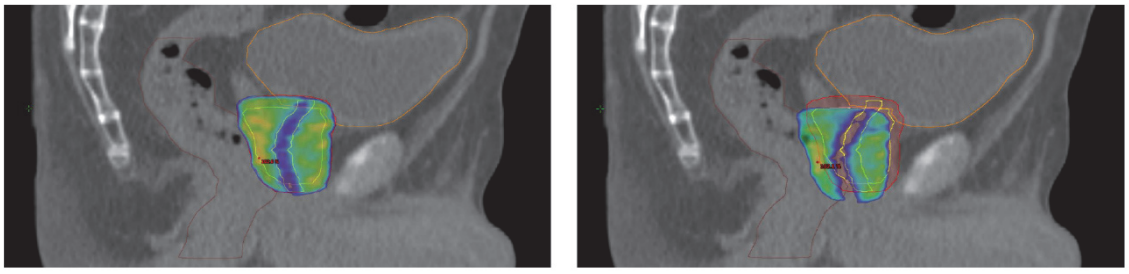

FIGURE 15 Motion-inclusive dose distributions for motion correction strategies A (left) and C (right) for a fraction with largest mean 3D displacement (7.4 mm) observed in strategy C. Delivered dose (strategy A, on left) hit the target precisely. Doses ≥ 95% of the prescribed dose are shown. Dose sparing in urethra region is seen in the colder area crossing through the PTV. [III]

4.3.3 The cumulative effect of five fractions

Running cumulative variation in PTVD95% and CTVD99% was calculated for 16 patients for which all of the five fractions could be reconstructed in each motion correction strategy. Cumulative differences to planned values are plotted as a function of treated fractions in figure 16. For strategies A and B, the differences decreased after third fraction but for some patients in strategy C, the differences increased even at the last fraction. Larger than 1% reduction in cumulative CTVD99%, and 5% reduction in cumulative PTVD95%, of five fractions, were seen only for the same 4 patients in strategy C. Maximum dose reduction in CTVD99% and PTVD95% after five fractions was -1.9 and -12.5%, respectively. Mean (±SD) differences to the planned values in CTVD99% after five fractions were -0.3 ± 0.2, -0.4 ± 0.3 and -0.7 ± 0.5% in strategies A, B and C, respectively. Corresponding differences for PTVD95% were -0.9 ± 0.5, -1.2 ± 0.7 and -3.6 ± 3.3%.

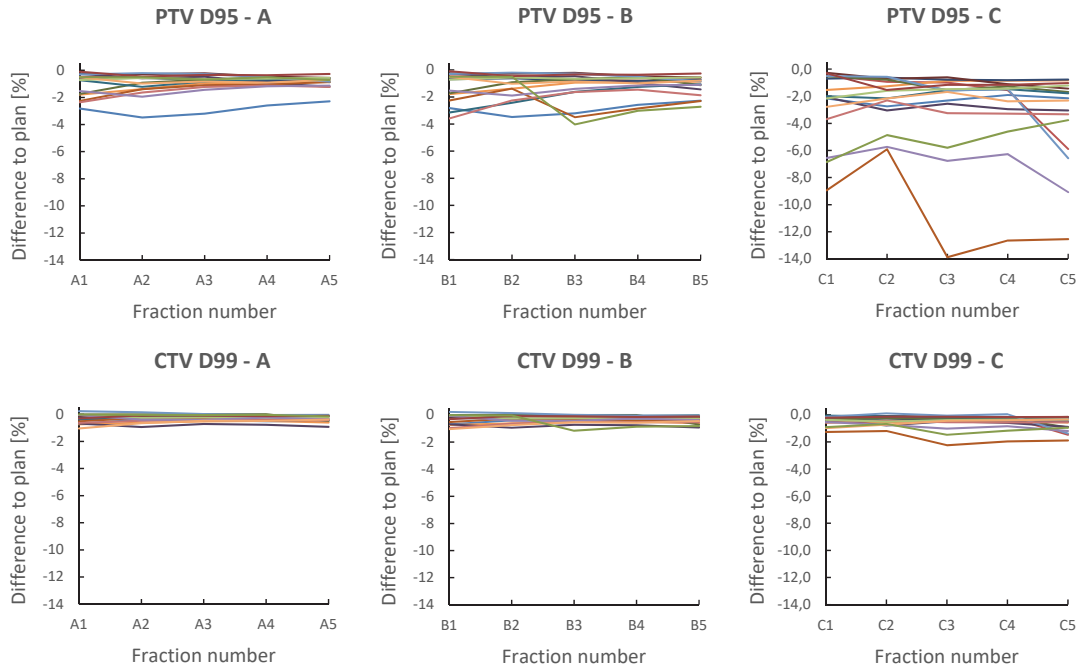

FIGURE 16 Cumulative difference in PTVD95% and CTVD99% as a function of treated fractions between motion-inclusive and planned values. A, B and C refer to motion correction strategies as explained in the text. Each curve corresponds to a patient. [III]

4.3.4 The effect of prostate motion on doses to risk organs

Mean, SD and maximum differences of the dose volume parameters between motion-inclusive and planned dose distributions for bladder and rectum in each motion correction strategy are presented in table 9. Box-plots for motion induced dose differences in rectum V96.2%, V65% and bladder V90% and V65% are

presented in figure 17. In general, motion of the prostate exposed larger volumes of the OARs to high doses, whereas lower dose volumes were less affected. Relative increase of the high dose volumes was substantial in both rectum and bladder due to small planned absolute volumes exposed to the high doses. However, absolute volumes corresponding to maximum percentual increase were small: for rectum V100%, V96.2% and V65% they were 0.6, 2.9 and 5.9 cm3 (strategy A), 1.3, 4.2 and 14.8 cm3 (strategy B) and 0.9, 7.5 and 15.3 cm3 (strategy C). For bladder V100%, V90% and V65% they were 0.9, 3.2 and 8.3 cm3 (strategy A), 0.9, 3.1 and 8.3 cm3 (strategy B) and 2.6, 7.5 and 14.5 cm3 (strategy C). Delivered maximum absolute volumes of rectum V100%, V96.2% and V65% were 2.9, 4.9 and 13.2 cm3 (strategy A), 2.9, 4.9 and 14.8 cm3 (strategy B) and 2.3, 7.5 and 15.3 cm3 (strategy C). Delivered maximum volumes of bladder V100%, V90% and V65% were 8.0, 17.5 and 31.3 cm3 (strategy A), 8.0, 17.3 and 31.1 cm3 (strategy B) and 13.1, 24.0 and 46.5 cm3 (strategy C). Mean ± SD absolute V100% values in strategies A, B and C were 0.6 ± 0.6, 0.6 ± 0.6 and 0.6 ± 0.5 cm3 for rectum and 1.9 ± 1.4, 1.8 ± 1.4 and 2.0 ± 1.6 cm3 for bladder, respectively. Mean ± SD absolute V96.2% for rectum were 1.6 ± 0.9, 1.6 ± 1.0 and 1.6 ± 1.1 cm3 in strategies A, B and C, respectively. Maximum point dose to the rectum in a single fraction was 7.6-7.7 Gy in each strategy, and maximum cumulative point dose to the rectum after five fractions was 37.4 Gy in each strategy.

TABLE 9 Mean, SD and maximum percentual differences in calculated OAR dose parameters between motion-inclusive and planned dose distributions over all patients and fractions. The table is modified from Study III.

	Strategy A			Strategy B			Strategy C		
	Mean	SD	Max	Mean	SD	Max	Mean	SD	Max
V100% bladder	9.5	63.9	325.4	6.6	62.6	323.0	44.5	170.6	1095.8
V90% bladder	-0.6	22.0	89.9	-1.8	23.6	88.1	8.6	59.9	347.4
V65% bladder	-0.2	13.7	43.6	-0.9	15.1	43.0	2.4	33.3	149.8
V100% rectum	55.1	159.4	913.0	81.3	265.9	2004.7	83.6	224.2	1347.9
V96.2% rectum	3.6	39.7	116.5	7.6	51.4	292.8	8.1	77.9	413.9
V65% rectum	2.2	25.5	65.5	4.6	31.7	174.5	2.5	51.3	269.3

4.3.5 Correlation between prostate motion and dosimetric effect

The dosimetric effect in parameters PTVD95%, PTVsubCTVD95% and PTV mean dose correlated strongly with mean of absolute AP, SI and 3D displacements of the prostate (r = 0.74 – -0.89). Strong correlations were found also for urethra D99% and mean absolute SI displacement (r = -0.81), bladder V100%, V90% and mean SI displacement (r = -0.71 and r = -0.84, respectively) and rectum V96.2%, V90% and mean AP displacements (r = 0.91 for both). Differences to planned value in rectum V96.2% and V90% against mean AP displacement are presented in figure 18. Differences between motion-inclusive and planned bladder V100% and V90% against mean SI displacement are presented in figure 19.

in figure 18. Differences between motion-inclusive and planned bladder V100% and V90% against mean SI displacement are presented in figure 19.

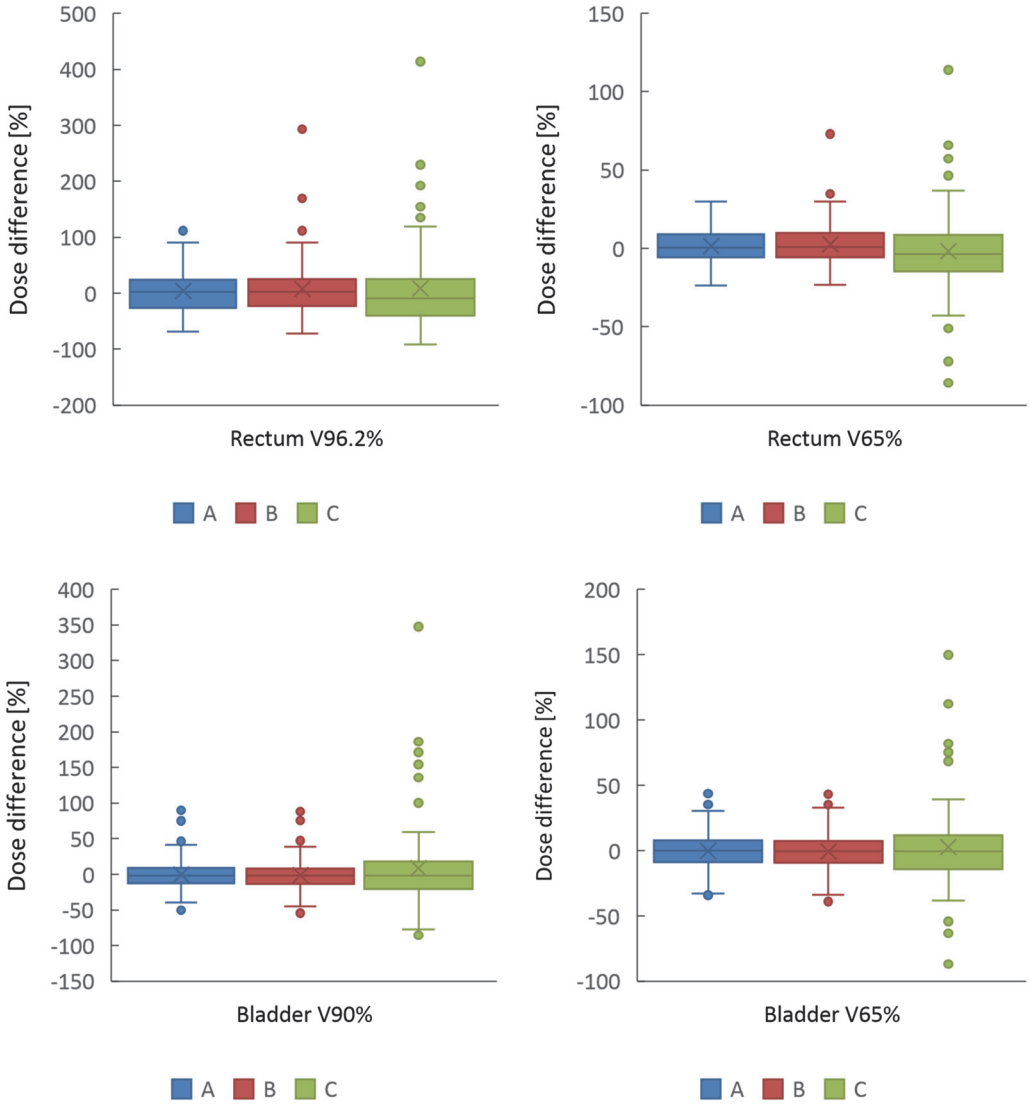

FIGURE 17 The distribution of dose differences between motion-inclusive and planned DVH parameters for rectum and bladder in motion correction strategies A, B and C. The box limits represent the median and 25th and 75th percentiles. The cross shows the mean value. The whiskers extend up to the largest values that are less than or equal to 1.5 times the interquartile range or down to the smallest values that are larger than 1.5 times the interquartile range. Dots outside the whiskers represent outliers.

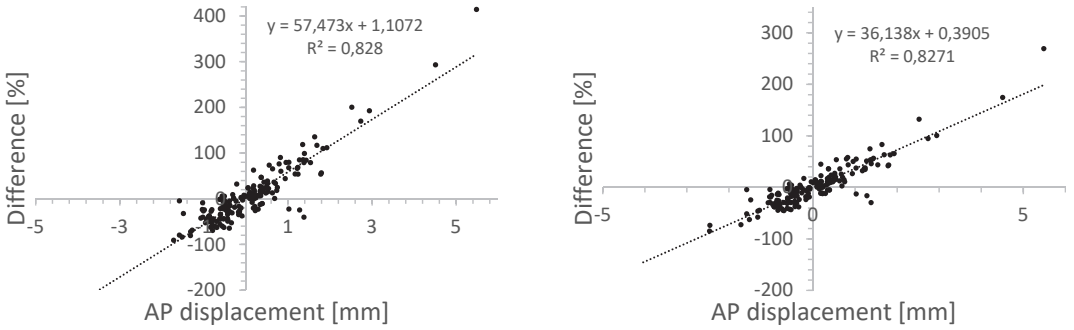

FIGURE 18 Differences to planned values in motion-inclusive rectum V96.2% (left) and V90% (right) as a function of mean AP displacement of the prostate. There was a linear dependency between rectum volumes getting high doses and mean AP displacement. Positive displacement corresponds anterior direction.

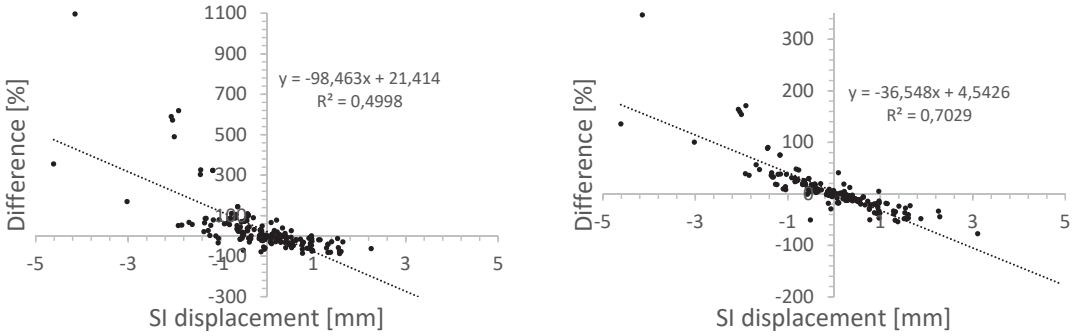

FIGURE 19 Differences to planned values in motion-inclusive bladder V100% (left) and V90% (right) as a function of mean SI displacement of the prostate. Linear dependency between bladder volumes getting high doses and mean SI displacement was not obvious at superior (negative) displacements > 1 mm, especially for bladder V100%.

5 DISCUSSION

5.1 Immobilizing effect of the RR

The comparison of the intrafraction motion patterns of the prostate between RR and non-RR fractions shows that the use of RR increased the prostate motion. The motion increased in every direction except anterior and the 3D motion patterns between RR and non-RR fractions were significantly different ($p < 0.03$). At individual level, the motion increase was significant for 13 patients out of 22 investigated and for only two patients the result was opposite. Largest increase in the motion was seen in inferior and posterior directions. The insertion of the RR is uncomfortable for the patient causing tension to muscles in the pelvis and the motion increase seen was most probably a consequence of a muscle relaxation after the placing of the RR. Muscle relaxation explains some of the inferior and posterior motion seen also after the normal treatment setup without the RR [31, 34] and with the RR this effect is supposedly emphasized. Additionally, applied retraction creates empty space posteriorly to the prostate, which decreases the support from the posterior tissues and potentially enables larger posterior prostate motion. Relaxation time was included in the motion data and analysis as the motion tracking was initiated immediately after the RR placement. It is probable, that after a certain amount of time during which the pelvic muscles relax, the position of the prostate with the RR in place would stabilize. A plateau seen in increase of the inferior displacements ≥ 1 mm for RR fractions (figure 9) may be an indication of prostate stabilization after about 6-8 min from the patient setup, though the small amount of data at 6-10 minute intervals decreases the reliability of the data. However, to implement a waiting time for muscle relaxation after the insertion of the RR would prolong the overall duration of the treatment session, which in turn would reduce the effective machine time available for treatments. Overall, the probability of the prostate displacement increased as a function of tracking time for both RR and non-RR fractions, indicating, that if no corrective actions are made, the treatment should be initialized as soon as possible after the

patient setup and using of treatment techniques with shorter treatment delivery time would be beneficial for the patient.

Results found in this thesis are in contrast to results of Legge et al [82] who found larger than 3 mm prostate displacements only 0.4% of the treatment time, when RR was used. However, they analyzed the motion only during the beam on time and not during the pre-treatment setup period, which was done in the present study. Thus, the data of Legge et al did not include the muscle relaxation time, which was the most probable reason for the increased motion with the RR in the present study, and therefore the results are not fully comparable. In addition, the motion data in the study of Legge et al comprised only of 19 fractions of 10 patients and they did not have comparative motion data without the RR in place [82]. Results of this thesis differ also from the results of de Leon et al [83], who found reduced prostate motion when the RR was used. They measured the prostate displacement in planning phase of the treatment, using cine MRI. MRI imaging typically comprises of initial localization imaging used for setting up the field-of-view (FOV) over which the actual MR images are acquired. Usually several different imaging sequences are acquired and all of them take variable amount of time in the range of few minutes. It is unclear how much time had passed between the insertion of the RR and the start of cine-MRI in the study of de Leon et al, but it is probable, that their data did not include the relaxation period thus making their results incomparable to the results of this thesis. In addition, to reproduce the bladder filling at imaging and treatment, De Leon et al used indwelling catheters which affect the orientation of the prostate and position of the urethra [84, 85]. It is reasonable to assume that the use of catheters may also affect the prostate intrafraction motion. Therefore, the applicability of their results is limited to similar setting with catheters.

Results of this thesis, revealing increased prostate motion with the RR in a clinical setting were opposite to what was expected. Increased prostate motion decreases the accuracy of the treatment delivery and therefore the use of RR would be inferior to a treatment setting without the RR. Additionally, it was seen that the RR creates separation between rectum and prostate mainly near the apex of the prostate thus limiting its potential on reducing the rectal doses. Due to the lack of the MRI image data of the prostate and rectum with the RR in place, rectum could not be contoured reliably and quantitative analysis of the effect of the RR on rectal doses were not performed in the present study. Findings of the dose sparing effect of the RR are contradictory in literature [86, 87]. The uncertainty of the dose sparing effect together with the findings of increased prostate motion with the RR led to a conclusion of not using it in further prostate RT treatments in Tampere University Hospital.

The use of the RayPilot had some technical issues that were related to the transmitter implantation and removal after the treatment course. With three patients the transmitter angle was out of operation limits and with another three, the transmitter stopped working prior to or during the treatment course. These patients were not included in the analysis. In two other cases, the transmitter cable snapped at the post-treatment removal of the transmitter and the

transmitter were stuck in the patient. It seems that some patients create fibrosis around the transmitter which obstructs the transmitter removal effectively and that transmitter cables are not designed strong enough for these cases. The patients with stuck transmitters are followed-up and the transmitters have not caused any special concerns. However, the transmitter cables were found unreliable and the use of the RayPilot system was discontinued.

5.2 Localization accuracy of the electromagnetic tracking devices and the relevance of the number and stability of the surrogate markers

The aim of the Study II was to compare the accuracy of the RayPilot and Calypso systems with orthogonal kV imaging using fiducial markers in detecting prostate translations in prostate RT.

Results of the study revealed that the localization accuracy of the Calypso system was comparable to kV imaging using FMs. Mean differences of the couch shifts/isocenter offsets between the methods were negligible and at least 98.6% of the differences in each direction were within 2 mm. The results are in agreement with findings in the literature, which show submillimeter to millimeter mean differences between Calypso and kV imaging/CBCT imaging [63, 88–90]. Mean 3D shift differences of 1.5 ± 0.9 mm and 1.9 ± 1.2 mm between Calypso and radiographic imaging, found by Willoughby et al [62] and Kupelian et al [33], respectively, were probably influenced by the prostate intrafraction motion, as the observations made with different methods were temporally separated by 3-5 minutes.

Mean differences in couch shifts between the RayPilot and kV imaging were less than 0.5 mm for AP and LR translations, but -2.2 ± 2.4 mm in SI direction, indicating that on average, the RayPilot located the prostate 2.2 mm inferior to its position assessed with kV imaging. The variance in the differences was also larger between RayPilot and kV imaging than between Calypso and kV imaging, which is seen in larger SD and LOA values. Apart from the LR direction, for which the differences were on the acceptable limit, the LOAs were considerable larger than the acceptable 2 mm and only 64.6% of the AP and 44.0% of the SI differences were within 2 mm. Other studies comparing the accuracy of RayPilot with kV imaging has not been made in similar clinical setting than in the present study. Kindblom et al [61] compared the positioning accuracy of the system with kV imaging in a setting where the transmitter was inserted into the prostatic urethra within a dilation catheter and found average (±SD) absolute and relative 3D difference of 2.7±1.2 and 1.7±1.0 mm, respectively. Biston et al [91] compared the observations of known translations and rotations in a phantom setup between RayPilot and transperineal US system and found absolute differences less than 0.5 mm. Rotations of the plastic sphere representing prostate resulted

in systematic shifts up to 4.4 mm in the measured translations and were a consequence of off-center setup of the transmitter [91].

In order to evaluate the factors affecting the accuracy of the different localization methods, the stability of the surrogate markers were investigated. Gold seed fiducial markers, as well as Calypso transponders showed excellent positional stability, with small variability in intermarker distances, similar for both methods and in agreement with the findings in literature [33, 92–96]. Larger marker migrations on the order of few millimeters were rare and seen only for a few patients. Differences in displacements observed between Calypso and kV imaging were small and detailed analysis of the effect of marker migration was not performed. However, change in the marker position, if remedial actions are not made, can affect the accuracy of the method, which was seen in the patient with 3.8 mm superior transponder migration. For this patient, the mean (±SD) difference in SI isocenter shifts between the Calypso and kV imaging was 1.2 ± 0.5 mm, while for any other patient the corresponding difference was less than 0.9 mm. The difference is explained by the inclusion of migrated transponder in the Calypso localization plan whereas the localization with kV imaging was performed matching only the two stable transponders. Interesting individual case was the voiding of one transponder due to transponder being implanted too near to the urethra. The phenomenon is rare, but similar incident has been reported in the literature [33, 95] and it emphasizes the importance of avoiding urethra region when implanting the transponders.

The stability of the RayPilot transmitters was measured relative to the geometric CP of the three gold FMs. Small migration or position change of a single marker has negligible effect on the geometric CP of the three markers [97] and thus the CP was deemed as an appropriate reference point for assessing the change in transmitter position. Results revealed considerable variation in the transmitter position along the treatment course, especially in AP and SI directions. In addition, averaged over all fractions, inferiorly directed mean (±SD) shift of 1.8 ± 2.0 mm in transmitter position was detected. Position instability of the transmitter has been observed also elsewhere [91, 98]. The effect of the positional instability of the transmitter on localization accuracy of the RayPilot system was investigated by correcting the RayPilot readings with the observed transmitter shifts and comparing the resulting values with observations made with kV imaging. The correction decreased the differences between the methods, but the differences were still clinically unacceptable, indicating that although the positional instability of the transmitter is likely the major error source deteriorating the localization accuracy of the RayPilot system, it does not explain solely the differences seen between the methods. The definition of the transmitter CP coordinates from the planning CT was found prone to positioning errors up to 2 mm, due to limited resolution of the CT image, even though slice thicknesses of 0.5-1 mm were used. Accurate localization of the transmitter CP in CT image requires image windowing and/or the use of image intensity profile tools and is prone to inter- and intra-observer errors. The CT data was carefully reviewed in retrospect and errors ≥ 0.5 mm in the CP coordinates were corrected prior to

analyzing the data. Time synchronization between the RayPilot and treatment system was not done for some of the fractions due to human error. For these fractions the synchronization was done retrospectively by matching the timing of treatment field start and end times between the systems. Method was not exact and residual error between the methods was approximately ± 15 s and ± 30 s at its worst. Intrafraction motion of the prostate was analyzed from the 3 min period around the imaging time points to evaluate whether the prostate motion could have affected the results. In 98.4% of the any 30 s time interval within the three minute periods the absolute shift of the prostate in any direction was less than 1 mm, which is also the resolution of the RayPilot suggested couch shifts, indicating that the possible effect of the intrafraction motion on the RayPilot observations was insignificant.

Main limitation of the RayPilot is that it is based on the use of a single transmitter acting as a surrogate for prostate position. Thus, due to the off-center implantation of the transmitter, the translations observed by the RayPilot may not correspond accurately the translations of the isocenter, or the prostate, when the prostate is rotated. Biston et al [91] showed that 15° pitch and yaw rotations of the transmitter may cause systematic shifts up to 2.3, 3.8 and 4.4 mm to the monitoring results in AP, SI and LR directions, respectively. The magnitude and direction of the shifts depend on the position of the transmitter relative to the isocenter and phantom tests with centered transmitter showed less than 2 mm shifts for rotations > 15° [91]. In practice, the urethra region restricts implanting the transmitter within the center of the prostate. The position of the transmitter relative to the isocenter may also change if the prostate is deformed. Variations in rectum filling may cause significant prostate deformations, which can affect more to the posterior than anterior periphery of the prostate [30]. Thus, depending on the placing of the transmitter in the prostate, prostate deformations may change the position of the transmitter relative to the isocenter, or prostate center of the gravity, in an unpredictable way. Prostate deformations and rotations affect also the positions of gold seed markers or Calypso transponders, but the effect of marker displacements on the geometric CP of the three markers is small as shown by Pouliot et al [97]. The use of at least two, but preferably three, markers in daily prostate target alignment is also supported by the study of Kudchadker et al [99].

Rotations of the prostate may have affected also the RayPilot tracking results of the Study I but as the prostate motion was assessed relative to the initial position of the transmitter/prostate at the start of the tracking, the effects of interfraction rotations were cancelled out. Thus, the possible effects would have had to be due to intrafraction prostate rotations. The intrafraction rotations could not be analyzed without imaging data throughout the fraction. However, as the transmitter position varied among the patients, it is probable that the effect of the possible rotations partially averaged out and affected only minimally the differences seen in motion patterns between RR and non-RR fractions over the whole patient population.

In conclusion, due to the positional instability of the transmitters and the limitations of the single point tracking method, the absolute localization accuracy of the RayPilot is not good enough for localization of treatments with high precision requirements, such as prostate SBRT, and the use of RayPilot for intrafraction motion monitoring should be combined with independent localization methods, like kV imaging using FMs. The localization accuracy of the Calypso was found comparable to kV imaging using FMs and could thus be used as stand-alone system for treatment localization and intrafraction position correction in prostate RT, including SBRT.

5.3 Dosimetric benefit of continuous motion monitoring based motion correction and threshold based beam gating

The aim of the Study III was to evaluate the dosimetric benefit of continuous motion monitoring based treatment localization and intrafraction motion correction strategy in contrast to conventional imaging based localization methods that are applied prior to treatment delivery.

5.3.1 Prostate motion during the beam delivery

During the treatment, prostate was displaced most in strategy C and least in strategy A. The average displacement in strategy B was only little larger than in strategy A. The difference between strategy C and strategies A and B is explained by the prostate motion occurring during the CBCT acquisition, image matching and interpretation which may take on the order of 5 min. During the delay, the prostate may be displaced and its position in the CBCT does not perfectly represent the prostate position at the treatment. Additional motion correction prior to treatment corrects the CBCT residual error induced by the motion and explains smaller displacement in strategy B. The beam gating in strategy A reduced the motion even further but the difference to strategy B was small. In general, the motion was small in each motion correction strategy: the intrafraction motion in any direction was within 3 mm for more than 95% of the beam delivery time in strategy C and more than 98% in strategy B. In strategy A, the beam gating kept the prostate within motion tolerances and the prostate motion were within 2 mm in any direction for more than 98% of the beam delivery time. Likelihood of the prostate motion increases with time after initial alignment but the increase occurs slowly: the observed percentage of time for at least 3 mm prostate displacement by the fifth minute of the tracking time is around 10% and by the tenth minute around 20% [31, 34]. As the setup period might take longer than the actual beam delivery with modern VMAT-FFF techniques, the prostate motion and motion correction during the setup may be of more importance than the motion during the beam delivery. This is backed up by the observed small difference in average prostate displacement between strategies A and B.

Observed motion in all strategies was smaller than what has been reported in literature: Langen et al [34] observed prostate being displaced > 3 mm for 13.6% of the tracking time, while Tong et al [31] found at least 3 mm prostate shifts for 10.7% of the tracking time. However, the tracking times were much longer in these studies, as the tracking time included also the setup time, whereas in the present study, the motion was analyzed only from the beam delivery time excluding beam pauses. In addition, the use of VMAT with high dose rate FFF beams in this study ensured extremely fast treatment delivery, when compared to IMRT techniques used in the previous studies [31, 34]. This reduced the occurrence of large displacements, which is in accordance with the findings of Li et al [100]. Motion was largest in AP and SI directions and smallest in LR direction, which is consistent with literature [31, 33–35].

5.3.2 Dosimetric effect of the intrafraction motion

Motion induced dose effects increased with motion and were smallest in motion correction strategy A and largest in strategy C. Target dose deficits were mostly limited to PTV periphery and CTV was affected only little, indicating that the applied CTV-to-PTV margins covered most of the motion effects, even in strategy C. However, larger motion induced dose deviations affecting also the CTV dose coverage were observed for individual fractions, which is seen in the box-plot outliers in figure 14. Largest dose reductions in CTV mean dose and CTVD99% were -2.2% and -7.1% in strategy C, while they were -0.5% and -2.5% in strategy A and -0.5% and -3.5% in strategy B, respectively (table 7). According to the dose-response of prostate cancer in conventionally fractionated or moderately hypofractionated RT without hormonal therapy, 2-7% CTV dose reductions of the whole treatment, could lead up to 5-16% decrease in tumor control probability (TCP) [101, 102]. However, the effect is dependent on the risk class [101–103], and on the other hand, not evaluated for extremely hypofractionated treatments. It can be argued, that the motion induced dose deficits in SBRT would have larger impact on cancer control than conventionally fractionated or moderately hypofractionated treatments due to limited number of fractions and high fraction doses of SBRT, which would support the use of continuous motion monitoring based treatment localization and threshold based beam gating to ensure the correct target dose coverage.

Prostate motion has also an effect on the doses received by the nearby organs at risk. Due to steep dose gradients even small error in target alignment may expose larger volumes of bladder and rectum to high doses. This was seen in higher relative increase of rectum and bladder high dose volumes, while the lower dose volumes were less affected. Increase was largest in strategy C and smallest in strategy A, and the change in volumes getting high doses was linear with mean AP displacement (rectum) (figure 18) and mean SI displacement (bladder), although the linearity was not obvious for bladder at superior displacements larger than 1 mm (figure 19). However, maximum absolute volumes exposed to high doses were small in each strategy. Rectum maximum doses larger than 37.4 Gy and rectum D1cm3 > 35 Gy in prostate SBRT have been

associated with elevated bowel problems affecting long-term quality of life (QOL) [23, 24]. Grade 2 or higher rectal bleeding has been associated with rectal V38Gy ≥ 2 cm3, use of anticoagulants and the presence of hemorrhoids [22]. Severe, grade 3+ delayed rectal toxicity has been associated with the rectal wall V50Gy > 3 cm3 and treatment of > 35% circumference of rectal wall to 39 Gy [19]. On the grounds of the clinical evidence, severe rectal toxicity can be expected to be rare for patients receiving 35-36.25 Gy in five fractions but the treatment may have effect on QOL and for that reason rectum doses should be kept as low as possible. In this regard, it is reasonable to use reduced posterior PTV margins and continuous motion tracking with threshold based gating to ensure the most accurate treatment delivery. Further dose-escalation would possibly benefit from additional use of spacer hydrogels to increase the prostate-rectum separation. Accurate treatment delivery would also minimize the high doses to bladder, which have been associated with urinary symptoms following SBRT of the prostate [25, 26].

Motion induced target dose deficits observed in the current study are similar to a findings in literature: Colvill et al [104] observed maximum dose decrease of -19.2% and -34.2% in CTVD99% and PTVD95%, respectively, in a single fraction of conventionally fractionated VMAT. If gating would have been used, these figures would have reduced to -0.7% and -2.7%, respectively [104]. Langen et al [41] evaluated the dosimetric effect of intrafraction motion in conventionally fractionated step-and-shoot IMRT and found mean (±1 SD) change of -0.2 ± 0.5% in CTVD95% and -0.5 ± 1.1% in PTVD95%. Largest reductions in CTV and PTV were -6.4% and -12.7%, respectively [41]. In VMAT treatments comprising of conventionally fractionated and extremely hypofractionated patients, an average drop of -6.2% in PTVD95% was found, when the mean of the highest 50% of the motion was > 3mm [105]. Although the dose deficits in individual fractions may be substantial, the cumulative dosimetric effect is reduced in a long treatment course due to averaging of localization errors [40–42]. However, in an extremely hypofractionated setting the averaging of errors may not be evident, as shown in this thesis. In strategy C, the cumulative effect even increased for some patients (figure16). These patients exhibited large prostate motion and benefitted from more accurate treatment localization that was applied in actually delivered treatments (strategy A). The use of gating improved the rectal and bladder dosimetry when compared to non-gated motion correction strategies, which is consistent with literature [104].

The previous studies that investigated the dosimetric effect of intrafraction prostate motion have either assumed ideal setup, or included the residual setup error in the analysis and have not specifically addressed the dosimetric effect of the motion during the setup period [40, 41, 104–106]. In the current study, the relevance of the prostate motion during the setup could be evaluated by comparing the dosimetric differences between strategies B and C, whereas comparison between strategies A and B reveals the benefit of beam gating and continuous motion monitoring based motion correction. Small differences between strategies A and B indicate that the benefit of the gating was small, when

the residual setup error after the initial alignment was corrected immediately prior to irradiation. Larger dosimetric differences between strategies B and C indicate, that this additional pre-treatment motion correction had more impact than beam gating and continuous monitoring based motion correction. This is explained by the setup period taking longer time than the actual treatment, which increases the relevance of prostate motion during the setup period. It is noteworthy, that the results apply to VMAT treatments utilizing high dose rate FFF beams, which minimizes the beam delivery time, and to the CTV-to-PTV margins used in this study. While the benefit of gating and motion corrections during the treatment might be of less importance with this technique, they might be necessary in treatments having longer beam delivery time. Beam delivery time of a prostate SBRT treatment with CyberKnife is significantly higher than with VMAT [107, 108], which increases the probability of intrafraction prostate motion and necessitates the motion correction in CyberKnife treatments. Van de Water et al [109] found, that optimal target coverage for CyberKnife treatments with 3 mm PTV margin would require translational and rotational motion corrections up to 5° between 60 and 180 seconds [109]. Larger extent rotational corrections were required for 0 mm margin plans [109]. The threshold based beam gating and repositioning of the patient are also required with other treatment techniques, if the PTV margins were to be reduced further [40, 44, 110]. This is backed up also by the results of this study, as the dose coverage of the PTV, which can be considered as the CTV with zero margins, was maintained best in strategy A.

The results of this study suggest, that additional motion correction immediately prior to treatment delivery without beam gating would be adequate for most of the patients and fractions treated with VMAT-FFF and 3-5 mm CTV-to-PTV margins, whereas the single CBCT-guided localization might compromise the target coverage for patients exhibiting large prostate motion. However, continuous motion monitoring based motion correction strategy with threshold based beam gating is needed to ensure the best CTV dose coverage and minimized OAR doses for all fractions and all patients.

5.3.3 Benefits and tradeoffs of real-time motion management

Main advantage of the real-time prostate motion tracking with Calypso system is that it enables the detection of sudden shifts in prostate position which may remain unnoticed with only pre-treatment imaging based localization, or with methods using sparse imaging during the treatment. It also enables immediate beam interruption and quick re-positioning of the patient if the motion tolerances are exceeded thus enabling accurate treatment delivery and the possibility to reduce the PTV-to-CTV margins. However, the ferromagnetic core of the Calypso transponders produce large artefacts in MRI images [64], which reduces the utilization of the MRI in treatment planning and negates the post-treatment follow-up with the MRI. Alternative for Calypso in the future could be the KIM method, which utilizes continuous kV imaging of the gold markers during the treatment and probability density function for the prostate position, acquired before the treatment, to provide real-time 3D position of the prostate [49–55]. This method

is not yet commercially available but it has already been tested and used clinically for motion monitoring [52] and also for beam gating [53] in prostate radiotherapy. KIM has also been used in prostate RT utilizing MLC tracking, where the MLC aperture is adjusted during the treatment to follow the tumor motion [111]. The advantages of the KIM are that it does not require additional equipment, it does not prevent MRI imaging and besides of the translations it can track also the target rotations [54, 112, 113]. Dynamic prostate rotations during the treatment may cause substantial CTV dose deficits due to interplay effect between prostate rotations and MLC motion in VMAT treatments [114], and could be of interest to be accounted for in the treatment by beam gating, for instance. It is noteworthy, that the motion tracking methods that are based on the tracking of implanted markers cannot account for seminal vesicles, which can experience significantly larger motion than the prostate and may not move in unison with the prostate in real-time [115]. Thus, if seminal vesicles are included in the treatment that is localized using the intraprostatic markers, an additional margin is required for seminal vesicle motion [115].

5.3.4 Motion-including dose reconstruction and adaptive radiotherapy

The used dose reconstruction method is based on shifting of the sub-beam isocenters according to the observed prostate motion which allows the use of single planning CT to reconstruct the dose. Disadvantage of the used method is that it does not take into account target or OAR deformation and assumes that the OARs move along with the target, which reduces the accuracy of the reconstructed doses. In addition, the method cannot account for target rotations. However, the role of motion-inclusive dose reconstruction will increase along the ongoing development of treatment techniques and equipment, which is leading towards adaptive radiotherapy, where the treatment plan is adapted according to the daily changes in patient anatomy or intrafraction target motion [116–122]. In this regard, motion-including dose reconstruction should consider also the dynamic changes in patient anatomy, which could be a basis for future investigations and development of the dose modelling methods. In prostate RT, reconstructed dose parameters of the actually delivered dose have also been shown to correlate more strongly with observed toxicity than the planned dose parameters and thus the reconstructed dose could potentially be used to predict the treatment toxicity [123].

6 CONCLUSIONS

In the present thesis, methods to increase the accuracy of treatment delivery and decrease the rectum dose in radiotherapy for prostate cancer were investigated. Specifically, the effect of rectal dose sparing device on intrafraction motion of the prostate was investigated by utilizing electromagnetic real-time motion tracking of the prostate. The localization accuracy of two modern electromagnetic tracking devices in prostate cancer radiotherapy was assessed in comparison with fiducial marker based kV imaging. Finally, the dosimetric benefit of continuous motion monitoring based motion correction and beam gating in prostate SBRT was evaluated and compared with pre-treatment imaging based localization methods. The findings of the thesis formed the grounds for the current implementation of prostate SBRT in Tampere University Hospital, in which regard the thesis reached its aims. The main conclusions of the thesis were:

1) The use of the RR was found to increase the intrafraction prostate motion in a standard clinical setting of prostate cancer radiotherapy, without additional waiting time for muscle relaxation. Increased motion reduces the accuracy of the treatment delivery and the use of the RR was discontinued.

2) The localization accuracy of the RayPilot system was affected by the positional instability of the transmitters and the observed accuracy of the system did not meet the requirements for the treatment localization in prostate cancer radiotherapy. The system could be used for real-time motion tracking but the treatment localization should be verified by other setup techniques. The localization accuracy of the Calypso system was found to be comparable to orthogonal kV imaging of fiducial markers and the system could be used in treatment localization in place of kV imaging.

3) Single pre-treatment CBCT-guided treatment localization was susceptible to intrafraction prostate motion and could result in clinically relevant CTV dose deficits in prostate SBRT for patients exhibiting large prostate motions. Additional pre-treatment motion correction increased the accuracy and was adequate for most of the fractions and patients. Continuous motion monitoring based motion correction and beam gating ensured high CTV dose coverage and minimized OAR doses for all fractions.

Future development of prostate SBRT includes further dose escalation both to the whole prostate gland, even in a single-fraction [124], and in the context of simultaneous boosting of dominant intraprostatic tumor lesions, for which several trials are under way [8, 125]. These treatment schemes require highly accurate treatment delivery accounting for intrafraction prostate displacements to preserve the urethra and OAR doses at acceptable level and to ensure the accurate localization of focal boosting. However, the detection and delineation of the dominant tumor lesions are based on MRI, which restricts the use of EM localization methods in focal boosting. Additionally, the use of the MRI in treatment follow-up and diagnosing of recurrent disease is increasing, which creates the need for the development of MRI-compatible motion tracking methods, and predicts that the prostate motion tracking with imaging-based methods will become more common.

REFERENCES

[1] Ferlay J, Colombet M, Soerjomataram I, Dyba T, Randi G, Bettio M, et al. Cancer incidence and mortality patterns in Eurepe: estimates for 40 countries and 25 major cancers in 2018. Eur J Cancer 2018;103:356–87.

[2] Barnett GC, West CML, Dunning AM, Elliott RM, Coles CE, Pharoah PDP, et al. Normal tissue reactions to radiotherapy: towards tailoring treatment dose by genotype. Nat Rev Cancer 2009;9:134–42.

[3] Brenner DJ, Hall EJ. Fractionation and protraction for radiotherapy of prostate carcinoma. Int J Radiat Oncol Biol Phys 1999;43:1095–1101.

[4] Dasu A, Toma-Dasu I. Prostate alpha/beta revisited - an analysis of clinical results from 14 168 patients. Acta Oncol 2012;51:963–74.

[5] Miralbell R, Roberts SA, Zubizarreta E, Hendry HH. Dose-fractionation sensitivity of prostate cancer deduced from radiotherapy outcomes of 5,969 patients in seven international institutional datasets: α/β = 1.4 (0.9-2.2) Gy. Int J Radiat Oncol Biol Phys 2012;82:e17–e24.

[6] Vogelius IR, Bentzen SM. Dose response and fractionation sensitivity of prostate cancer after external beam radiation therapy: a meta-analysis of randomized trials. Int J Radiat Oncol Biol Phys 2018;100:858–65.

[7] Brenner DJ. Fractionation and late rectal toxicity. Int J Radiat Oncol Biol Phys 2004;60:1013–15.

[8] Draulans C, De Roover R, van der Heide UA, Haustermans K, Pos F, Smeenk RJ, et al. Stereotactic body radiotherapy with optional focal lesion ablative microboost in prostate cancer: topical review and multicenter consensus. Radiother Oncol 2019;140:131–42.

[9] Pan HY, Jiang J, Hoffman KE, Tang C, Choi SL, Nguyen Q, et al. Comparative toxicities and cost of intensity-modulated radiotherapy, proton radiation, and stereotactic body radiotherapy among younger men with prostate cancer. J Clin Oncol 2018;36:1823–30.

[10] Sher DJ, Parikh RB, Mays-Jackson S, Punglia RS. Cost-effectiveness analysis of SBRT versus IMRT for low-risk prostate cancer. Am J Clin Oncol 2014:37;215–21.

[11] Parthan A, Pruttivarasin N, Davies D, Taylor DCA, Pawar V, Biljani A, et al. Comparative cost-effectiveness of stereotactic body radiation therapy versus intensity-modulated and proton radiation therapy for localized prostate cancer. Front Oncol 2012;2:81.

[12] Dearnaley D, Syndikus I, Mossop H, Khoo V, Birtle A, Bloomfield D, et al. Conventional versus hypofractionated high-dose intensity-modulated radiotherapy for prostate cancer: 5-year outcomes of the randomised, non-inferiority, phase 3 CHHiP trial. Lancet Oncol 2016;17:1047–60.

[13] Lee WR, Dignam JJ, Amin MB, Bruner DW, Low D, Swanson GP, et al. Randomized phase III noninferiority study comparing two radiotherapy fractionation schedules in patients with low-risk prostate cancer. J Clin Oncol 2016;34:2325–32.

[14] Catton CN, Lukka H, Gu C, Martin JM, Supiot S, Chung PWM, et al. Randomized trial of a hypofractionated radiation regimen for the treatment of localized prostate cancer. J Clin Oncol 2017; 35:1884–1890.

[15] Widmark A, Gunnlaugsson A, Beckman K, Thellenberg-Karlsson, C, Hoyer M, Lagerlund M, et al. Ultra-hypofractionated versus conventionally fractionated radiotherapy for prostate cancer: 5-year outcomes of the HYPO-RT-PC randomized, non-inferiority, phase 3 trial. Lancet 2019;394:385–95.

[16] Brand DH, Tree AC, Ostler P, van der Voet H, Loblaw A, Chu W, et al. Intensity-modulated fractionated radiotherapy versus stereotactic body radiotherapy for prostate cancer (PACE-B): acute toxicity findings from an international, randomised, open-label, phase 3, non-inferiority trial. Lancet Oncol 2019;20:1531–43.

[17] Kishan AU, Dang A, Katz AJ, Mantz CA, Collins SP, Aghdam N, et al. Long-term outcomes of stereotactic body radiotherapy for low-risk and intermediate-risk prostate cancer. JAMA Netw Open 2019;2(2):e188006.

[18] Jackson WC, Silva J, Hartman HE, Dess RT, Kishan AU, Beeler WH, et al. Stereotactic body radiation therapy for localized prostate cancer: a systematic review and meta-analysis of over 6,000 patients treated on prospective studies. Int J Radiat Oncol Biol Phys 2019;104:778–89.

[19] Kim DWN, Cho LC, Straka C, Christie A, Lotan Y, Pistenmaa D, et al. Predictors of rectal tolerance observed in a dose-escalated phase 1-2 trial of stereotactic body radiation therapy for prostate cancer. Int J Radiat Oncol Biol Phys 2014;89:509–17.

[20] Kim DWN, Straka C, Cho LC, Timmerman R. Stereotactic body radiation therapy for prostate cancer: review of experience of a multicenter phase I/II dose-escalation study. Front Oncol 2014;4:319.

[21] Bauman G, Ferguson M, Lock M, Chen J, Ahmad B, Venkatesan VM, et al. A phase 1/2 trial of brief androgen suppression and stereotactic radiation therapy (FASTR) for high-risk prostate cancer. Int J Radiat Oncol Biol Phys 2015;92:856–62.

[22] Musunuru HB, Davidson M, Cheung P, Vesprini D, Liu S, Chung H, et al. Predictive parameters of symptomatic hematochezia following 5-fraction gantry-based SABR in prostate cancer. Int J Radiat Oncol Biol Phys 2016;94:1043–51.

[23] Elias E, Helou J, Zhang L, Cheung P, Deabreu A, D'Alimonte L, et al. Dosimetric and patient correlates of quality of life after prostate stereotactic ablative radiotherapy. Radiother Oncol 2014;112:83–8.

[24] Wang K, Chen RC, Kane BL, Medbery CA, Underhill KJ, Gray JR, et al. Patient and dosimetric predictors of genitourinary and bowel quality of life after prostate SBRT: secondary analysis of a multi-institutional trial. Int J Radiat Oncol Biol Phys 2018;102:1430–7.

[25] Kole TP, Tong M, Wu B, Lei S, Obayomi-Davies O, Chen LN, et al. Late urinary toxicity modeling after stereotactic body radiotherapy (SBRT) in the definitive treatment of localized prostate cancer. Acta Oncol 2016;55:52–8.

[26] Repka MC, Kole TP, Lee J, Wu B, Lei S, Yung T, Collins BT, Suy S, Dritschilo A, Lynch JH, Collins SP. Predictors of acute urinary symptom flare following stereotactic body radiation therapy (SBRT) in the definitive treatment of localized prostate cancer. Acta Oncol 2017;56:1136–8.

[27] Langen K M, Jones DT. Organ motion and its management. Int J Radiat Oncol Biol Phys 2001;50:265–78.

[28] van Herk M. Errors and margins in radiotherapy. Semin Radiat Oncol 2004;14:52–64.

[29] Padhani AR, Khoo VS, Suckling J, Husband JE, Leach MO, Dearnaley DP. Evaluating the effect of rectal distension and rectal movement on prostate gland position using cine MRI. Int J Radiat Oncol Biol Phys 1999;44:525–33.

[30] Ghilezan MJ, Jaffray DA, Siewerdsen JH, van Herk M, Shetty A, Sharpe MB, et al. Prostate gland motion assessed with cine-magnetic resonance imaging (cine-MRI). Int J Radiat Oncol Biol Phys 2005;62:406–17.

[31] Tong X, Chen X, Li J, Xu Q, Lin M, Chen L, et al. Intrafractional prostate motion during external beam radiotherapy monitored by a real-time target localization system. J Appl Clin Med Phys 2015;16(2):51–61.

[32] Ballhausen H, Li M, Hegemann N-S, Ganswindt U, Belka C. Intra-fraction motion of the prostate is a random walk. Phys Med Biol 2015;60:549–63.

[33] Kupelian P, Willoughby T, Mahadevan A, Djemil T, Weinstein G, Jani S, et al. Multi-institutional clinical experience with the Calypso system in localization and continuous, real-time monitoring of the prostate gland during external radiotherapy. Int J Radiat Oncol Biol Phys 2007;67:1088–98.

[34] Langen KM, Willoughby TR, Meeks SL, Santhanam A, Cunningham A, Levine L, et al. Observations on real-time prostate gland motion using electromagnetic tracking. Int J Radiat Oncol Biol Phys 2008;71:1084–90.

[35] Lin Y, Liu T, Yang W, Yang X, Khan MK. The non-Gaussian nature of prostate motion based on real-time intrafraction tracking. Int J Radiat Oncol Biol Phys 2013;87:363–9.

[36] Moseley DJ, White EA, Wiltshire KL, Rosewall T, Sharpe MB, Siewerdsen JH, et al. Comparison of localization performance with implanted fiducial markers and cone-beam computed tomography for on-line image-guided radiotherapy of the prostate. Int J Radiat Oncol Biol Phys 2007;67:942–53.

[37] Barney BM, Lee J, Handrahan D, Welsh KT, Cook JT, Sause WT. Image-guided radiotherapy (IGRT) for prostate cancer comparing kV imaging of fiducial markers with cone beam computed tomography (CBCT). Int J Radiat Oncol Biol Phys 2011;80:301–5.

[38] O'Neill AG, Jain S, Hounsell AR, O'Sullivan JM. Fiducial marker guided prostate radiotherapy: a review. Br J Radiol 2016;89(1068):20160296.

[39] Goff PH, Harrison LB, Furhang E, Ng E, Bhatia S, Trichter F, et al. 2D kV orthogonal imaging with fiducial markers is more precise for daily image guided alignments than soft-tissue cone beam computed tomography for prostate radiation therapy. Adv Radiat Oncol 2017;2:420–8.

[40] Li HS, Chetty IJ, Enke CA, Foster RD, Willoughby TR, Kupelian PA, et al. Dosimetric consequences of intrafraction prostate motion. Int J Radiat Oncol Biol Phys 2008;71:801–12.

[41] Langen KM, Chauhan B, Siebers JV, Moore J, Kupelian PA. The dosimetric effect of intrafraction prostate motion on step-and-shoot intensity-modulated radiation therapy plans: magnitude, correlation with motion parameters, and comparison with helical tomotherapy plans. Int J Radiat Oncol Biol Phys 2011;84:1220–5.

[42] Adamson J, Wu Q, Yan D. Dosimetric effect of intrafraction motion and residual setup error for hypofractionated prostate intensity-modulated radiotherapy with online cone beam computed tomography image guidance. Int J Radiat Oncol Biol Phys 2011;80:453–61.

[43] Choi HS, Kang KM, Jeong BK, Song JH, Lee Y H, Ha IB, et al. Analysis of motion-dependent clinical outcome of tumor tracking stereotactic body radiotherapy for prostate cancer. J Korean Med Sci 2018;33:e107.

[44] Litzenberg DW, Balter JM, Hadley SW, Sandler HM, Willoughby TR, Kupelian PA, Levine L. Influence of intrafraction motion on margins for prostate radiotherapy. Int J Radiat Oncol Biol Phys 2006;65:548–53.

[45] Li JS, Jin L, Pollack A, Horwitz EM, Buyyounouski MK, Price RA, et al. Gains from real-time tracking of prostate motion during external beam radiation therapy. Int J Radiat Oncol Biol Phys 2009;75:1613–20.

[46] Jin J, Yin F, Tenn SE, Medin PM, Solberg TD. Use of the Brainlab Exactrac x-ray 6D system in image-guided radiotherapy. Med Dosim 2008;33:124–34.

[47] Xie Y, Djajaputra D, King CR, Hossain S, Ma L, Xing L. Intrafractional motion of the prostate during hypofractionated radiotherapy. Int J Radiat Oncol Biol Phys 2009;72:236–46.

[48] Kaur G, Lehmann J, Greer P, Simpson J. Assessment of the accuracy of truebeam intrafraction motion review (IMR) system for prostate treatment guidance. Australas Phys Eng Sci Med 2019;42:585–598.

[49] Poulsen PR, Cho B, Langen K, Kupelian P, Keall PJ. Three-dimensional prostate position estimation with a single x-ray imager utilizing the spatial probability density. Phys Med Biol 2008;53:4331–4353.

[50] Poulsen PR, Cho B, Keall PJ. Real-time prostate trajectory estimation with a single imager in arc radiotherapy: a simulation study. Phys Med Biol 2009;54:4019–4035.

[51] Ng JA, Booth JT, Poulsen PR, Fledelius W, Worm ES, Eade T, et al. Kilovoltage intrafraction monitoring for prostate intensity modulated arc therapy: first clinical results. Int J Radiat Oncol Biol Phys 2012;84:e655–e661.

[52] Keall PJ, Ng JA, O'Brien R, Colvill E, Huang C, Poulsen PR, et al. The first clinical treatment with Kilovoltage Intrafraction Monitoring (KIM): a real-time image guidance method. Med Phys 2015;42:354–8.

[53] Keall PJ, Ng JA, Juneja P, O'Brien R, Huang C, Colvill E, et al. Real-time 3D image guidance using a standard LINAC: measured motion, accuracy, and precision of the first prospective clinical trial of Kilovoltage Intrafraction Monitoring–guided gating for prostate cancer radiation therapy. Int J Radiat Oncol Biol Phys 2016;94:1015–1021.

[54] Nguyen DT, O'Brien R, Kim J, Huang C, Wilton L, Greer P, et al. The first clinical implementation of a real-time six degree of freedom target tracking system during radiation therapy based on Kilovoltage Intrafraction Monitoring (KIM). Radiother Oncol 2017;123:37–42.

[55] Hewson EA, Nguyen DT, O'Brien R, Kim J, Montanaro T, Moodie T, et al. The accuracy and precision of the KIM motion monitoring system used in the multi-institutional TROG 15.01 Stereotactic Prostate Ablative Radiotherapy with KIM (SPARK) trial. Med Phys 2019;46:4725–37.

[56] Noel C, Parikh PJ, Roy M, Kupelian P, Mahadevan A, Weinstein G, et al. Prediction of intrafraction prostate motion: accuracy of pre- and post-treatment imaging and intermittent imaging. Int J Radiat Oncol Biol Phys 2009;73:692–8.

[57] Dobler B, Mai S, Ross C, Wolff D, Wertz H, Lohr F, et al. Evaluation of possible prostate displacement induced by pressure applied during transabdominal ultrasound image acquisition. Strahlenther Oncol 2006;182:240–6.

[58] Li M, Hegemann N, Manapov F, Kolberg A, Thum PD, Ganswindt U, et al. Prefraction displacement and intrafraction drift of the prostate due to perineal ultrasound probe pressure. Strahlenther Oncol 2017;193:459–65.

[59] Mate TP, Krag D, Wright JN, Dimmer S. A new system to perform continuous target tracking for radiation and surgery using non-ionizing alternating current electromagnetics. Int J Comput Assisted Radiol Surg 2004;1268:425–30. (CARS 2004—Proc. of the 18th Int. Congress and Exhibition (Chicago, USA, 23–26 June 2004)).

[60] Balter JM, Wright JN, Newell LJ, Friemel B, Dimmer S, Cheng Y, et al. Accuracy of a wireless localization system for radiotherapy. Int J Radiat Oncol Biol Phys 2005;61:933–7.

[61] Kindblom J, Ekelund-Olvenmark A, Syren H, Iustin R, Braide K, Frank-Lissbrant I, et al. High precision transponder localization using a novel electromagnetic positioning system in patients with localized prostate cancer. Radiother Oncol 2009;90:307–11.

[62] Willoughby TR, Kupelian PA, Pouliot J, Shinohara K, Aubin M, Roach M, et al. Target localization and real-time tracking using the Calypso 4D localization system in patients with localized prostate cancer. Int J Radiat Oncol Biol Phys 2006;65:528–34.

[63] Bell LJ, Eade T, Kneebone A, Hruby G, Alfieri F, Bromley R, et al. Initial experience with intra-fraction motion monitoring using Calypso guided volumetric modulated arc therapy for definitive prostate cancer treatment. J Med Radiat Sci 2017;64(1):25–34.

[64] Zhu X, Bourland JD, Yuan Y, Zhuang T, O'Daniel J, Thongphiew D, et al. Tradeoffs of integrating real-time tracking into IGRT for prostate cancer treatment. Phys Med Biol 2009;54:N393–N401.

[65] Mok G, Benz E, Vallee J, Miralbell R, Zilli T. Optimization of radiation therapy techniques for prostate cancer with prostate-rectum spacers: a systematic review. Int J Radiat Oncol Biol Phys 2014;90:278–88.

[66] Karsh LI, Gross ET, Pieczonka CM, Aliotta PJ, Skomra CJ, Ponsky LE, Nieh PT, Han M, Hamstra DA, Shore ND. Absorbable hydrogel spacer use in prostate radiotherapy: a comprehensive review of phase 3 clinical trial published data. Urology 2017;115:39–44.

[67] Whalley D, Hruby G, Alfieri F, Kneebone A, Eade T. SpaceOAR hydrogel in dose-escalated prostate cancer radiotherapy: rectal dosimetry and late toxicity. Clin Oncol 2016;28:e148–e154.

[68] Hwang ME, Mayeda M, Liz M, Goode-Marshall B, Gonzalez L, Elliston CD, et al. Stereotactic body radiotherapy with periprostatic hydrogel spacer for localized prostate cancer: toxicity profile and early oncologic outcomes. Radiat Oncol 2019;14:136.

[69] Aminsharifi A, Kotamarti S, Silver D, Schulman A. Major complications and adverse events related to the injection of the SpaceOAR hydrogel system before radiotherapy for prostate cancer: review of the manufacturer and user facility device experience database. J Endourol 2019;33:868-71.

[70] Wachter S, Gerstner N, Dorner D, Goldner G, Colotto A, Wambersie A, et al. The influence of a rectal balloon tube as internal immobilization device on variations of volumes and dose-volume histograms during treatment course of conformal radiotherapy for prostate cancer. Int J Radiat Oncol Biol Phys 2002;52:91–100.

[71] Both S, Wang KK, Plastaras JP, Deville C, Ad VB, Tochner Z, et al. Real-time study of prostate intrafraction motion during external beam radiotherapy with daily endorectal balloon. Int J Radiat Oncol Biol Phys 2011;81:1302–9.

[72] Wang KK, Vapiwala N, Deville C, Plastaras JP, Scheuermann R, Lin H, et al. A study to quantify the effectiveness of daily endorectal balloon for prostate intrafraction motion management. Int J Radiat Oncol Biol Phys 2012;83:1055–63.

[73] Smeenk RJ, Louwe RJ, Langen KM, Shah AP, Kupelian PA, van Lin EN, et al. An endorectal balloon reduces intrafraction prostate motion during radiotherapy. Int J Radiat Oncol Biol Phys 2012;83:661–9.

[74] Jones BL, Gan G, Kavanagh B, Miften M. Effect of endorectal balloon positioning errors on target deformation and dosimetric quality during prostate SBRT. Phys Med Biol 2013;58:7995–06.

[75] Isacsson U, Nilsson K, Asplund S, Morhed E, Montelius A, Turesson I. A method to separate the rectum from the prostate during proton beam radiotherapy of prostate cancer patients. Acta Oncol 2010;49:500–5.

[76] Holupka EJ, Kaplan ID, Burdette EC, Svensson GK. Ultrasound image fusion for external beam radiotherapy for prostate cancer. Int J Radiat Oncol Biol Phys 1996;35:975–84.

[77] Franz AM, Schmitt D, Seitel A, Chatrasingh M, Echner G, Oelfke U, et al. Standardized accuracy assessment of the calypso wireless transponder tracking system. Phys Med Biol 2014;59:6797–810.

[78] Bland JM, Altman DG. Statistical methods for assessing agreement between two methods of clinical measurement. Lancet 1986;327(8476):307–10.

[79] Bland JM, Altman DG. Measuring agreement in method comparison studies. Stat Methods Med Res1999;8(2):135–60.

[80] Santanam L, Malinowski K, Hubenshmidt J, Dimmer S, Mayse ML, Bradley J, et al. Fiducial-based translational localization accuracy of electromagnetic tracking system and on-board kilovoltage imaging system. Int J Radiat Oncol Biol Phys 2008;70**:**892–99.

[81] Poulsen PR, Schmidt ML, Keall P, Worm ES, Fledelius W, Hoffman L. A method of dose reconstruction for moving targets compatible with dynamic treatments. Med Phys 2012;39(10):6237–46.

[82] Legge K, Nguyen D, Ng JA, Wilton L, Richardson M, Booth J, et al. Real-time intrafraction prostate motion during linac based stereotactic radiotherapy with rectal displacement. J Appl Clin Med Phys 2017;18(6):130–6.

[83] de Leon J, Jameson MG, Rivest-Henault D, Keats S, Rai R, Arumugam S, et al. Reduced motion and improved rectal dosimetry through endorectal immobilization for prostate stereotactic body radiotherapy. Br J Radiol 2019;92:20190056.

[84] Litzenberg DW, Muenz DG, Archer PG, Jackson WC, Hamstra DA, Hearn JW, et al. Changes in prostate orientation due to removal of a Foley catheter. Med Phys 2018;45:1369–78.

[85] Dekura Y, Nishioka K, Hashimoto T, Miyamoto N, Suzuki R, Yoshimura T, et al. The urethral position may shift due to urethral catheter placement in the treatment planning for prostate radiation therapy. Radiat Oncol 2019;14:226.

[86] Nicolae A, Davidson M, Easton H, Helou J, Musunuru H, Loblaw A, et al. Clinical evaluation of an endorectal immobilization system for use in prostate hypofractionated stereotactic ablative body radiotherapy (SABR). Radiat Oncol 2015;10:122.

[87] Mahdavi SR, Ghaffari H, Modif B, Rostami A, Relazi R, Janani L. Rectal retractor application during image-guided dose-escalated prostate radiotherapy. Strahlenther Oncol 2019;195:923–33.

[88] Ogunleye T, Rossi PJ, Jani AB, Fox T, Elder E. Performance evaluation of Calypso 4D localization and kilovoltage imagine guidance systems for interfraction motion management of prostate patients. Scientific World Journal 2009;9:449–58.

[89] Foster RD, Pistenmaa DA, Solberg TD. A comparison of radiographic techniques and electromagnetic transponders for localization of the prostate. Radiat Oncol 2012;7:101.

[90] Hamilton DG, McKenzie DP, Perkins AE. Comparison between electromagnetic transponders and radiographic imaging for prostate localization: a pelvic phantom study with rotations and translations. J Appl Clin Med Phys 2017;18:43–53.

[91] Biston M, Zaragori T, Delcoudert L, Fargier-Voiron M, Munoz A, Gorsse C, et al. Comparison of electromagnetic transmitter and ultrasound imaging for intrafraction monitoring of prostate radiotherapy. Radiother Oncol 2019;136:1–8.

[92] Litzenberg D, Dawson LA, Sandler H, Sanda MG, McShan DL, Ten Haken RK, et al. Daily prostate targeting using implanted radiopaque markers. Int J Radiat Oncol Biol Phys 2002;52:699–703.

[93] Poggi MM, Gant DA, Sewchand W, Warlick WB. Marker seed migration in prostate localization. Int J Radiat Oncol Biol Phys 2003;56:1248–51.

[94] Kupelian P, Willoughby TR, Meeks SL, Forbes A, Wagner T, Maach M, et al. Intraprostatic fiducials for localization of the prostate gland: monitoring intermarker distances during radiation therapy to test for marker stability. Int J Radiat Oncol Biol Phys 2005;62:1291–6.

[95] Litzenberg DW, Willoughby TR, Balter JM, Sandler HM, Wei J, Kupelian PA, et al. Positional stability of electromagnetic transponders used for prostate localization and continuous, real-time tracking. Int J Radiat Oncol Biol Phys 2007;68:1199–206.

[96] van der Heide UA, Kotte AN, Dehnad H, Hofman P, Lagenijk JJ, van Vulpen M. Analysis of fiducial marker-based position verification in the external beam radiotherapy of patients with prostate cancer. Radiother Oncol 2007;82:38–45.

[97] Pouliot J, Aubin M, Langen KM, Liu Y-M, Pickett B, Shinohara K, et al. (Non)-migration of radiopaque markers used for on-line localization of the prostate with an electronic portal imaging device. Int J Radiat Oncol Biol Phys 2003;56:862–6.

[98] Braide K, Lindencrona U, Welinder K, Götstedt J, Ståhl I, Pettersson N, et al. Clinical feasibility and positional stability of an implanted wired transmitter in a novel electromagnetic positioning system for prostate radiotherapy. Radiother Oncol 2018;128:336–42.

[99] Kudchadker RJ, Lee AK, Yu ZH, Johnson JL, Zhang L, Zhang Y, et al. Effectiveness of using fewer implanted fiducial markers for prostate target alignment. Int J Radiat Oncol Biol Phys 2009;74:1283–9.

[100] Li JS, Lin M, Buyyounouski MK, Horwitz EM, Ma C. Reduction of prostate intrafractional motion from shortening the treatment time. Phys Med Biol 2013;58:4921–32.

[101] Cheung R, Tucker SL, Dong L, Kuban D. Dose-response for biochemical control among high-risk prostate cancer patients after external beam radiotherapy. Int J Radiat Oncol Biol Phys 2003;56:1234–40.

[102] Tamponi M, Gabriele D, Maggio A, Stasi M, Meloni GB, Conti M, et al. Prostate cancer dose-response, fractionation sensitivity and repopulation parameters evaluation from 25 international radiotherapy outcome data sets. Br J Radiol 2019;92(1098):20180823.

[103] Cheung R, Tucker SL, Lee AK, de Crevoisier R, Dong L, Kamat A. Dose-response characteristics of low- and intermediate-risk prostate cancer treated with external beam radiotherapy. Int J Radiat Oncol Biol Phys 2005;61:993–1002.

[104] Colvill E, Poulsen PR, Booth JT, O'Brien RT, Ng JA, Keall PJ. DMLC tracking and gating can improve dose coverage for prostate VMAT. Med Phys 2014;41:091705.

[105] Juneja P, Colvill E, Kneebone A, Eade T, Ng JA, Thwaites DI, Keall P, Kaur R, Poulsen P, Booth JT. Quantification of intrafraction prostate motion and its dosimetric effect on VMAT. Australas Phys Eng Sci Med 2017;40:317–324.

[106] Lovelock MD, Messineo AP, Cox BW, Kollmeier MA, Zelefsky MJ. Continuous monitoring and intrafraction target position correction during treatment improves target coverage for patients undergoing SBRT prostate therapy. Int J Radiat Oncol Biol Phys 2015;91:588–94.

[107] Seppälä J, Suilamo S, Tenhunen M, Sailas L, Virsunen H, Kaleva E, et al. Dosimetric comparison and evaluation of 4 stereotactic body radiotherapy techniques for the treatment of prostate cancer. Technol Cancer Res Treat 2017;16:238–45.

[108] Scobioala S, Kittel C, Elsayad K, Kroeger K, Oertel M, Samhouri L, et al. A treatment planning study comparing IMRT techniques and cyber knife for stereotactic body radiotherapy of low-risk prostate carcinoma. Radiat Oncol 2019;14:143.

[109] van de Water S, Valli L, Aluwini S, Lanconelli N, Heijmen B, Hoogeman M. Intrafraction prostate translations and rotations during hypofractionated robotic radiation surgery: dosimetric impact of correction strategies and margins. Int J Radiat Oncol Biol Phys 2014;88:1154–60.

[110] Zhang P, Mah D, Happersett L, Cox B, Hunt M, Mageras G. Determination of action thresholds for electromagnetic tracking system-guided hypofractionated prostate radiotherapy using volumetric arc therapy. Med Phys 2011;38(7):4001–8.

[111] Keall PJ, Nguyen DT, O'Brien R, Caillet V, Hewson E, Poulsen PR, et al. The first clinical implementation of real-time image-guided adaptive radiotherapy using a standard linear accelerator. Radiother Oncol 2018;127:6–11.

[112] Tehrani JN, O'Brien RT, Poulsen PR, Keall P. Real-time estimation of prostate tumor rotation and translation with a kV imaging system based on an iterative closest point algorithm. Phys Med Biol 2013;58:8517–33.

[113] Kim J, Nguyen DT, Booth JT, Huang C, Fuangrod T, Poulsen P, et al. The accuracy and precision of Kilovoltage Intrafraction Monitoring (KIM) six degree-of-freedom prostate motion measurements during patient treatments. Radiother Oncol 2018;126:236–43.

[114] Muurholm CG, Ravkilde T, Skouboe S, Eade T, Nguyen DT, Booth J, et al. Dose reconstruction including dynamic six-degree of freedom motion during prostate radiotherapy. J Phys: Conf Ser 2019;1305:012053.

[115] Gill S, Dang K, Fox C, Bressel M, Kron T, Bergen N, et al. Seminal vesicle intrafraction motion analysed with cinematic magnetic resonance imaging. Radiat Oncol 2014;9:174.

[116] Fast MF, Kamerling CP, Ziegenheim P, Menten MJ, Bedford JL, Nill S, et al. Assessment of MLC tracking performance during hypofractionated prostate radiotherapy using real-time dose reconstruction. Phys Med Biol 2016;61:1546–62.

[117] Kamerling CP, Fast MF, Ziegenheim P, Menten MJ, Nill S, Oelfke U. Online dose reconstruction for tracked volumetric arc therapy: real-time implementation and offline quality assurance for prostate SBRT. Med Phys 2017;44:5997–6007.

[118] Ravkilde T, Skouboe S, Hansen R, Worm E, Poulsen PR. First online real-time evaluation of motion-induced 4D dose errors during radiotherapy delivery. Med Phys 2018;45:3893–903.

[119] Hunt A, Hansen VN, Oelfke U, Nill S, Hafeez S. Adaptive radiotherapy enabled by MRI guidance. Clin Oncol 2018;30:711–9.

[120] Skouboe S, Ravkilde T, Bertholet J, Hansen R, Worm ES, Muurholm CG, et al. First clinical real-time motion-including tumor dose reconstruction during radiotherapy delivery. Radiother Oncol 2019;139:66–71.

[121] Skouboe S, Poulsen PR, Muurholm CG, Worm E, Hansen R, Høyer M, et al. Simulated real-time dose reconstruction for moving tumors in stereotactic liver radiotherapy. Med Phys 2019;46:4738–48.

[122] Menten MJ, Mohajer JK, Nilawar R, Bertholet J, Dunlop A, Pathmanathan AU, et al. Automatic reconstruction of the delivered dose of the day using MR-linac treatment log files and online MR imaging. Radiother Oncol 2020;145:88–94.

[123] Shelley LEA, Scaife JE, Romanchikova M, Harrison K, Forman JR, Bates AM, et al. Delivered dose can be a better predictor of rectal toxicity than planned dose in prostate radiotherapy. Radiother Oncol 2017;123:466–71.

[124] Zilli T, Scorsetti M, Zwahlen D, Franzese C, Förster R, Giaj-Levra N, et al. ONE SHOT - single shot radiotherapy for localized prostate cancer: study protocol of a single arm, multicenter phase I/II trial. Radiat Oncol 2018;13:166.

[125] Herrera FG, Valerio M, Berthold D, Tawadros T, Meuwly J, Vallet V, et al. 50-Gy stereotactic body radiation therapy to the dominant intraprostatic nodule: results from a phase 1a/b trial. Int J Radiat Oncol Biol Phys 2019;103:320–34.

ORIGINAL PAPERS

I

THE EFFECT OF RECTAL RETRACTOR ON INTRAFRACTION MOTION OF THE PROSTATE

by

Vanhanen, A. & Kapanen, M. 2016

Biomedical Physics & Engineering Express 2 035021

DOI: 10.1088/2057-1976/2/3/035021

Biomedical Physics & Engineering Express

PAPER

The effect of rectal retractor on intrafraction motion of the prostate

A Vanhanen[1,2] and M Kapanen[1,2]

[1] Department of Oncology, Unit of Radiotherapy, Tampere University Hospital, PO Box 2000, FI-33521 Tampere, Finland
[2] Department of Medical Physics, Medical Imaging Center, Tampere University Hospital, PO Box 2000, FI-33521 Tampere, Finland

E-mail: antti.vanhanen@pshp.fi

OPEN ACCESS

RECEIVED
4 March 2016

REVISED
11 May 2016

ACCEPTED FOR PUBLICATION
26 May 2016

PUBLISHED
5 July 2016

Keywords: prostate radiotherapy, hypofractionation, rectal retractor, intrafraction motion, real-time motion tracking

Abstract

Rectal retractors (RR) are used in prostate radiotherapy to retract part of the rectal wall further from the prostate in order to lower the rectal dose and toxicity. The aim of this study was to investigate the effect of RR on intrafraction motion of the prostate. Intrafraction motion of the prostate with RR and without it was recorded with electromagnetic real-time tracking system. Intrafractional motion data of 260 RR fractions and 351 non-RR fractions from 22 patients was analyzed. 3D and unidirectional motion patterns between RR and non-RR fraction datasets were compared in terms of percentage time at displacement $\geqslant$1, 2, 3, 4, 5 and 6 mm over 6 and 10 min of tracking time. Temporal patterns of the prostate motion were evaluated by re-binning the motion data in 1 min time intervals. The percentage time at displacement was larger in RR data compared to non-RR data in every direction (except anterior) and for every motion magnitude considered. For non-RR fractions the percentage of time of $\geqslant$1, 2, 3, 4, 5 and 6 mm 3D displacements within 10 min of tracking time were 44.8%, 16.0%, 6.4%, 2.9%, 1.4% and 0.5%, respectively. For RR fractions the corresponding percentages were 69.6%, 32.8%, 15.3%, 7.4%, 3.7% and 2.2%, respectively. The difference in 3D motion between the datasets was statistically significant ($p < 0.03$). Largest increase in the motion was seen in inferior and posterior directions when the RR was used. Motion increased linearly as a function of elapsed tracking time in both RR and non-RR datasets but the increase was more rapid in RR fractions. The use of RR increases the intrafraction motion of the prostate which can lead to inaccurate treatment localization and delivery thus questioning the justification of its use.

1. Introduction

In recent years there has been growing interest in hypofractionated radiotherapy (RT) for prostate cancer. This is due to the fact that prostate cancer is considered to have a low alpha–beta ratio relative to surrounding normal tissues tissues (Dasu and Toma-Dasu 2012, Vogelius and Bentzen 2013). In radiobiological point of view hypofractionation could lead to a better tumor control with fewer or same level of normal tissue complications compared to standard fractionation (Brenner and Hall 1999). Compared to standard fractionation, lower number of fractions and increased fraction doses may lead to a more significant underdosage of the target and overdosage of the normal tissues if the target is not hit accurately. As a consequence more emphasis should be laid on preserving the normal tissue doses at acceptable level and on accurate treatment localization.

In order to minimize rectal toxicity, several methods to reduce the dose to the rectum have been proposed. Among these are spacer gels and biodegradable balloons that are implanted to the interspace of prostate and rectum to increase the prostate-rectum separation. These methods can create a separation even up to 20 mm which results in significantly diminished rectal volumes exposed to high doses (Mok *et al* 2014). Disadvantages of these methods are related to the positioning of the spacer that usually cannot be corrected and to the invasive implantation procedures that can cause complications (Mok *et al* 2014). Another method for rectum sparing is the use of inflatable endorectal balloon (ERB) (Wachter *et al* 2002, Smeenk *et al* 2010). This method increases the distance of posterior rectal wall from the prostate but pushes the anterior rectal wall against the prostate. Reductions in high- and intermediate-dose regions of rectum wall have been reported (Smeenk *et al* 2010).

Disadvantage of the ERBs is the variation in daily reproducibility of the ERB position and shape that can cause deformations in the prostate (Jones *et al* 2013).

An alternative to spacer gels and rectal balloons in rectum dose sparing is a rectal retractor (RR). In this method a rectal rod is inserted into the rectum and the distance between rectum wall and the prostate is increased by retracting the rectum posteriorly (Isacsson *et al* 2010, Nilsson *et al* 2014, Nicolae *et al* 2015). One comparative treatment planning study shows that the RR significantly decreases rectal wall doses in the high dose region (Nilsson *et al* 2014) whereas in another study with similar device statistical differences were not found (Nicolae *et al* 2015).

It has been assessed from transrectal ultrasound (US) imaging during RT and from comparison of pre- and post-RT cone beam computed tomography (CBCT) images that RR may minimize intrafraction movement of the prostate during RT (Holupka *et al* 1996, Nicolae *et al* 2015). However, this has not been measured for the same patient group using real-time motion data recorded during actual RT.

In the present study the effect of RR (Rectafix™, Scanflex Medical AB, Täby, Sweden) on prostate intrafraction motion is investigated. This is accomplished by comparing real-time intrafraction motion data of patients treated partly with the RR and without it. Three dimensional (3D) and unidirectional displacements in anterior–posterior (AP), superior–inferior (SI) and left–right (LR) directions are determined in terms of percentage time at a displacement and compared between the RR and non-RR fractions. It is commonly assumed that the RR has stabilizing effect on prostate motion and the goal was to evaluate the magnitude of this effect. If the prostate motion was halted by the RR, the need for a real-time motion tracking could be questioned. The intrafraction motion data was acquired using real-time electromagnetic tracking system, RayPilot® (Micropos Medical AB, Gothenburg, Sweden). The study is part of a clinical trial (ClinicalTrials.gov ID: NCT02319239) which aims at developing extremely hypofractionated protocol for prostate cancer with minimized rectal toxicity.

2. Materials and methods

2.1. Patients and treatment

Study was approved by ethical committee of Pirkanmaa Hospital District (R14009) and the written consent to participate was obtained from each included patient. Twenty-eight patients with biopsy-proven prostate adenocarcinoma were recruited in the study between April 2014 and July 2015. They were treated with volumetric modulated arc therapy (VMAT) on a Varian TrueBeam STx accelerator (Varian Medical Systems, Palo Alto, CA) using two full arcs and 6 MV flattened beams. Twelve patients were treated using moderate hypofractionation schedule 20×3 Gy based on CHHiP-trial (Dearnaley *et al* 2012). Ten patients were treated using conventional schedule with 39×2 Gy. If seminal vesicles (SV) were included in the treatment, the dose to SVs was 20×2.3 Gy in moderate hypofractionation schedule administered by simultaneous integrated boost technique and 28×2 Gy in conventional schedule. RR was used in first 10 out of 20 or in first 15 out of 39 fractions to increase the distance between rectum wall and prostate.

2.2. Treatment planning and localization

Three gold seed fiducial markers were implanted transrectally in US guidance into the prostate for treatment localization. Before pre-RT imaging and treatment sessions, patients were instructed to empty their rectum and to have full bladder. Enemas were used before the magnetic resonance imaging (MRI) and CT simulation but not before treatment sessions because repetitively administered enemas were thought to be too exhausting to patients in long treatment course. A few days after the implantation, an MRI scan without the RR was acquired for target delineation. After the MRI, a RayPilot transmitter was implanted into the prostate for real-time electromagnetic motion tracking. Transmitter implantation was performed transperineally, using endorectal US guidance. The aim was to place the transmitter centrally into another, preferably more prominent one, of the lateral lobes of the prostate, trying to avoid the urethra, and midway of the apex and base of the prostate. Two computed tomography (CT) scans, first without the RR and immediately after with the RR, were acquired for treatment planning. Treatment plans were generated for both CT scans as the treatment consisted of RR and non-RR fractions. Toshiba Aquilion LB with 0.5–1 mm slice thickness was used to detect transmitter central point with high precision. 2 mm slices were reconstructed for the actual dose calculation. The planning target volume (PTV) was formed adding 5 mm isotropic margin around the clinical target volume that was either prostate alone or prostate and full SVs. The choice of 5 mm PTV margins was based on clinical protocol of daily image-guided marker alignment. Dose optimization and calculation was performed using Eclipse treatment planning system (Varian Medical Systems, Palo Alto, CA). To ensure the correct position of the RR and bladder filling, CBCT-scan was acquired before each treatment with RR. CBCT was acquired also for every other non-RR fraction to check the bladder and rectum filling. The actual target localization was performed by acquiring orthogonal kV-image pair of the prostate and matching it to the reference image pair obtained from the planning CT using three implanted gold seeds as fiducial markers. Treatment couch corrections proposed by image

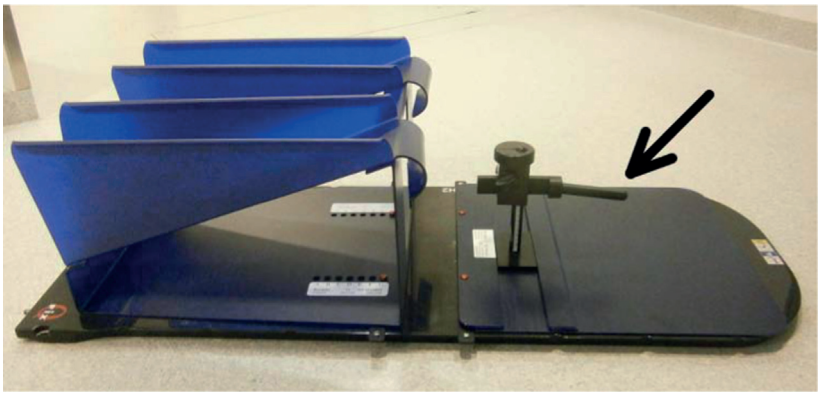

Figure 1. Rectafix consists of a rectal rod (black arrow), an adjustable vertical column and a leg support. The height of the leg support is 300 mm.

matching were performed to match the plan isocenter to the machine isocenter. Prostate intrafraction motion was tracked continuously starting immediately after the initial patient positioning on treatment couch (non-RR fractions) and when RR placement was accomplished (RR-fractions). Thus the tracking included CBCT- and kV-imaging and ended after the radiation delivery was complete. As the tracking was started after initial positioning procedures, the observed motion was not influenced by extraneous disturbances, such as RR placement. If the position of the RR had to be adjusted after the CBCT check, the tracking was stopped, reset and started over after the correction was done. Couch correction shifts during the tracking were canceled out from the observed motion data by subtracting the couch shift values in question from subsequent data points. Tracking the motion during the imaging in addition to irradiation provides information for planning of the timeline of the whole treatment session, e.g. potential stabilization time needed after patient setup and prostate movement during image guidance and treatment delivery.

2.3. Rectal retraction

The RR consists of a cylindrical rectal rod (diameter 20 mm, length 110 mm) which is locked to an adjustable vertical column. The column and leg support are attached to a baseplate (figure 1) which is fixed to the treatment couch or RayPilot detector plate. Indexed fixation holes on the leg support ensure the reproducible positioning of the leg support relative to vertical column. Electrically non-conductive fixation bars were used for fixation of the RR to avoid electromagnetic interference on RayPilot motion detection. The retraction of the rectal wall is achieved by mechanically pushing the rectal rod posteriorly. Vertical position of the rectal rod can be recorded with the help of a numeric scale on both sides of the vertical column. The extent of the retraction was limited by the discomfort of the patient and the achieved retraction (vertical position of the rectal rod) at the CT simulation was recorded for reproducible retraction at the treatment sessions. The positioning of the patient and the retraction achieved at the CT simulation were reproduced at every treatment fraction. The use of recorded retraction index and CBCT-imaging at every RR fraction to check the vertical and longitudinal position of the rod minimized the variability in RR position between fractions and different persons performing the retraction. The retraction was reproduced with millimeter precision and the depth of the RR insertion into the rectum had to cover the prostate and differ less than 1–2 cm compared to planning CT. Since the mechanical stretching may induce rectal complications if the RR would be used in large number of fractions (Nilsson *et al* 2014), the use of the rod was limited to 10 fractions with moderately hypofractionated patients and to 15 fractions with conventionally fractionated patients. RR was chosen to be used at the beginning fractions of the treatment course as the rectal mucosa usually becomes more irritated along the treatment course due to the irradiation. Langen *et al* (2008) studied the prostate intrafraction mobility during treatment course finding no difference between the observed motion at the beginning and end of the treatment course. Based on this, the choice of non-randomized scheduling of RR fractions was considered justified.

Within fractions without the RR, in-house developed knee support having femur angle comparable to most commercial solutions was used (figure 2).

2.4. Intra-fraction motion tracking

The RayPilot system consists of a transmitter which is implanted into the prostate and a receiver plate which is positioned on the treatment couch. The transmitter consisting of the transmitting part (length 17 mm, diameter 3 mm) and a cable (length 383 mm, diameter 1.6 mm) is attached to the receiver plate during each fraction to activate the transmitter. Signal sent by the transmitter is read by the receiver antennas in the receiver system and the position of the transmitter is

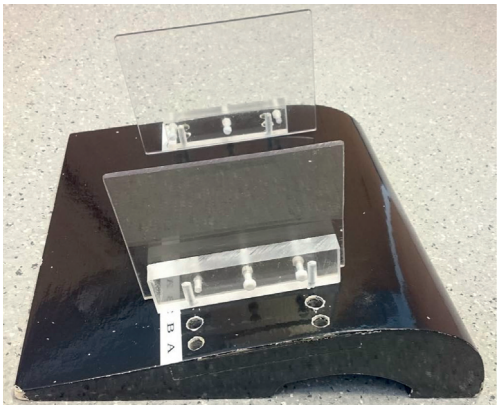

Figure 2. In-house developed knee support that was used in non-RR fractions. The height of the knee support is 110 mm.

located. The position is given in LR, SI and AP directions at 30 Hz frequency. The system measures also the rotation around the vertical axis (yaw) and rotation around the lateral axis (pitch). The active measurement volume is 10 cm × 10 cm × 10 cm and the vertical position of the measurement volume is adjustable. The operation limits for the transmitter angle are ±40° ±5% (pitch and yaw). Reported 3D resolution of the system, measured in laboratory environment, is 0.8 mm (±0.6) mm (Kindblom *et al* 2009). The RayPilot system is calibrated to the treatment room isocenter and based on the known relationship between transmitter center and treatment isocenter in the planning CT the system allows treatment localization, in addition to motion tracking. However, in this study the RayPilot was only used for the tracking of the intrafraction motion. The collected intrafraction motion data was saved in 1 s time resolution for further analysis. No treatment interruptions were made based on the detected intrafraction motion of the prostate.

2.5. Data processing

There was a small, sub-millimeter, bias in initial zero-point position tracked which is a result of a finite measurement resolution of the RayPilot system. The bias was eliminated by subtracting the initial position reading from subsequent position points in all translational directions. As the tracking time included treatment couch corrections, the shifts made to the couch were seen in raw tracking data. To analyze the pure prostate motion, the shifts were canceled out by subtracting couch shift values in question from subsequent data points. The effect of instrumental noise and radiofrequency disturbances were reduced by filtering the data using first order low-pass filter. To avoid the changes in phase response, the data was filtered bidirectionally in time and averaged. Gaussian measurement noise characteristics of the RayPilot system differ a little bit depending on measurement direction and therefore different smoothing factors (α) for different directions were used. Smoothing factors were $\alpha = 0.15$, $\alpha = 0.15$ and $\alpha = 0.1$ for LR, SI and AP directions, respectively. In addition to the Cartesian motion data, 3D vectors were calculated for the motion analysis.

2.6. Data analysis

Intrafraction motion was assessed by calculating absolute prostate displacement in each direction relative to its initial position at the beginning of the tracking. The extent, directionality and duration of prostate displacements were investigated. For this purpose, percentages of time at 3D and unidirectional displacements $\geqslant$1, 2, 3, 4, 5 and 6 mm were determined for 6 and 10 min tracking times. The percentage is the fraction of time when the pre-processed time-displacement curve is equal to or above the given displacement value. Temporal patterns of prostate motion were also investigated. To accomplish this, the percentages of time at displacements $\geqslant$1, 2, 3, 4, 5 and 6 mm were determined for 1 min tracking time intervals ranging from 0 to 10 min. The percentage times were determined separately for all RR fractions and all non-RR fractions and separately for the whole patient population and individual patients. Due to the variability in the duration of treatment sessions, the percentage times at displacements were calculated up to 10 min of tracking time to maintain adequate amount of data at the last minutes. The effect of RR on intrafraction motion was evaluated by comparing 3D and unidirectional motion patterns between RR and non-RR fractions. Comparisons between the RR and non-RR fractions were made for individual patients and for the whole patient population.

2.7. Statistical analysis

To evaluate the time dependence of prostate displacement, Pearson correlation coefficients between percentage time at a displacement and tracking time were calculated for each direction and 3D vector. Correlation was defined for displacements $\geqslant$1, 2, 3, 4, 5 and 6 mm.

Nonparametric two-sample Kolmogorov–Smirnov test was used to estimate differences in intrafraction motion patterns between the RR and non-RR fractions. The distributions of percentage time at a displacement in 1 min intervals within 10 min tracking time were compared between both fraction datasets. The comparisons were made for displacements $\geqslant$1, 2, 3, 4, 5 and 6 mm in each direction.

The paired Wilcoxon signed-rank test was applied to test the difference in percentage times with and without the RR at displacements $\geqslant$1, 2, 3, 4, 5 and 6 mm within 6 and 10 min. Differences in left, right, superior, inferior, anterior, posterior and 3D directions were tested. In addition to comparisons between fraction datasets over whole population, comparisons of 3D motion patterns were made for all individual

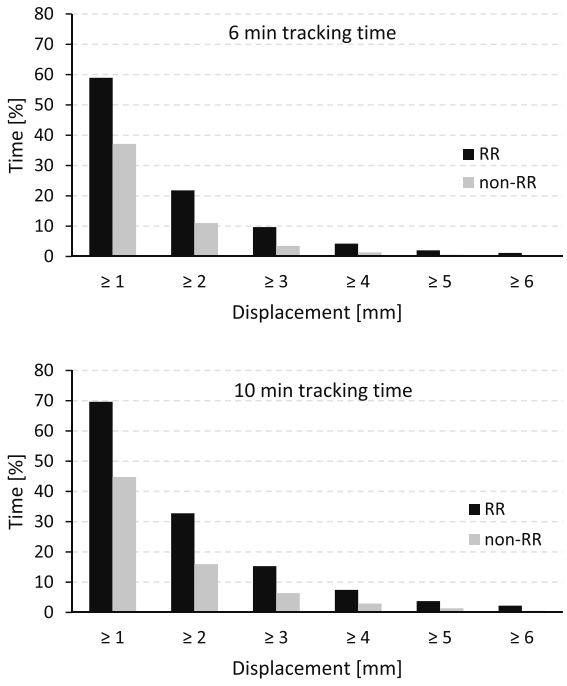

Figure 3. Percentage of tracking time of 3D displacements within 6 and 10 min for RR and non-RR fractions. The use of RR increased the intrafraction motion of the prostate and the difference in 3D motion between RR and non-RR fractions was statistically significant ($p < 0.03$).

patients. For a small subgroup of four patients having very small prostate motion the testing was limited to displacements $\geqslant$1, 1.5, 2, 2.5, 3 and 3.5 mm. All tests were conducted with significance level of 0.05.

3. Results

3.1. 3D motion analysis for RR and non-RR data

Technical problems with the cables of three of the implanted transmitters and transmitter pitch or yaw angle being out of operating limits with three patients prevented motion data collection partly or entirely thus leading to exclusion of these patients from the analysis. As a consequence, usable motion data was available for 22 patients out of 28 patients recruited, and the final number of fractions analyzed was 260 with the RR and 351 without it. Mean tracking time $\pm$ standard deviation for fractions with the RR was 540 $\pm$ 150 s and 450 $\pm$ 150 s for fractions without the RR. Difference in mean tracking times largely resulted from the different number of CBCTs between RR and non-RR fractions and the time required for RR position confirmation in RR fractions. Tracking time of 247 RR fractions (95.0%) and 276 non-RR fractions (80.7%) covered at least 6 min whereas 58 RR fractions (22.3%) and 26 non-RR fractions (7.5%) covered at least 10 min. The percentage time of 3D prostate displacements over 6 and 10 min of tracking time for both fraction datasets are shown in figure 3. The percentage time at 3D displacement was larger in RR fractions compared to non-RR fractions for every motion magnitude considered within both 6 and 10 min of tracking time. For non-RR fractions the percentage times of $\geqslant$1, 2, 3, 4, 5 and 6 mm 3D displacements were 37.2%, 11.0%, 3.5%, 1.4%, 0.6% and 0.3% within 6 min, and 44.8%, 16.0%, 6.4%, 2.9%, 1.4% and 0.5% within 10 min, respectively. For RR fractions the corresponding percentages were 59.0%, 21.8%, 9.7%, 4.2%, 2.0% and 1.2% within 6 min, and 69.6%, 32.8%, 15.3%, 7.4%, 3.7% and 2.2% within 10 min, respectively. The difference in 3D motion between RR and non-RR fractions was statistically significant ($p < 0.03$) for both 6 and 10 min of tracking time. The power of the test for the 3D differences within 10 min of tracking time was 0.90.

3.2. 3D analysis for individual patients

The percentage time of 3D displacements of the prostate in RR and non-RR fractions over 10 min of tracking time for individual patients are shown in table 1. The analysis reveals that for 13 patients out of 22 the 3D motion of the prostate was significantly larger ($p < 0.05$) with RR than without it. For two patients the observed motion was milder within RR fractions compared to non-RR fractions and the difference was statistically significant ($p < 0.05$). For

Table 1. Percentage time of 3D prostate displacements in RR and non-RR fractions within 10 min of tracking time for individual patients.

	Displacement											
	⩾1 mm		⩾2 mm		⩾3 mm		⩾4 mm		⩾5 mm		⩾6 mm	
Patient	RR	non-RR	RR	non-RR	RR	non-RR	RR	non-RR	RR	non-RR	RR	non-RR
1	75.7	44.3	35.0	16.0	17.3	8.8	1.3	6.6	0.0	2.6	0.0	0.5
2	70.8	68.2	36.3	36.4	2.5	13.2	0.0	5.4	0.0	2.8	0.0	0.4
3*	71.6	38.2	38.8	13.0	22.6	2.2	11.1	0.0	6.2	0.0	2.3	0.0
4*	77.4	5.6	53.5	0.0	25.4	0.0	13.8	0.0	11.1	0.0	10.7	0.0
5*	70.2	23.4	21.4	8.8	10.0	0.0	0.9	0.0	0.3	0.0	0.1	0.0
6*	90.1	70.3	67.7	34.8	49.3	9.8	28.3	3.9	16.6	0.2	4.6	0.0
7*	66.9	49.9	44.4	8.7	25.6	2.4	14.9	1.0	6.9	0.3	3.3	0.0
8	69.5	58.2	22.8	24.8	2.1	8.1	0.0	2.9	0.0	0.2	0.0	0.0
9*	65.0	12.0	29.6	0.2	2.2	0.0	0.0	0.0	0.0	0.0	0.0	0.0
10**	66.9	70.4	13.4	27.9	0.0	11.3	0.0	9.7	0.0	4.8	0.0	0.0
11*	57.4	29.1	13.5	1.4	1.0	0.0	0.0	0.0	0.0	0.0	0.0	0.0
12*	57.1	26.1	6.4	1.3	1.0	0.0	0.0	0.0	0.0	0.0	0.0	0.0
13*	88.2	74.8	65.2	43.0	50.5	17.9	28.4	5.7	11.3	3.2	7.6	0.9
14*	85.1	34.2	65.9	7.7	39.5	1.2	21.8	0.2	9.4	0.0	7.1	0.0
15*	59.1	24.5	5.1	0.0	0.4	0.0	0.0	0.0	0.0	0.0	0.0	0.0
16	49.2	40.3	5.0	6.5	0.0	1.0	0.0	0.4	0.0	0.0	0.0	0.0
17	62.2	31.5	7.2	9.5	0.0	3.0	0.0	0.0	0.0	0.0	0.0	0.0
18*	80.4	35.9	39.1	5.7	21.4	4.8	15.7	1.1	8.2	0.0	7.5	0.0
19	73.2	65.9	40.8	37.1	8.5	20.8	0.0	10.7	0.0	4.7	0.0	1.2
20**	46.5	75.5	17.4	41.0	0.5	20.3	0.0	3.9	0.0	1.8	0.0	0.4
21*	87.5	76.4	69.7	49.7	40.9	30.3	22.1	14.9	13.3	7.3	5.7	3.5
22	64.4	46.7	19.3	16.1	4.6	9.2	0.3	8.0	0.0	6.0	0.0	5.0

*$p < 0.05$, RR-motion larger than non-RR motion.
**$p < 0.05$, non-RR motion larger than RR motion.

Table 2. Percentage of time of unidirectional prostate displacements for RR and non-RR fractions within 6 min of tracking time.

		Displacement					
		⩾1 mm	⩾2 mm	⩾3 mm	⩾4 mm	⩾5 mm	⩾6 mm
Left	RR	6.8	1.9	0.8	0.1	0.0	0.0
	non-RR	5.6	1.4	0.3	0.2	0.0	0.0
Right	RR	7.2	1.6	0.2	0.1	0.0	0.0
	non-RR	4.8	0.6	0.1	0.0	0.0	0.0
Superior	RR	4.0	1.3	0.6	0.2	0.0	0.0
	non-RR	2.4	0.9	0.3	0.0	0.0	0.0
Inferior	RR	26.4	6.4	2.6	1.2	0.6	0.6
	non-RR	7.1	0.8	0.2	0.0	0.0	0.0
Anterior	RR	6.1	2.0	0.9	0.4	0.1	0.1
	non-RR	7.5	2.5	0.8	0.5	0.3	0.2
Posterior	RR	24.2	6.9	2.6	1.5	0.8	0.7
	non-RR	13.1	3.2	0.9	0.1	0.0	0.0

rest of the patients statistically significant difference was not seen.

3.3. Directional analysis

Percentage times at unidirectional displacements within 6 and 10 min tracking time for both fraction datasets are shown in tables 2 and 3, respectively. Least motion was seen in LR direction. LR displacements ⩾5 mm were not seen in RR data and were negligible (0.01%) in non-RR data. The motion was quite evenly distributed between left and right directions, although the movement was slightly more emphasized in left direction in both RR and non-RR data and more frequent in RR data than in non-RR data ($p = 0.08$ left, power = 0.90; $p = 0.07$ right, power = 0.76).

SI motion in non-RR fractions was approximately of the same order as LR motion in non-RR fractions and no displacements ⩾5 mm were seen. In RR fractions SI motion was notable larger. Motion was more frequent in RR fractions than in non-RR fractions in superior and especially in inferior direction. Differences between the two datasets were statistically significant ($p < 0.03$, power ⩾ 0.86) in both superior and inferior directions.

Table 3. Percentage of time of unidirectional prostate displacements for RR and non-RR fractions within 10 min of tracking time.

		Displacement					
		⩾1 mm	⩾2 mm	⩾3mm	⩾4 mm	⩾5 mm	⩾6 mm
Left	RR	9.4	3.5	1.6	0.4	0.0	0.0
	non-RR	7.5	1.8	0.5	0.2	0.0	0.0
Right	RR	9.7	2.4	0.3	0.1	0.0	0.0
	non-RR	6.0	0.9	0.1	0.0	0.0	0.0
Superior	RR	6.0	2.4	1.1	0.3	0.1	0.0
	non-RR	3.8	1.5	0.6	0.1	0.0	0.0
Inferior	RR	35.0	10.3	4.4	2.0	1.0	0.8
	non-RR	9.4	1.4	0.3	0.0	0.0	0.0
Anterior	RR	8.6	4.1	2.1	0.9	0.2	0.1
	non-RR	9.3	3.6	1.5	0.8	0.4	0.2
Posterior	RR	30.5	9.1	3.8	2.3	1.3	0.9
	non-RR	17.5	5.6	2.2	0.4	0.1	0.0

Most of the motion in non-RR group was seen in AP direction. Anterior motion was comparable between the groups whereas posterior motion was more frequent in RR group than in non-RR group. The difference in posterior motion distribution between the groups was statistically significant ($p < 0.03$, power $= 0.90$).

3.4. Time dependence

Temporal patterns of the prostate motion were evaluated by re-binning the percentage of time at displacements against 1 min tracking time intervals. Temporal pattern of 3D motion is plotted for displacements ⩾2, 3, 4, 5 and 6 mm (figure 4) and unidirectional temporal patterns are plotted for displacements ⩾2, 3 and 5 mm (figure 5). 3D motion of the prostate increased as a function of elapsed tracking time whether the RR was used or not and the correlation of the percentage time of 3D displacement with tracking time was significant for all the displacements considered. For 3D deviations ⩾2, 3, 4 and 5 mm the increment of percentage time at displacement was linear with tracking time in RR and non-RR fractions, though the linearity was more pronounced in RR fractions. The 3D motion beyond 6 mm increased linearly with elapsed tracking time in RR fractions whereas displacements of at least 6 mm were rare in non-RR group and the linearity of the tracking time dependence was not evident. Common for all the displacements considered was that the percentage time at displacement grew faster in RR fractions than in non-RR fractions.

LR motion increased as a function of elapsed tracking time and the increase of the motion was linear for RR fractions in left direction. The probability of larger displacement along the elapsed tracking time increased also in right direction but the linearity was not clear. LR motion was more time independent when RR was not used.

The probability of inferior displacements ⩾2 and 3 mm grew as a function of tracking time ($p < 0.05$) and the increase was more linear and steep in RR fractions than in non-RR fractions. The increase of the percentage time at superior displacements ⩾1, 2 and 3 mm was mild and comparable between the two datasets. Displacements of at least 5 mm in inferior direction were seen only in RR fractions and the probability of at least 5 mm displacement increased as a function of elapsed tracking time. Large displacements in superior direction were negligible and time independent.

The percentage time at displacement ⩾1, 2 and 3 mm increased as a function of tracking time in anterior and posterior directions in both groups ($p < 0.05$). Posterior motion beyond 5 mm was negligible in non-RR group but increased as a function of tracking time in RR group. Large (⩾5 mm) anterior motion was time independent in both groups.

Statistically significant differences in temporal patterns of the motion between RR and non-RR fractions were found in inferior motion beyond 3 mm ($p \leqslant 0.015$) and in posterior motion for displacements ⩾5 mm ($p < 0.05$). Differences in inferior motion were near the significance level for displacements ⩾1 and 2 mm ($p = 0.055$).

4. Discussion

In the current study the effect of the RR on prostate intrafraction motion was examined using real-time motion tracking over every treatment fraction and the whole treatment course. Results of the study suggest that the RR increases the prostate motion instead of stabilizing it. Compared to non-RR fractions the percentage time at displacement in RR fractions was effectively larger in every direction (with the exception of anterior) and for any displacement considered. The difference in 3D motion patterns between RR and non-RR fractions was statistically significant ($p < 0.03$). Differences in 3D motion were evaluated also at individual level. For 13 out of 22 patients the RR

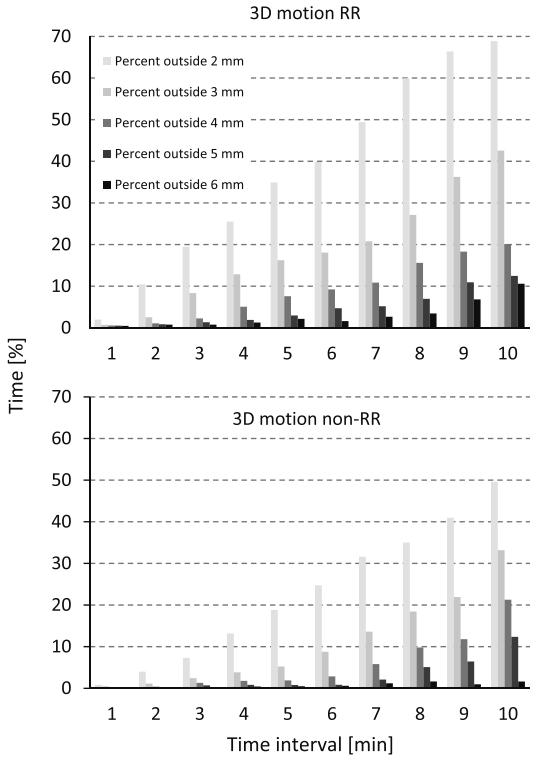

Figure 4. Percentage of time at 3D prostate displacements as a function of elapsed tracking time. Motion increased linearly in both RR and non-RR fractions but the increase was more rapid in RR fractions.

caused significant increase in intrafraction motion of the prostate. For only two patients the intrafraction motion was significantly reduced with the RR.

These results are conflicting with the results of Nicolae *et al* (2015) who observed prostate immobilization with endorectal immobilization device (EIS) comparable to immobilization with ERB. However, it has to be pointed out that the clinical implementation of the EIS system differs from RR as the knee support used and therefore the femur angle is different between the two systems. Nicolae *et al* (2015) also used pre- and post-treatment CBCT-imaging as a motion tracking method which misses the motion information (e.g. transient excursions of the prostate) during the actual treatment and which has been proven to be insensitive in determining intrafraction prostate motion (Noel *et al* 2009). Results of the current study are based on continuous motion tracking thus representing more accurate and comprehensive view of prostate intrafraction motion between two different clinical practical implementations.

Directional analysis of the motion was performed to clarify more rigorously the effect of RR on prostate motion. Overall the LR motion was mildest and most of the motion was seen in SI and AP directions in both RR and non-RR fractions. This finding was expected as the prostate is surrounded laterally by muscular structures which restricts the LR motion of the prostate and directs the motion mainly in AP and SI directions (Lin *et al* 2013). The use of RR increased the intrafraction motion in all but anterior direction but the biggest differences between RR and non-RR fractions were seen in superior, inferior and posterior directions. Especially the increase in inferior and posterior motion was notable. In addition to increased frequency in inferior and posterior motion the magnitude of the motions increased in RR fractions compared to non-RR fractions. Over 3 mm displacements in inferior direction and over 4 mm displacements in posterior direction were seen only in RR fractions. Without the RR there can be seen slight emphasis on inferiorly directed motion and more clearly posteriorly directed motion which is consistent with many earlier findings (Langen *et al* 2008, Bittner *et al* 2010, Li *et al* 2013, Tong *et al* 2015).

Several reasons can explain the increased motion with RR. The RR and the retraction cause discomfort which may increase the muscular tension. Changes in tension may be larger than in normal patient setup and might lead to increased motion of the whole pelvis and the prostate. Greatly increased posterior and inferior motion could be a consequence of the posteriorly

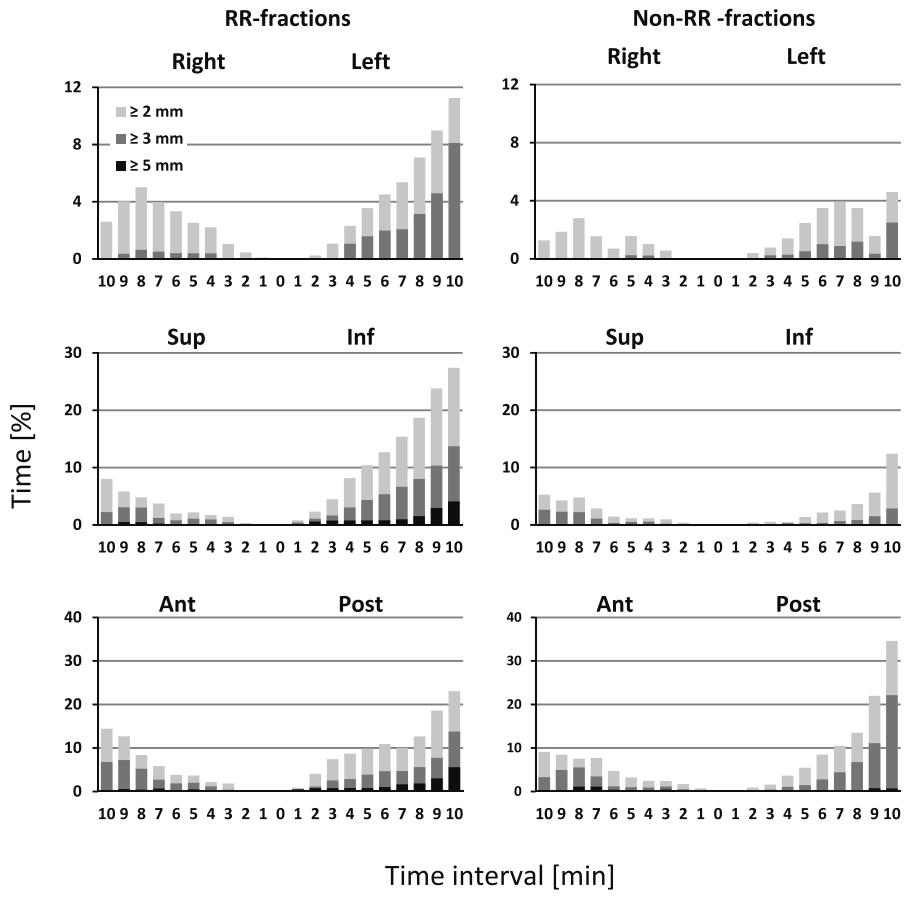

Figure 5. Percentage of time at unidirectional prostate displacements as a function of elapsed tracking time. Largest increase in the motion was seen in inferior and posterior directions when the RR was used.

directed retraction which creates empty space posteriorly to the prostate eliminating the supporting act of the posterior tissues. Phenomenon seems to be opposite when compared to the use of ERBs which create supporting structure posteriorly to the prostate and which have been reported to reduce the motion especially in AP direction (Smeenk *et al* 2012, Wang *et al* 2012). The greatest separation between rectum and prostate with the RR is achieved at the inferior part of the prostate-rectum interface. This might direct the motion more in posterior and inferior directions as the muscular tension relaxes. Filling of the bladder during the tracking time might also push the prostate towards inferior and posterior directions.

Continuous drifting describes well the motion type of the prostate in majority of the fractions investigated in the present study. This supports the hypothesis that the observed motion is mainly a consequence of a muscle relaxation. With many patients the prostate was quite stable and sudden excursions, related probably to peristaltic motion (Langen *et al* 2008), were seen rarely. However, as pointed out by earlier studies, there can be substantial transitions in the prostate motion that can be unpredictable (Kupelian *et al* 2007, Tong *et al* 2015).

Flattening of the motion curves as a function of elapsed tracking time were seen in some of the individual fractions in both RR and non-RR datasets but was not evident in motion patterns over all fractions except for small ($\leqslant$1 mm) 3D motions (data not shown). Instead, temporal patterns of the motion (figures 4 and 5) reveal that the motion increased linearly as a function of elapsed tracking time in both fraction datasets for most of the displacements considered. For RR fractions the increase in motion was notably faster. Generally, our findings of increasing probability of prostate intrafraction motion with tracking time are consistent with previously reported results (Langen *et al* 2008, Ballhausen *et al* 2015, Tong *et al* 2015). Li *et al* (2013) reported that the magnitude of the intrafraction motion of the prostate would not significantly change after 9 min of treatment time. Their tracking

data did not include the localization time which might take even 4–6 min from initial setup to the start of treatment delivery based on our own clinical experiences. Taking into account the localization time the possible saturation of the magnitude of the motion could be seen actually 13–15 min after the initial setup and might be impractical to wait in normal clinical routine. Possible stabilization that could be related to a relaxation of the patient was not seen in neither of the fraction datasets within the examined 10 min of tracking time in the present study. This suggests that within the first 10 min after the initial setup no stabilizing or relaxing time is needed between patient setup, image guidance and treatment with and without the RR. Relative differences in 3D motion are nearly the same between 6 and 10 min datasets for both fraction datasets reflecting the linear increase in the probability of the motion and indicating that the observed difference in intrafraction motion between RR and non-RR fractions is independent of tracking time. However, it has to be pointed out that the effect of RR on intrafraction motion with longer than 10 min tracking times after the initial setup is not known.

Increase in the probability of the motion with elapsed tracking time emphasizes the importance of shorter treatment times that are achievable with modern treatment techniques such as VMAT and flattened filter free (FFF) beams. It should also be realized that the prostate motion affects also to the accuracy of image guided treatment localization and thus the delay between imaging and couch corrections should be minimized. The time that is required for image guidance depends on the imaging modality and the experience of the personnel. Orthogonal kV imaging based image guidance in prostate RT takes about 2.5 min in our department and delivery of 2 Gy fraction dose with two full VMAT treatment arcs will take approximately 2 min. Using 10 MV FFF beams even the dose of 7.25 Gy, that is common in prostate SBRT, can be delivered within 2 to 3 min.

The observed 3D motion of the prostate in non-RR fractions was generally smaller than seen in literature: the percentage of time at displacements $\geqslant$3 mm and $\geqslant$5 mm within 10 min of tracking time was 6.4% and 1.4%, respectively. Tong *et al* (2015) observed 12% accumulated time of at least 3 mm displacement for all treatment fractions completed within 10 min. For at least 5 mm displacement the corresponding percentage was about 2% (Tong *et al* 2015, figure 2). Wang *et al* (2012) observed prostate displacements of $>$3 mm and $>$5 mm for 11.7% $\pm$ 7.0% and 3.1% $\pm$ 2.2% within 6 min of tracking time. Corresponding percentages for 6 min tracking time in the current study were 3.5% and 0.6%. Langen *et al* (2008) observed prostate displacements of $>$3 mm and $>$5 mm for 13.6% and 3.3% of total treatment time (mean tracking time 10 $\pm$ 2 min), respectively. Nearly similar percentages of time observed also Li *et al* (2009) (13.4% and 1.8%) for tracking times ranging from 10 to 20 min. However, these results are not fully comparable to the current results as they are proportional to different tracking times. The assessments of motion patterns were restricted to maximum of 10 min of tracking time because majority of the fractions were completed in less than 10 min and low number of longer tracking times might not represent well the motion in general population. There are many explanations for the differences in non-immobilized motion. One reason might be the differences in treatment preparation, e.g. rectum and bladder filling. In the present study the patients were concisely instructed to empty the rectum before each treatment whereas in the study of Langen *et al* (2008) bladder or rectum preparations were not performed before CT-simulation or daily treatment fractions. No special requirements for rectum filling before treatments in non-ERB group have been mentioned in the study of Wang *et al* (2012) either and there is no mention about it in the study of Li *et al* (2009). However, in the study of Tong *et al* (2015) patients were instructed to come to all simulations and treatments with empty rectum and full bladder. Rectal movements and related rectal distension have been shown to result in significant displacements of the prostate (Padhani *et al* 1999) which implies that empty rectum in the current patient data might explain some of the differences between the current and literature results.

Interestingly the observed 3D motion in RR fractions was comparable to or more frequent than findings of non-immobilized prostate motion in literature (Langen *et al* 2008, Li *et al* 2009, Wang *et al* 2012, Tong *et al* 2015). In these studies the intrafraction motion was tracked using electromagnetic Calypso® system (Balter *et al* 2005, Willoughby *et al* 2006) in which three localization transponders are implanted into the prostate. With the RayPilot used in the present study a wired transmitter is implanted into the prostate leaving the cable running out from the perineum. The cable may induce fibrosis to the perineal tissues surrounding the cable which might reduce the tissue mobility and have minor stabilizing effect on prostate as the transmitter part is connected to the cable. However, this should be verified with comparative measurements with different tracking methods and consistent patient groups.

It can be argued if the use of RR would affect the prostate motion of subsequent non-RR fractions. If this was the case, it may be assumed that the effect would have been largest at the beginning of the non-RR fractions. However, the observed prostate motion of the first five non-RR fractions did not differ from the motion of last five non-RR fractions of the treatment course. Based on these findings, it is unlikely that the use of RR would have affected to the prostate motion at subsequent non-RR fractions. To test this rigorously, would require larger cohorts of patients treated separately with or without the RR, which was out of scope of this study.

One of the limitations of the present study is the small amount of patient data that might explain some of the differences in observed non-immobilized prostate motion results between our study and literature. It is noteworthy that patient inclusion criteria excluded for example hip transplant patients and our results might not be fully representative to that particular group of patients. To compensate small number of patients, all the patients were treated partly with and without the RR thus making the comparison of the motion data between RR and non-RR fractions comparable. This also enabled the comparison of motion patterns at individual level which deepened the knowledge of RR's effect with different anatomies. The placement of the transmitter is important as prostate deformations might have an influence on detected intrafraction motion. Comparison of RR and non-RR motion data for individual patients reduced also the possible effect of non-ideal transmitter placement on observed difference in intrafraction motion patterns as the measurement point was the same for all fractions for the same patient. It is noteworthy that RayPilot tracking is based on tracking of single point inside the prostate which does not necessarily reflect the motion of SVs or deformations of the prostate. Thus the analysis of intrafraction motion of the SVs and the effects of prostate deformations are not included in the present study. If SVs are included in treatment their possible motion should be compensated with reasonable margins and deformations of the prostate should always be verified with imaging, e.g. CBCT.

In the present study the analysis of motion was limited to translational movements. The analysis of intrafraction prostate rotations (pitch and yaw) and their connection to translational movements would require more extensive investigation which was out of scope of this study. The impact of increased motion with RR on treatment margins was not investigated in this study either but will be explored in future studies. However, it is obvious that increased motion should be taken into account by increasing margins or by exploiting real-time motion monitoring.

Femur angle against couch surface was steeper in RR fractions (population mean $44.2^\circ \pm 4.2^\circ$) than in non-RR fractions (population mean $16.6^\circ \pm 2.4^\circ$) due to differences in knee supports between RR and non-RR fractions. Knee support affects to the position of rectum and prostate (Steenbakkers *et al* 2004) but whether it has an effect on prostate motion is not known or has not bee reported in the literature. In-house developed knee support was used in all fractions with two patients in the current study. For one of these two patients the motion distributions between RR and non-RR fractions were similar and for the other the motion was significantly larger in RR fractions than in non-RR fractions. These findings suggest that the leg support is not the cause of the observed difference in motion patterns but its effect cannot be fully excluded and should be confirmed with further investigation.

The primary benefit of the RR is thought to be the rectum dose sparing in prostate RT. However, this has been questioned by the results of Nicolae *et al* (2015) who did not see a difference in rectum dose distribution between treatment plans calculated with and without the EIS similar to the RR. Results of the present study suggest that the use of RR increases the intrafraction motion of the prostate although the observed motion even with the RR was generally small. However, increased motion can lead to inaccurate treatment localization and delivery increasing the uncertainty of dose sparing of the RR. Based on these results, we do not recommend the use of it. Controversy in dose sparing of the RR require further investigation and the final effect of RR on rectal side effects should be verified by clinical data.

5. Conclusions

In the present study the effect of the RR on intrafraction motion of the prostate was assessed for the first time using real-time motion tracking. The results imply that the use of the RR increases intrafraction motion when compared to motion data recorded in normal patient setup without the RR. The difference in percentage time at 3D displacement was 1%–25% depending on the magnitude of the displacement and the difference between the motion patterns between RR and non-RR fractions was statistically significant. This finding is important because it is opposite to the general assumptions based on transrectal US findings. The increased movement, if not corrected properly, may lead to a degradation of the delivered dose to the target and expose organs at risk to higher doses. Further clinical and planning studies might be needed to evaluate the dose sparing effect of the RR in detail.

Acknowledgments

This study was financially supported by the Seppo Nieminen funding, Grant number 15012, Tampere University Hospital and by the Eila Vehmas foundation, Tampere University Hospital. Oncologist Petri Reinikainen is acknowledged for recruiting the patients and the transmitter implantations. The authors declare that they have no conflict of interest.

References

Ballhausen H, Li M, Hegemann N-S, Ganswindt U and Belka C 2015 Intra-fraction motion of the prostate is a random walk *Phys. Med. Biol.* **60** 549–63

Balter J M, Wright J N, Newell L J, Friemel B, Dimmer S, Cheng Y, Wong J, Vertatschitsch E and Mate T P 2005 Accuracy of a wireless localization system for radiotherapy *Int. J. Radiat. Oncol. Biol. Phys.* **61** 933–7

Bittner N, Butler W M, Reed J L, Murray B C, Kurko B S, Wallner K E and Merrick G S 2010 Electromagnetic tracking of intrafraction prostate displacement in patients externally

immobilized in the prone position *Int. J. Radiat. Oncol. Biol. Phys.* **77** 490–5

Brenner D J and Hall E J 1999 Fractionation and protraction for radiotherapy of prostate carcinoma *Int. J. Radiat. Oncol. Biol. Phys.* **43** 1095–101

Dasu A and Toma-Dasu I 2012 Prostate alpha/beta revisited—an analysis of clinical results from 14 168 patients *Acta Oncol.* **51** 963–74

Dearnaley *et al* 2012 Conventional versus hypofractionated high-dose intensity-modulated radiotherapy for prostate cancer: preliminary safety results from the CHHiP randomized controlled trial *Lancet Oncol.* **13** 43–54

Holupka E J, Kaplan I D, Burdette E C and Svensson G K 1996 Ultrasound image fusion for external beam radiotherapy for prostate cancer *Int. J. Radiat. Oncol. Biol. Phys.* **35** 975–84

Isacsson U, Nilsson K, Asplund S, Morhed E, Montelius A and Turesson I 2010 A method to separate the rectum from the prostate during proton beam radiotherapy of prostate cancer patients *Acta Oncol.* **49** 500–5

Jones B L, Gan G, Kavanagh B and Miften M 2013 Effect of endorectal balloon positioning errors on target deformation and dosimetric quality during prostate SBRT *Phys. Med. Biol.* **58** 7995–8006

Kindblom J, Ekelund-Olvenmark A, Syren H, Iustin R, Braide K, Frank-Lissbrant I and Lennernäs B 2009 High precision transponder localization using a novel electromagnetic positioning system in patients with localized prostate cancer *Radiother. Oncol.* **90** 307–11

Kupelian P *et al* 2007 Multi-institutional clinical experience with the Calypso system in localization and continuous, real-time monitoring of the prostate gland during external radiotherapy *Int. J. Radiat. Oncol. Biol. Phys.* **67** 1088–98

Langen K M, Willoughby T R, Meeks S L, Santhanam A, Cunningham A, Levine L and Kupelian P A 2008 Observations on real-time prostate gland motion using electromagnetic tracking *Int. J. Radiat. Oncol. Biol. Phys.* **71** 1084–90

Li J S, Jin L, Pollack A, Horwitz E M, Buyyounouski M K, Price R A and Ma C 2009 Gains from real-time tracking of prostate motion during external beam radiation therapy *Int. J. Radiat. Oncol. Biol. Phys.* **75** 1613–20

Li J S, Lin M, Buyyounouski M K, Horwitz E M and Ma C 2013 Reduction of prostate intrafractional motion from shortening the treatment time *Phys. Med. Biol.* **58** 4921–32

Lin Y, Liu T, Yang W, Yang X and Khan M K 2013 The non-Gaussian nature of prostate motion based on real-time intrafraction tracking *Int. J. Radiat. Oncol. Biol. Phys.* **87** 363–9

Mok G, Benz E, Vallee J, Miralbell R and Zilli T 2014 Optimization of radiation therapy techniques for prostate cancer with prostate-rectum spacers: a systematic review *Int. J. Radiat. Oncol. Biol. Phys.* **90** 278–88

Nicolae A, Davidson M, Easton H, Helou J, Musunuru H, Loblaw A and Ravi A 2015 Clinical evaluation of an endorectal immobilization system for use in prostate hypofractionated stereotactic ablative body radiotherapy (SABR) *Radiat. Oncol.* **10** 122

Nilsson K, Johansson A K, Montelius A, Turesson I, Heikkinen R O, Ljung G and Isacsson U 2014 Decreasing the dose to the rectal wall by using a rectal retractor during radiotherapy of prostate cancer: a comparative treatment planning study *J. Radiother.* **2014** 680205

Noel C, Parikh P J, Roy M, Kupelian P, Mahadevan A, Weinstein G, Enke C, Flores N, Beyer D and Levine L 2009 Prediction of intrafraction prostate motion: accuracy of pre- and post-treatment imaging and intermittent imaging *Int. J. Radiat. Oncol. Biol. Phys.* **73** 692–8

Padhani A R, Khoo V S, Suckling J, Husband J E, Leach M O and Dearnaley D P 1999 Evaluating the effect of rectal distension and rectal movement on prostate gland position using cine MRI *Int. J. Radiat. Oncol. Biol. Phys.* **44** 525–33

Smeenk R J, Louwe R J, Langen K M, Shah A P, Kupelian P A, van Lin E N and Kaanders J H 2012 An endorectal balloon reduces intrafraction prostate motion during radiotherapy *Int. J. Radiat. Oncol. Biol. Phys.* **83** 661–9

Smeenk R J, Teh B S, Butler E B, van Lin E N and Kaanders J H 2010 Is there a role for endorectal balloons in prostate radiotherapy? A systematic review *Radiother. Oncol.* **95** 277–82

Steenbakkers R J, Duppen J C, Betgen A, Lotz H, Remeijer P, Fitton I, Nowak P J, van Herk M and Rasch C R 2004 Impact of knee support and shape of tabletop on rectum and prostate position *Int. J. Radiat. Oncol. Biol. Phys.* **60** 1364–72

Tong X, Chen X, Li J, Xu Q, Lin M, Chen L, Price R A and Ma C-M 2015 Intrafractional prostate motion during external beam radiotherapy monitored by a real-time target localization system *J. Appl. Clin. Med. Phys.* **16** 5013

Vogelius I R and Bentzen S M 2013 Meta-analysis of the alpha/beta ratio for prostate cancer in the presence of an overall time factor: bad news, good news, or no news? *Int. J. Radiat. Oncol. Biol. Phys.* **85** 89–94

Wachter S, Gerstner N, Dorner D, Goldner G, Colotto A, Wambersie A and Pötter R 2002 The influence of a rectal balloon tube as internal immobilization device on variations of volumes and dose-volume histograms during treatment course of conformal radiotherapy for prostate cancer *Int. J. Radiat. Oncol. Biol. Phys.* **52** 91–100

Wang K K, Vapiwala N, Deville C, Plastaras J P, Scheuermann R, Lin H, Ad V B, Tochner Z and Both S 2012 A study to quantify the effectiveness of daily endorectal balloon for prostate intrafraction motion management *Int. J. Radiat. Oncol. Biol. Phys.* **83** 1055–63

Willoughby T R *et al* 2006 Target localization and real-time tracking using the Calypso 4D localization system in patients with localized prostate cancer *Int. J. Radiat. Oncol. Biol. Phys.* **65** 528–34

II

LOCALIZATION ACCURACY OF TWO ELECTROMAGNETIC TRACKING SYSTEMS IN PROSTATE CANCER RADIOTHERAPY: A COMPARISON WITH FIDUCIAL MARKER BASED KILOVOLTAGE IMAGING

by

Vanhanen, A. & Syrén, H. & Kapanen, M. 2018

Physica Medica vol 56, 10-18

DOI: 10.1016/j.ejmp.2018.11.007

Physica Medica 56 (2018) 10–18

Contents lists available at ScienceDirect

Physica Medica

journal homepage: www.elsevier.com/locate/ejmp

Original paper

Localization accuracy of two electromagnetic tracking systems in prostate cancer radiotherapy: A comparison with fiducial marker based kilovoltage imaging

A. Vanhanen[a,b,*], H. Syrén[c], M. Kapanen[a,b]

[a] Department of Oncology, Unit of Radiotherapy, Tampere University Hospital, POB-2000, 33521 Tampere, Finland
[b] Department of Medical Physics, Medical Imaging Center, Tampere University Hospital, POB-2000, 33521 Tampere, Finland
[c] Micropos Medical AB, Gothenburg, Sweden

ARTICLE INFO

Keywords:
Radiotherapy
Prostate
Interfraction motion
Intrafraction motion
Fiducial markers
kV-imaging
RayPilot
Calypso

ABSTRACT

The aim of this study was to evaluate the localization accuracy of electromagnetic (EM) tracking systems RayPilot (Micropos Medical AB) and Calypso (Varian Medical Systems) in prostate cancer radiotherapy. The accuracy was assessed by comparing couch shifts obtained with the EM methods to the couch shifts determined by simultaneous fiducial marker (FM) based orthogonal kilovoltage (kV) imaging. Agreement between the methods was compared using Bland-Altman analysis. Interfractional positional stability of the FMs, RayPilot transmitters and Calypso transponders was investigated. 582 fractions from 22 RayPilot patients and 335 fractions from 26 Calypso patients were analyzed. Mean (± standard deviation (SD)) differences between RayPilot and kV imaging were 0.3 ± 2.2, −2.2 ± 2.4 and −0.0 ± 1.0 mm in anterior-posterior (AP), superior-inferior (SI) and left-right (LR) directions, respectively. Corresponding 95% limits of agreement (LOA) were ± 4.3, ± 4.7 and ± 2.1 mm around the mean. Mean (± SD) differences between Calypso and kV imaging were −0.2 ± 0.6, 0.1 ± 0.5 and −0.1 ± 0.4 mm in AP, SI and LR directions, respectively, and corresponding LOAs were ± 1.3, ± 1.0 and ± 0.8 mm around the mean. FMs and transponders were stable: SD of intermarker and intertransponder distances was 0.5 mm. Transmitters were unstable: mean caudal transmitter shift of 1.8 ± 2.0 mm was observed. Results indicate that the localization accuracy of the Calypso is comparable to kV imaging of fiducials and the methods could be used interchangeably. The localization accuracy of the RayPilot is affected by transmitter instability and the positioning of the patient should be verified by other setup techniques. The study is part of clinical trial NCT02319239.

1. Introduction

Accurate treatment localization is crucial part of modern radiotherapy. Its importance is emphasized in prostate radiotherapy as the prostate position is known to change relative to bony structures and skin surface between the fractions (interfraction motion) [1–3] and during the treatment (intrafraction motion) [4–6]. The motion is mainly caused by variations in rectum and bladder filling and it can range up to 1–2 cm during the treatment course [7], intrafraction motion being generally smaller in extent, typically less than 5 mm [5,6]. Inaccuracies in the localization may deteriorate the target dose distribution [8]. Uncertainties in treatment localization, target delineation and treatment delivery are covered by planning target volume (PTV) margins around the clinical target volume (CTV). However, PTV margins expand the irradiated volume thus exposing larger volumes of nearby critical organs to high doses. High doses in rectum and bladder (especially trigone region) has been associated with late rectal bleeding [9] and incidence of acute and late urinary toxicity [9,10], respectively. Uncertainties in localization, and thus PTV margins, could be reduced by accurate and frequently performed localization methods.

Several localization methods, such as ultra-sound (US), kilovoltage (kV) and megavoltage (MV) imaging, cone beam computed tomography (CBCT) and the use of fiducial markers (FM) have been applied in image-guided radiotherapy (IGRT) of the prostate. US methods increase the localization accuracy when compared to positioning based only on skin marks [11] but clinically unacceptable accuracy have also been reported [12]. US probe pressure can cause prostate displacement if handled without care, which have been seen both for transabdmominal [13] and transperineal probes [14]. Several studies have compared the accuracy of US localization methods to kV and MV imaging using FMs

* Corresponding author.
E-mail address: antti.vanhanen@pshp.fi (A. Vanhanen).

https://doi.org/10.1016/j.ejmp.2018.11.007
Received 18 August 2018; Received in revised form 2 October 2018; Accepted 10 November 2018

and found latter methods outperforming the US [11,15,16]. MV and kV imaging as such have poor soft tissue contrast and positioning of the patient is based on alignment of bony structures. CBCT imaging provides three-dimensional (3D) information of the imaging volume but the poor soft tissue contrast limits the accuracy of identifying the prostate from surrounding tissues. FMs implanted into the prostate provide a surrogate for prostate position, as they are made of radiopaque material and are discerned well in kV or MV images. Implantation of the FMs is made prior to treatment planning and the localization is based on alignment of the markers in reference images and kV or MV images (2D match) or markers in planning CT and CBCT images (3D match). FMs have been in use since the 1990s and the feasibility of FMs in the IGRT of the prostate has been shown in many studies [2,17,18]. Imaging of FMs has proven to be reliable localization method having accuracy on the order of ≤ 1 mm [19] which reduces the systematic positioning error [20] and enables the margin reduction [21,22]. The imaging of FMs together with 3D soft tissue analysis is currently the most effective and widely available localization technique in the IGRT of the prostate [23] and is established practice in many radiotherapy clinics.

To monitor continuously the organ intrafraction motion a real-time electromagnetic (EM) localization system, Calypso (Varian Medical Systems), was introduced [24,25]. Calypso consists of three transponders implanted into the prostate and an EM source/receiver array which is setup above the patient during the treatment. Calypso provides real-time 3D position information of the three transponders and thus the prostate and can be used for localization and intrafraction motion tracking. Another EM tracking system currently in the market is RayPilot (Micropos Medical AB), which consists of a wired transmitter, implanted into the prostate for the treatment course and removed afterwards, and a detector array which is setup on the treatment couch [26]. RayPilot provides the 3D position of the transmitter in real-time and can also be used in localization and tracking of the prostate. EM systems provide a non-ionizing alternative to kV- and MV-imaging systems and high sampling rate of the systems guarantees that positional information of the prostate is not missed during the treatment.

The localization accuracy of Calypso have been investigated in many studies both in laboratory conditions [19,25,27–29] and in clinical situations [4,5,30–33] whereas there is a lack of information about the localization accuracy of RayPilot in clinical environment. Kindblom et al. [26] reported submillimeter accuracy of RayPilot in phantom fixture and compared 3D positional difference between RayPilot and orthogonal X-ray imaging when the transmitter was implanted in a urethral catheter. However, urethral catheter implantation does not represent the intended application method of implanting the transmitter into the prostate gland.

The aim of this study is to investigate the localization accuracy of the RayPilot and Calypso systems in comparison with fiducial marker based localization for a group of clinically treated prostate cancer patients. This is accomplished by comparing the translational couch shifts, proposed by the EM systems and couch shifts proposed by FM based kV-image alignment acquired simultaneously with the EM systems. Couch shifts represent the isocenter offsets recorded by the localization method in question. The stability and migration of the RayPilot transmitter, the gold seed fiducials and Calypso transponders are evaluated as well. To our knowledge, this is the first large study investigating the accuracy of the RayPilot system in clinical environment. The study is part of a clinical trial (ClinicalTrials.gov NCT02319239) which aims at developing extremely hypofractionated treatment protocol for prostate cancer.

2. Materials and methods

2.1. Electromagnetic localization methods

2.1.1. RayPilot tracking system

The RayPilot system is described in more detail in a previous study [34]. The system consists of a wired transmitter implanted into the prostate, a receiver plate positioned on the treatment couch and software for the transmitter position evaluation. Transmitter signal is read by the receiver plate which is calibrated to the machine isocenter and based on the coordinates of the transmitter coil center point (CP) and treatment isocenter in the planning CT, the system can locate the correct isocenter position relative to the observed transmitter position. The sampling frequency is 30 Hz and the location of the transmitter is given in AP, SI and LR directions. In addition to translational directions, the pitch (rotation around the LR axis) and yaw (rotation around the AP axis) angles of the transmitter are given. According to precision tests performed in a laboratory setting, the localization uncertainty of the two RayPilot systems used in this study is 0.60 ± 0.46 mm (radial mean $\pm$ SD).

2.1.2. Calypso tracking system

The Calypso system, its operating principle and transponders have been described in detail in earlier publications [24,25,35] and described here only briefly. The Calypso system consists of three transponders implanted into the prostate and EM source/receiver coil array positioned above the patient. The array detects the locations of the transponders which respond to EM signals sent by the array. The system is calibrated to the machine isocenter and the target alignment is based on the relations between the planned isocenter and transponder positions and detected transponder positions. The sampling frequency is 25 Hz (Calypso version 3.0) thus enabling real-time tracking besides of initial localization. The system gives the translational (AP, SI and LR) offsets of the isocenter which in isocenter tracking mode include the rotational offset compensation measured at the start of the localization and tracking. Rotational compensation is not used if the isocenter lies too far from the centroid of the transponders. Rotational changes are not compensated during the tracking either, but the translations are continuously tracked. Reported precision and accuracy of the system is 0.4 ± 0.4 mm and 0.1 ± 0.1 mm, respectively [28].

2.2. Patients and localization data acquisition

2.2.1. Patients with RayPilot

In this study, prostate localization data with the RayPilot was retrospectively gathered from a motion data of a previous study investigating the effect of rectal retractor device (RR) on prostate intrafraction motion [34]. Details of the patients, fractionation, treatment setup and planning are presented in that study and are covered here briefly, with the emphasis on localization procedures. Twelve patients were treated using moderate hypofractionation schedule 20×3 Gy based on CHHip-trial [36] and ten patients were treated using conventional schedule 39×2 Gy. If seminal vesicles (SV) were included in the treatment, the dose to SVs was 20×2.3 Gy in moderate hypofractionation schedule administered by simultaneous integrated boost technique and 28×2 Gy in conventional schedule. Three gold seed fiducial markers (Gold lock 3, Beam point AB, Sweden) and RayPilot transmitter were implanted into the prostate in separate sessions, on the average 3 weeks apart, at least one week prior to planning CT scan. Transmitter was implanted transperineally and gold seeds transrectally, both using endorectal US guidance. Treatment started one week after the planning CT and the transmitter was removed after the last treatment fraction. Patients were setup supine on the treatment couch by aligning setup lasers with reference skin marks. CBCT scans were acquired for subset of the fractions to volume analysis prior to the treatment. Localization of the treatment based on kV imaging of

fiducial markers: two orthogonal (kV source angle 0° and 90°, or 270° and 180°) kV images were acquired and aligned with digitally reconstructed reference images obtained from the planning CT using three gold seeds as fiducials. Image alignment was performed online and manually by experienced radiotherapists and isocenter offsets were corrected by corresponding translational couch shifts. Couch shifts were recorded for further analysis. All patients were treated with a TrueBeam STx (Varian Medical Systems) linear accelerator. The motion tracking with RayPilot was initialized prior the imaging and continued throughout the treatment session. The time points of the kV image acquisition were retrieved from the treatment system database and couch shifts proposed by the RayPilot system at the corresponding time points were recorded retrospectively from the RayPilot motion data. To ensure the correspondence of the couch shifts, the clocks of the RayPilot and treatment system computers were synchronized in the beginning of every treatment session. To evaluate the possible migration of the gold seed fiducials and transmitters, their Cartesian coordinates were recorded from the CBCT images which were first registered to corresponding planning CT image.

2.2.2. Patients with Calypso

Twenty-six Calypso patients treated between January 2016 and December 2017 were included in the study. Fourteen of the patients were treated using moderate hypofractionation scheme 20 × 3 Gy according to CHHip-trial [36] and twelve of the patients were treated using extreme hypofractionation scheme 5 × 7 Gy or 5 × 7.25 Gy. In the case of 7.25 Gy fractions, the region of prostatic urethra was delineated and was planned to get 7 Gy using simultaneous-integrated boost (SIB) technique. CTV was the prostate alone and PTV was formed by adding 3 mm margin posteriorly and 5 mm elsewhere around the CTV. Treatment technique was volumetric modulated arc therapy (VMAT) using two full, or two partial arcs (gantry 240° − 120°). Energies used were 6 MV for moderate hypofractionation schedule and 10 MV flattening filter free (FFF) for extreme hypofractionation schedule. Higher maximum dose rate of the FFF beams shortens the delivery time of large doses per fraction and thus used for extreme hypofractionation. Treatments were delivered with a TrueBeam STx (Varian Medical Systems) linear accelerator. Three Calypso transponders (either 14 G or 17 G) were implanted transrectally into the prostate before the planning CT scan. Transponders were implanted in triangular pattern, with intention to place them at least 1 cm apart from each other and avoiding urethra. Planning CT scan, with 1 or 2 mm slice thickness, was acquired one week after the implantation so that the prostate swelling had been reduced and the position of the transponders had been stabilized. Transponder x-, y- and z-coordinates were derived from the planning CT and their geometric mean was chosen as the isocenter position. We did not see difference in the coordinates between 1 and 2 mm slice thicknesses. Transponder and isocenter coordinates were exported to Calypso control computer. The treatment started on average 2–3 weeks after the planning CT. Patients were setup supine on the treatment couch by aligning setup lasers with reference skin marks. Self-made knee support was used. After the initial positioning, the Calypso localization mode was used to align the treatment isocenter with machine isocenter. After this, the localization was confirmed by orthogonal kV image pair, using transponders as fiducials. For extreme hypofractionated patients, a CBCT scan was acquired as well, to check the filling status of rectum and bladder. After the treatment course, the raw localization and tracking data was exported from Calypso system database for further analysis. Time points of kV image acquisition were derived from the treatment system database and Calypso readings were recorded from the tracking data at the same time points. As the Calypso data is sampled at 25 Hz frequency, the readings were averaged over one second at the kV image time points. Couch shifts proposed by the kV image pair alignment reflect the deviation of treatment isocenter from machine isocenter at imaging time points and should ideally be equal to the Calypso readings at the same time points. Calypso computer clock and the TrueBeam treatment system clock were synchronized retrospectively matching the beam starting time recorded by Calypso radiation detector with the starting time retrieved from the treatment system database. To evaluate the positional stability of the transponders, intertransponder distances were recorded from the Calypso treatment reports.

2.3. Data analysis

2.3.1. Agreement between the methods

Bland-Altman analysis was used to evaluate the agreement between kV based couch shifts and couch shifts proposed by EM localization methods. Bland-Altman analysis quantifies the agreement between two methods of clinical measurements using the differences between the observations made using the two methods on the same subjects [37,38]. In the current study the differences between couch shifts between kV imaging and EM methods were calculated. Analysis consists of a plot of differences between the methods against their mean. The mean value is used because the true value is not exactly known. The systematic bias, which is estimated by the mean difference $\bar{d}$, and standard deviation σ of the differences were calculated. To evaluate the agreement, the 95% limits of agreement (LOA) were calculated. The LOA defines the range within which 95% of all the differences between the methods are expected to lie, assuming the differences are normally distributed. The LOA were calculated using Eq. (1).

$$LOA = \bar{d} \pm 1.96\sigma \quad (1)$$

If the differences within LOA are clinically acceptable, the two methods could be used interchangeably. Considering relatively tight PTV margins used in our clinic, differences larger than ± 2 mm were considered clinically unacceptable. The percentages of differences within ± 1 and ± 2 mm were calculated. Descriptive statistics of the difference distributions was determined. The normality of the difference distributions was analyzed with the Shapiro-Wilks test.

2.3.2. Positional stability of the markers, transponders and transmitter

The positional stability of the fiducial markers, Calypso transponders and RayPilot transmitter affects the accuracy of the corresponding localization method as all of the methods assume stationary position of the planned isocenter relative to any of the markers implanted. The positional stability was evaluated by analyzing the intermarker and intertransponder distances during the treatment course. Intermarker Euclidean distances for any pair of the gold seed markers were calculated using the Cartesian coordinates of the gold seed CPs obtained from the CBCT images. Distances between the Calypso transponders were obtained from the Calypso treatment reports. SD of the intermarker and intertransponder distances was used as a measure of the positional stability. The transmitter migration during the treatment course was evaluated by calculating the change in the relative position between the centroid of the gold seed fiducials and transmitter CP compared to the initial relative position in the planning CT. The migration of a single marker has minimal effect on the position of the centroid of the three markers [39] and thus the centroid was chosen as the reference point for the evaluation of transmitter position change. The change in the transmitter position was determined in AP, SI and LR directions. The mean, SD and maximum values of the position change were calculated.

3. Results

3.1. Difference in couch shifts

A total of 582 paired data points from 582 RayPilot fractions were included in the Bland-Altman analysis for each translational direction. The number of Calypso fractions analyzed was 335. For some of the

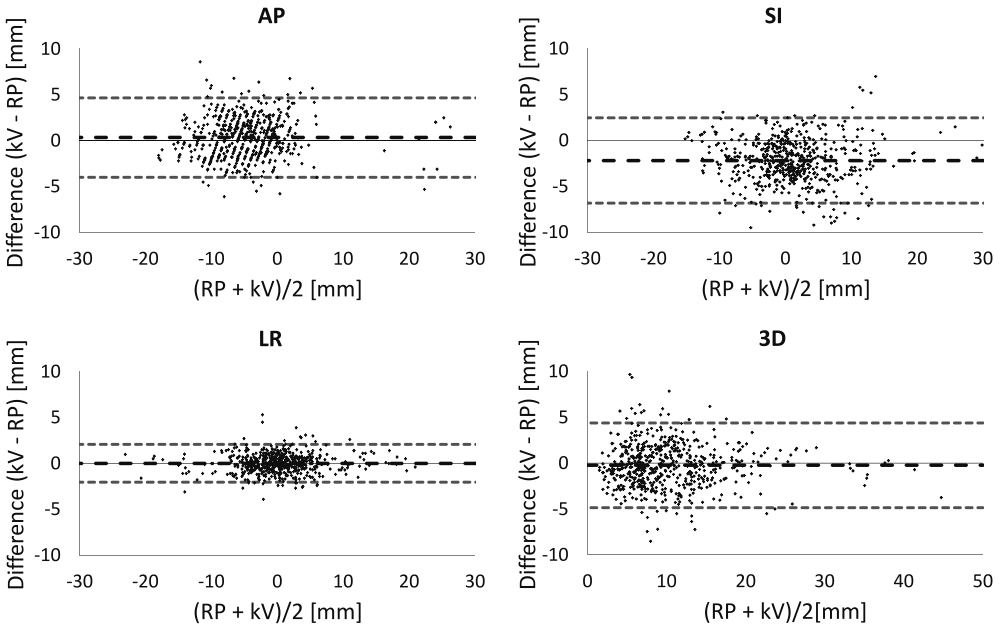

Fig. 1. Bland-Altman plots of the differences between RayPilot and kV imaging based couch shifts. Black dashed line shows mean difference, blue dashed lines represent 95% limits of agreement and black solid line is the line of identity.

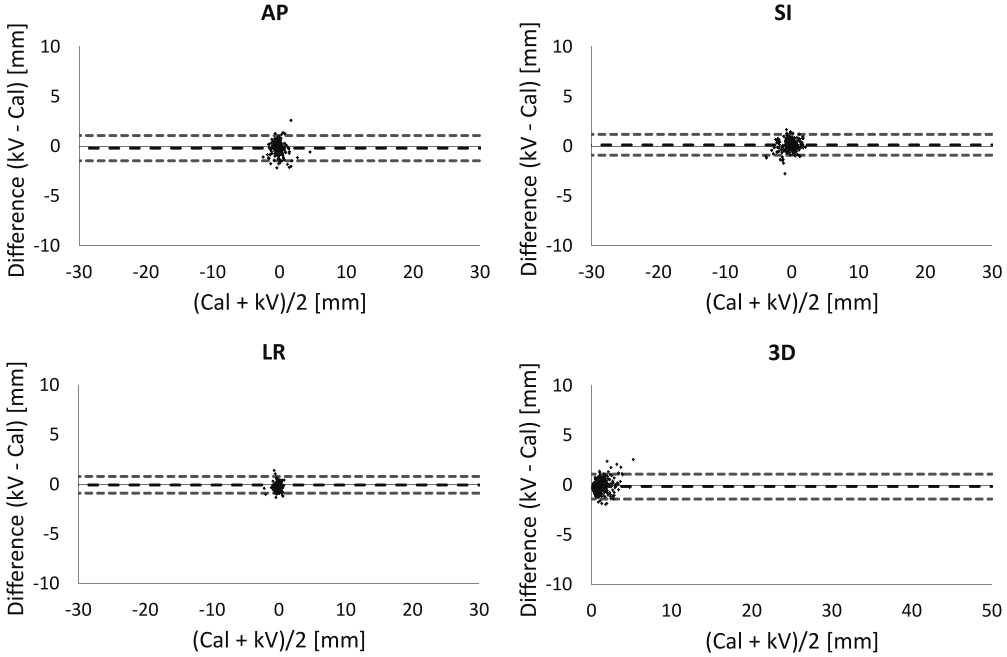

Fig. 2. Bland-Altman plots of the differences between Calypso and kV imaging based couch shifts. Black dashed line shows mean difference, blue dashed lines represent 95% limits of agreement and black solid line is the line of identity.

fractions one or both of the kV projections had to be repeated and these extra data points with corresponding Calypso readings were included in the analysis as well. SI information could be read from both orthogonal kV projections, whereas AP and LR information could be acquired only from projections perpendicular to corresponding axis. Eventually, for Calypso fractions, the number of paired data points included in the Bland-Altman analysis was 353, 700 and 347 for AP, SI and LR directions, respectively. Bland-Altman plots of the couch shift differences between RayPilot and kV imaging and between Calypso and kV imaging are presented in Figs. 1 and 2, respectively. Mean difference, SD, LOA

Table 1
The results of the Bland-Altman analysis: differences in couch shifts between RayPilot and kV imaging, and between Calypso and kV imaging. Positive values in AP-, SI- and LR-axes represent couch shifts towards anterior, inferior and left directions. All values are given in mm. Also presented are the percentages of differences within ± 1 and ± 2 mm.

	AP		SI		LR		3D	
	RayPilot	Calypso	RayPilot	Calypso	RayPilot	Calypso	RayPilot	Calypso
Bias (mean)	0.3	−0.2	−2.2	0.1	−0.0	−0.1	−0.2	−0.1
SD	2.2	0.6	2.4	0.5	1.0	0.4	2.4	0.6
Upper LOA	4.6	1.1	2.5	1.2	2.1	0.8	4.4	1.1
Lower LOA	−4.0	−1.5	−6.8	−0.9	−2.0	−0.9	−4.8	−1.4
≤1 mm [%]	32.3	88.7	22.9	93.1	69.4	96.5	35.2	88.8
≤2 mm [%]	64.6	98.6	44.0	99.6	94.8	100.0	63.4	99.1

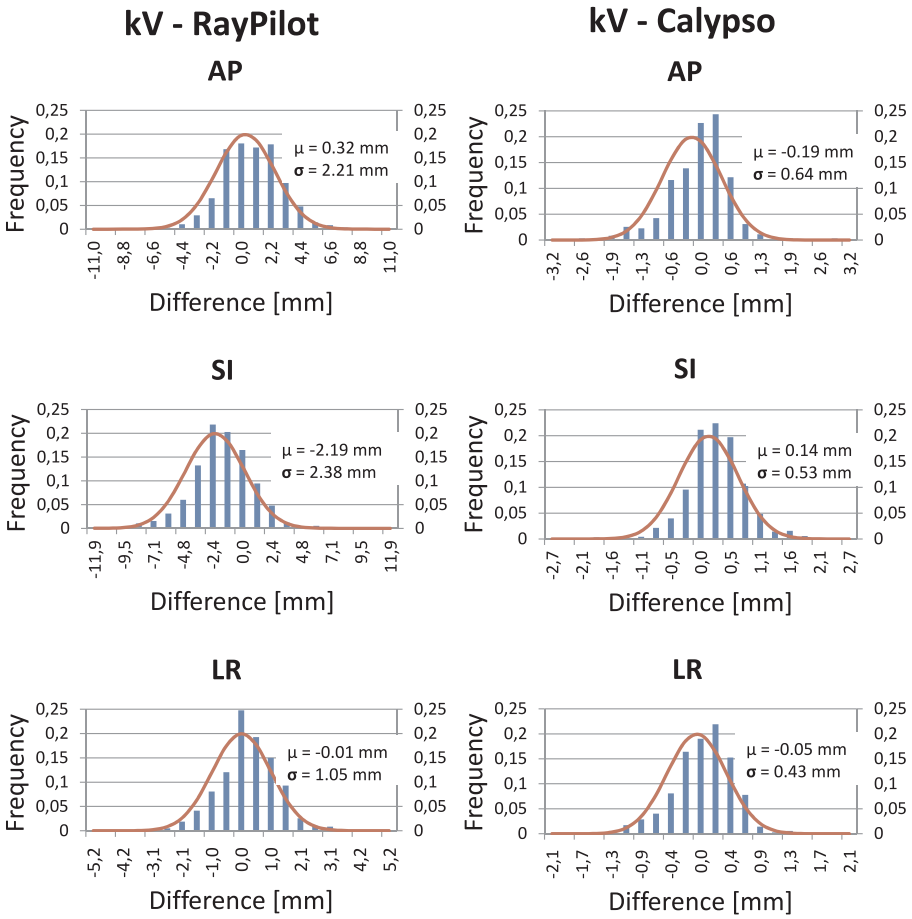

Fig. 3. Couch shift difference distributions in AP, SI and LR directions. Red curve is the normal distribution with the same mean and SD of the observed differences demonstrating good agreement and thus validity of the obtained LOA values.

and percentage of the differences within ± 1 and ± 2 mm are presented in Table 1. Positive values indicate couch shifts towards anterior, inferior and left directions and kV > RayPilot/Calypso. The LOAs for the AP, SI and LR couch shifts between RayPilot and kV imaging were ± 4.3, ± 4.7 and ± 2.1 mm around the mean, respectively. The LOAs for the AP, SI and LR couch shifts between Calypso and kV imaging were ± 1.3, ± 1.0 and ± 0.8 mm around the mean, respectively. Histograms of the difference distributions are presented in Fig. 3 and descriptive statistics of the distributions are presented in Table 2.

3.2. Positional stability of the markers, transponders and transmitter

The coordinates of the gold markers and transmitter CPs were determined for 324 RayPilot fractions over the treatment course and 44 planning CT images of the 22 RayPilot patients. Intermarker distances as well as the position of the transmitter CP relative to the centroid of the gold markers were calculated for all 368 instances. The mean SD of the intermarker distances was 0.5 mm. Gold seeds were generally very stable but for one patient one of the gold markers had migrated 6 mm

Table 2
Descriptive statistics of the difference distributions (all values are given in mm). Also presented are *p*-values of the Shapiro-Wilks normality tests.

	AP		SI		LR	
	kV-RayPilot	kV-Calypso	kV-RayPilot	kV-Calypso	kV-RayPilot	kV-Calypso
Mean	0.32	−0.19	−2.18	0.14	0.01	−0.05
SD	2.21	0.64	2.38	0.53	1.05	0.43
Skewness	0.154	−0.426	−0.124	−0.165	0.295	−0.210
Kurtosis	0.129	1.715	0.861	2.711	1.942	0.475
Shapiro-Wilks	0.129	0.000	0.001	0.000	0.000	0.008

Table 3
Position change of the RayPilot transmitter relative to the centroid of the gold seed markers during the treatment course. All values are given in mm.

	AP	SI	LR	3D
Mean	−0.3	−1.8	−0.2	2.8
SD	1.6	2.0	0.8	1.6
Max	−7.3	−7.6	−3.5	9.2

caudally between the first and the second fraction. The cause for such large migration was that the marker had drifted into the transmitter implantation canal, transmitter being implanted too near to the marker. For this patient the evaluation of the transmitter position stability was determined against the centroid of the two stabile gold markers. The change in the transmitter position relative to the centroid of the gold seeds was evaluated for 324 fractions and the mean, SD and maximum values of the position change are presented in Table 3. An example of intermarker distances and change in the transmitter position during the treatment course for a single patient are presented in Fig. 4. Transmitter position shifts were clearly visible in localization kV images as well (Fig. 5). The effect of the transmitter migration on the RayPilot positioning accuracy was evaluated by correcting the RayPilot readings with the offsets recorded from CBCT images and comparing couch shifts from migration corrected fractions against kV imaging based couch shifts from corresponding fractions using Bland-Altman analysis. The number of fractions in the analysis was 317. The results are presented in Table 4.

Calypso intertransponder distances were determined for all of the 335 fractions and 26 planning CT images. The mean SD of the Calypso intertransponder distances was 0.5 mm. Though the transponders were generally very stable, there were three occasions of larger migration: one transponder was implanted near the urethra and it was voided between the planning CT and the first treatment fraction. Similar incident has been reported also by Kupelian et al. [4] and Litzenberg et al. [35]. Voided transponder was excluded from the Calypso localization system and the tracking was executed with the two remaining transponders. In another patient one transponder had moved 6 mm caudally between the planning CT and the first fraction. As this patient was treated with extreme hypofractionation, new planning CT and treatment plan was made to ensure accurate localization and safe treatment. In third patient one transponder was placed near the rectum wall and it migrated cranially 3.8 mm during the treatment course. This had small effect on the localization accuracy of Calypso in SI direction, which was seen in > 1 mm mean difference in couch shifts between Calypso and kV imaging.

4. Discussion

In the current study the positioning accuracy of RayPilot and Calypso positioning systems was evaluated against the orthogonal kV imaging using fiducial markers by comparing the couch shifts proposed by the different methods.

Bland-Altman analysis shows that the differences between the RayPilot and kV imaging were largely dispersed in AP (range −6.1, 8.6 mm) and SI (range −10.3, 7.0 mm) directions. In addition to this, a notable mean difference (−2.2 ± 2.4 mm) was seen in SI direction indicating that RayPilot suggested larger superiorly directed couch shifts than kV imaging did. LOAs in AP and SI directions were above the clinically acceptable 2 mm limit and only 64.6% (AP) and 44.0% (SI) of the differences were within 2 mm. In a technical feasibility study, a difference of 1.7 ± 1.0 mm in a 3D position shift of the transmitter was found between RayPilot and orthogonal kV imaging [26]. In the current study the mean difference (± SD) between the 3D offsets was −0.23 ± 2.4 mm (range −8.5, 9.7 mm). The mean difference was smaller in the current study, but the variation in differences was larger. However, studies are not fully comparable because of a different kind of in vivo application of the transmitter and a lot smaller sample number in the study of Kindblom et al. [26].

In contrast to RayPilot, couch shifts proposed by Calypso agreed well with the couch shifts suggested by the kV imaging: mean differences were negligible and the scattering of differences around the mean was small. 98.6%, 99.6% and 100% of the differences in AP, SI and LR directions, respectively, were within 2 mm.

No trends were observed in the Bland-Altman analysis. Small differences between Calypso and kV imaging based localizations indicate

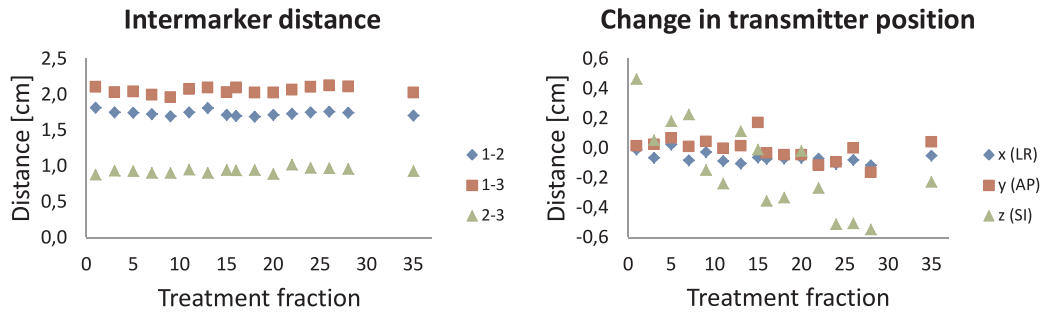

Fig. 4. On left: intermarker distances for one patient during the treatment course. On right: change in the distance between RayPilot transmitter and the centroid of the gold seed markers for the same patient.

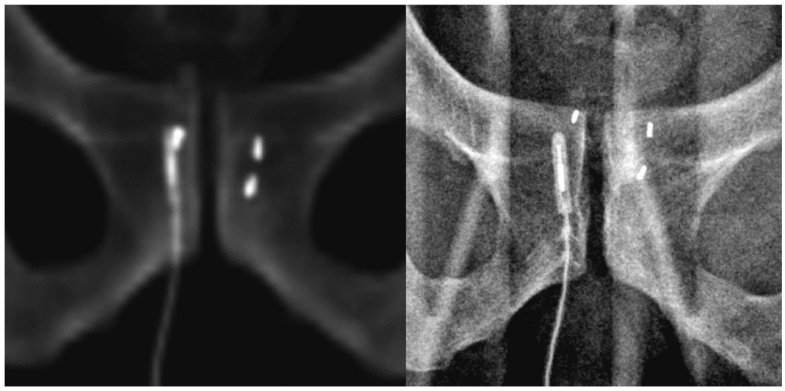

Fig. 5. On left: reference DRR-image of transmitter and gold seeds, reconstructed from planning CT. On right: corresponding kV-image at 28th treatment fraction. 5 mm caudal migration of the transmitter can be seen between the images. Difference on distance between the gold seeds and pubic bones reveals notable prostate interfraction motion.

Table 4
The results of the Bland-Altman analysis of the couch shift difference between migration corrected RayPilot values and kV imaging. All values are given in mm. Also presented are the percentages of differences within ± 1 and ± 2 mm.

	AP	SI	LR
Bias (mean)	0.1	−0.7	0.3
SD	1.7	1.9	1.2
Upper LOA	3.4	2.9	2.6
Lower LOA	−3.2	−4.3	−2.0
≤1 mm [%]	41.6	44.8	79.2
≤2 mm [%]	78.5	75.7	94.6

accurate performance of both of the methods. The uncertainty of the kV image guidance system including treatment couch movements was measured weekly according to the quality assurance (QA) program of Yoo et al. [40] and was ≤1 mm for all treatments in the current study. Thus it can be assumed that large differences between RayPilot and kV imaging are mainly due to inaccuracies related to RayPilot localization. Larger couch shifts seen with the RayPilot than with the Calypso in Bland-Altman plots are caused by the differences in localization procedure: the kV imaging was used as the primary localization method with RayPilot patients whereas it was used only to verify the Calypso localization with Calypso patients. However, this does not have any effect on the differences seen in the couch shifts between the RayPilot and kV imaging.

The differences between Calypso and kV imaging found in the current study agree with those found in literature: Bell et al. [33] compared the localization accuracy between Calypso and image guided techniques including orthogonal kV imaging and CBCT and found mean differences of 0.2, −0.6 and 0.6 mm in AP, SI and LR directions, respectively. Variation in all directions was less than 0.6 mm. Foster et al. [32] found mean differences (± SD) of −0.09 ± 1.40, 0.48 ± 1.50 and 0.08 ± 1.04 mm in AP, SI and LR directions, respectively, between Calypso and kV imaging. Mean differences between Calypso and kV imaging found by Ogunleye et al. [30] were 1.2 ± 0.9, 1.1 ± 0.9 and 0.7 ± 0.5 mm in AP, SI and LR directions, respectively. Earlier results of Willoughby et al. [31] and Kupelian et al. [4] showed average (± SD) 3D differences of 1.5 ± 0.9 mm and 1.9 ± 1.2 mm between Calypso and radiographic localizations, but their methods suffered from large time gap (3–5 min) between the localizations with different systems and their results were probably affected by the prostate intrafraction motion. Differences found in the current study are even close to the results reported in phantom studies [29–31]. Small differences observed in the current study are likely explained by the localization time points, which were defined and synchronized with high accuracy, thus eliminating the effect of prostate intrafraction motion. In addition, transponders were very stable, mean SD of the intertransponder distances was even smaller than seen elsewhere [4,35], confirming the consistency between the observed and planned geometries between the transponders and the isocenter. However, migration of the transponders, if large enough, may affect the Calypso localization accuracy, which was seen with the patient for which one of the transponders migrated 3.8 mm. In this kind of cases the kV image matching is based on the two stabile markers in our clinic, which might explain the difference seen between the two systems. Small changes in the position of the transponders did not seem to have clinically relevant effect on the localization accuracy of the Calypso which is consistent with the findings of Pouliot et al. [39] with gold seed markers. If larger migration is seen, it would be advisable to either exclude the migrated transponder from the localization plan, or to re-do the planning CT. However, defining a maximum allowable limit for the transponder migration was out of scope of this study.

Gold seed marker migration was negligible, which is consistent with earlier findings [18,41–43] and similar to Calypso transponders in the current study. Instead, considerable variation was seen in the position of the transmitter relative to the centroid of the gold seeds, especially in AP and SI directions. Most notably, averaged over all patients and fractions investigated, there was a systematic 1.8 ± 2.0 mm caudally directed shift of the transmitter when compared to the initial position in planning CT. Maximum shifts were 7.3 mm anteriorly and 7.6 mm caudally. These findings agree with the results of Braide et al. [44], who found mean SI and 3D transmitter shifts for different patients within a range of −2.3 to 4.5 mm, and 1.6–6.2 mm, respectively. The most probable reason for the caudal shift is that the transmitter cable remains outside of the body during the treatment course and is exposed to pulling forces which affects to the stability of the transmitter, if not handled with care. It is also possible, that some of the relative position shifts in SI and AP directions are consequence of prostate rotation around the lateral axis (pitch), which can have larger effect on transmitter than on gold seeds, especially if the transmitter is implanted into peripheral area of the prostate, far from the isocenter. Shifts in the SI position of the transmitter were seen over the whole treatment course, as can be seen in Fig. 4, and separate analysis of transmitter position shifts for RR and non-RR fractions (data not shown) showed no differences in detected position shifts indicating that the use of RR in part of the fractions did not have influence on the stability of the transmitter. Problems with the cable were seen in many occasions within the group of patients in this study. Changes in the SI position of the transmitter affected also to the AP position of the transmitter coil CP, in cases where the implantation angle was oblique.

Changes in rectum and bladder filling deform the prostate which may alter the distances between markers, transmitter and the isocenter. However, small changes in marker positions cause negligible displacement of their centroid [39], whereas the distance between single transmitter and the isocenter is directly affected. Thus the RayPilot

localization accuracy may have been affected by deformation in contrast to FMs. In general, due to prostate deformation, at least two fiducials are recommended to achieve accurate and reproducible alignment [45].

The effect of transmitter migration on the localization accuracy of the RayPilot was evaluated by comparing the migration corrected RayPilot localization values with corresponding kV-imaging based localization values. Mean difference and variation in differences decreased in AP and especially in SI direction but the LOAs were still larger than clinically acceptable 2 mm (Table 4). However, results indicate that the transmitter migration is likely the major factor deteriorating the absolute localization accuracy of the RayPilot. In addition to susceptibility to transmitter migration, the accuracy of the method is affected by the subjective determination of the transmitter coil CP coordinates from the planning CT. In spite of slice thickness from 0.5 to 1 mm used in planning CT [34], we noticed differences up to 2 mm in the CP position defined by different physicists, due to limited resolution of the CT images. Errors ≥ 0.5 mm in the transmitter CP were corrected retrospectively in the RayPilot localization data for the analysis but it was approximated that the residual error in the CP position determination was still ± 1 mm. Due to human error, manual time synchronization between treatment and RayPilot computers was not done in some fractions. In these cases the synchronization was done retrospectively by matching the treatment field start and end times with setup and treatment part records of the RayPilot tracking data. After the corrections, the residual time synchronization error was approximated to be within ± 15 s and ± 30 s at its worst. Time difference between the imaging modalities might cause inaccuracies to the data because of the intrafraction prostate motion and in order to evaluate its potential effect on localization differences, the tracking data was analyzed. Mean (± SD) absolute shift in prostate intrafraction position during any 10, 20, or 30 s intervals starting during the first 3 min of tracking in which the kV images were acquired, was $\leq 0.2 \pm 0.3$ mm. Maximum motion in any direction seen within 10, 20 and 30 s intervals, was 4.4, 8.1 and 9.7 mm, respectively. However, in 98.4% of the 30 s intervals, the motion was < 1 mm and in shorter intervals motions larger than 1 mm were even rarer. Motions < 1 mm did not affect much to the couch values suggested by the RayPilot, as the version of the RayPilot software used in this study reported the desired couch values in 1 mm resolution. Thus the prostate intrafraction motion may have had small, but practically negligible, effect on the differences seen between the RayPilot and kV imaging based localizations. Among the many possible sources of error is the couch bending which can be defined with an accuracy of 1 mm and which is defined for every patient and taken into account in the RayPilot software. It affects the AP and SI locations and might cause some variation seen in the results. RayPilot array was calibrated into the machine isocenter prior the treatments and the daily quality assurance checks were made in order to confirm the proper functioning of the device. As a conclusion, the accuracy of the RayPilot localization is affected by many factors including transmitter migration, deformation of the prostate, the uncertainty in determination of the transmitter CP, treatment couch bending and intrinsic precision and accuracy of the system. Though the absolute localization accuracy of the RayPilot may not be high enough for interfraction localization of the prostate, the tracking function could still be used for intrafraction motion tracking, as the tracking starting point can be calibrated to the initial isocenter defined by other means, such as kV or CBCT imaging, preferably with fiducial markers. However, the accuracy of the intrafraction motion tracking is based on the assumption of stable transmitter position during the treatment fraction. The examination of intrafraction stability of the transmitter and the accuracy of the intrafraction motion tracking were out of scope of this study.

Resolution of the DRR images could potentially affect to the accuracy of the matching of FMs. Using of thinner CT slices result in better resolution and visibility of the FMs in DRR images (measured FM length was on average 0.3 mm shorter in DRRs reconstructed from 1 mm slices compared to 2 mm slices) but the effect on the CPs and the centroid of the FMs is negligible. In addition, as the kV matching was performed similarly for all patients in the study, possible inaccuracies in kV matching did not affect to the results on the agreement between different EM methods and kV imaging.

Bland-Altman method assumes that the differences between the methods compared are normally distributed. According to Shapiro-Wilk test, only the differences in AP direction between RayPilot and kV imaging were normally distributed ($p > 0.05$). However, with the sample sizes > 300, Shapiro Wilk test may be unreliable [46,47] and difference histograms (Fig. 3) reveal that the differences are distributed quite evenly around the mean. According to skewness and kurtosis of the distributions, none of the distributions deviate substantially from the normal distribution. Threshold value for a clinically significant difference between the localization methods was chosen to be 2 mm. This value was based on the localization accuracy of the kV imaging of fiducial markers and relatively small PTV margins used in our clinic. Using looser criteria for the localization accuracy would require larger margins which would expose critical organs to higher doses.

One of the limitations of the current study is that it is a single-institution study having patient number of 22 with RayPilot and 26 with Calypso. Larger patient groups would give more insight into the effect of FM, transponder or transmitter placement on the accuracy of the corresponding localization method. However, the patient number and especially the number of fractions analyzed were large enough to show the differences between the localization methods. One clear benefit of this study is the comparison of the EM methods to simultaneously performed, and widely used, kV imaging of fiducials, which gives good conception of the accuracy of the EM methods in prostate localization. As the study was retrospective, preceding phantom studies were not carried out to evaluate the intrinsic limitations of the accuracy of the methods. However, calibration and regular QA of the systems ensured the repeatability and accuracy of the measurements.

5. Conclusions

The results of the current study indicate that, mainly due to the instability of the transmitter, the localization accuracy of the RayPilot system in clinical circumstances is not equivalent to kV imaging of fiducial markers and is not adequate for interfraction localization of the prostate as such. RayPilot could be used for intrafractional motion tracking, but the initial localization should be made by some other means such as kV or CBCT imaging of fiducial markers. Instead, the results imply that 95% of the differences between the localizations of Calypso and kV imaging of transponders as fiducials can be expected to lie within ± 1.3 in any of the AP, SI or LR axes, which was considered clinically acceptable. After confirming that the observed transponder geometry fits the planned geometry, Calypso may be used interchangeably with the kV imaging of fiducials. The advantage of the RayPilot is that the transmitter is removed after the treatment course enabling post-treatment follow up with magnetic resonance imaging (MRI), which is not possible with Calypso due to significant MRI artifacts from the transponders staying in the prostate. Independent clinical studies are needed to confirm the results of the current study regarding the localization accuracy of the RayPilot system.

Acknowledgements

This study was financially supported by the Seppo Nieminen funding, Grant number 15012, Tampere University Hospital. H Syrén is an employee of Micropos Medical AB.

References

[1] Balter JM, Sandler HM, Lam K, Bree RL, Lichter AS, Ten Haken RK. Measurement of prostate movement over the course of routine radiotherapy using implanted

markers. Int J Radiat Oncol Biol Phys 1995;31:113–8.
[2] Crook JM, Raymond Y, Salhani D, Yang H, Esche B. Prostate motion during standard radiotherapy as assessed by fiducial markers. Radiother Oncol 1995;37:35–42.
[3] Padhani AR, Khoo VS, Suckling J, Husband JE, Leach MO, Dearnaley DP. Evaluating the effect of rectal distension and rectal movement on prostate gland position using cine MRI. Int J Radiat Oncol Biol Phys 1999;44:525–33.
[4] Kupelian P, Willoughby T, Mahadevan A, Djemil T, Weinstein G, Jani S, et al. Multi-institutional clinical experience with the Calypso system in localization and continuous, real-time monitoring of the prostate gland during external radiotherapy. Int J Radiat Oncol Biol Phys 2007;67:1088–98.
[5] Langen KM, Willoughby TR, Meeks SL, Santhanam A, Cunningham A, Levine L, et al. Observations on real-time prostate gland motion using electromagnetic tracking. Int J Radiat Oncol Biol Phys 2008;71:1084–90.
[6] Tong X, Chen X, Li J, Xu Q, Lin M, Chen L, et al. Intrafractional prostate motion during external beam radiotherapy monitored by a real-time target localization system. J Appl Clin Med Phys 2015;16(2):51–61.
[7] Langen KM, Jones DT. Organ motion and its management. Int J Radiat Oncol Biol Phys 2001;50:265–78.
[8] Bell K, Dzierma Y, Morlo M, Nüsken F, Licht N, Rübe C. Image guidance in clinical practice – influence of positioning inaccuracy on the dose distribution for prostate cancer. Phys Med 2018;46:81–8.
[9] Landoni V, Fiorino C, Cozzarini C, Sanguineti G, Valdagni R, Rancati T. Predicting toxicity in radiotherapy for prostate cancer. Phys Med 2016;32:521–32.
[10] Improta I, Palorini F, Cozzarini C, Rancati T, Avuzzi B, Franco P, et al. Bladder spatial-dose descriptors correlate with acute urinary toxicity after radiation therapy for prostate cancer. Phys Med 2016;32:1681–9.
[11] Serago CF, Buskirk SJ, Igel TC, Gale AA, Serago NE, Earle JD. Comparison of daily megavoltage electronic portal imaging with marker seeds to ultrasound imaging or skin marks for prostate localization and treatment positioning in patients with prostate cancer. Int J Radiat Oncol Biol Phys 2006;65:1585–92.
[12] Robinson D, Liu D, Steciw S, Field C, Daly H, Saibishkumar EP, et al. An evaluation of the Clarity 3D ultrasound system for prostate localization. J Appl Clin Med Phys 2012;13(4):100–12.
[13] Dobler B, Mai S, Ross C, Wolff D, Wertz H, Lohr F, et al. Evaluation of possible prostate displacement induced by pressure applied during transabdominal ultrasound image acquisition. Strahlenther Oncol 2006;182:240–6.
[14] Li M, Hegemann N, Manapov F, Kolberg A, Thum PD, Ganswindt U, et al. Prefraction displacement and intrafraction drift of the prostate due to perineal ultrasound probe pressure. Strahlenther Oncol 2017;193:459–65.
[15] Van den Heuvel F, Powell T, Seppi E, Littrupp P, Khan M, Wang Y, et al. Independent verification of ultrasound based image-guided radiation treatment, using electronic portal imaging and implanted gold markers. Med Phys 2003;30(11):2878–87.
[16] Scarbrough TJ, Golden NM, Ting JY, Fuller CD, Wong A, Kupelian PA, et al. Comparison of ultrasound and implanted seed marker prostate localization methods: implications for image-guided radiotherapy. Int J Radiat Oncol Biol Phys 2006;65:378–87.
[17] Herman MG, Pisansky TM, Kruse JJ, Prisciandaro JI, Davis BJ, King BF. Technical aspects of daily online positioning of the prostate for three-dimensional conformal radiotherapy using and electronic portal imaging device. Int J Radiat Oncol Biol Phys 2003;57:1131–40.
[18] van der Heide UA, Kotte AN, Dehnad H, Hofman P, Lagenijk JJ, van Vulpen M. Analysis of fiducial marker-based position verification in the external beam radiotherapy of patients with prostate cancer. Radiother Oncol 2007;82:38–45.
[19] Santanam L, Malinowski K, Hubenshmidt J, Dimmer S, Mayse ML, Bradley J, et al. Fiducial-based translational localization accuracy of electromagnetic tracking system and on-board kilovoltage imaging system. Int J Radiat Oncol Biol Phys 2008;70:892–9.
[20] McNair HA, Hansen VN, Parker CC, Evans PM, Norman A, Miles E, et al. A comparison of the use of bony anatomy and internal markers for offline verification and an evaluation of the potential benefit of online and offline verification protocols for prostate radiotherapy. Int J Radiat Oncol Biol Phys 2008;71:41–50.
[21] Schallenkamp JM, Herman MG, Kruse JJ, Pisansky TM. Prostate position relative to pelvic bony anatomy based on intraprostatic gold markers and electronic portal imaging. Int J Radiat Oncol Biol Phys 2005;63:800–11.
[22] Chen J, Lee RJ, Handrahan D, Sause WT. Intensity-modulated radiotherapy using implanted fiducial markers with daily portal imaging: assessment of prostate organ motion. Int J Radiat Oncol Biol Phys 2007;68:912–9.
[23] O'Neill AG, Jain S, Hounsell AR, O'Sullivan JM. Fiducial marker guided prostate radiotherapy: a review. Br J Radiol 2016;89(1068):20160296.
[24] Mate TP, Krag D, Wright JN, Dimmer S. A new system to perform continuous target tracking for radiation and surgery using non-ionizing alternating current electromagnetics. Int J Comput Assisted Radiol Surg 2004;1268:425–30. (CARS 2004—Proc. of the 18th Int. Congress and Exhibition (Chicago, USA, 23–26 June 2004)).
[25] Balter JM, Wright JN, Newell LJ, Friemel B, Dimmer S, Cheng Y, et al. Accuracy of a wireless localization system for radiotherapy. Int J Radiat Oncol Biol Phys 2005;61:933–7.
[26] Kindblom J, Ekelund-Olvenmark A, Syren H, Iustin R, Braide K, Frank-Lissbrant I, et al. High precision transponder localization using a novel electromagnetic positioning system in patients with localized prostate cancer. Radiother Oncol 2009;90:307–11.
[27] Murphy MJ, Eidens R, Vertatschitsch E, Wright JN. The effect of transponder motion on the accuracy of the Calypso electromagnetic localization system. Int J Radiat Oncol Biol Phys 2008;72:295–9.
[28] Franz AM, Schmitt D, Seitel A, Chatrasingh M, Echner G, Oelfke U, et al. Standardized accuracy assessment of the calypso wireless transponder tracking system. Phys Med Biol 2014;59:6797–810.
[29] Hamilton DG, McKenzie DP, Perkins AE. Comparison between electromagnetic transponders and radiographic imaging for prostate localization: a pelvic phantom study with rotations and translations. J Appl Clin Med Phys 2017;18:43–53.
[30] Ogunleye T, Rossi PJ, Jani AB, Fox T, Elder E. Performance evaluation of Calypso 4D localization and kilovoltage imagine guidance systems for interfraction motion management of prostate patients. Sci World J 2009;9:449–58.
[31] Willoughby TR, Kupelian PA, Pouliot J, Shinohara K, Aubin M, Roach M, et al. Target localization and real-time tracking using the Calypso 4D localization system in patients with localized prostate cancer. Int J Radiat Oncol Biol Phys 2006;65:528–34.
[32] Foster RD, Pistenmaa DA, Solberg TD. A comparison of radiographic techniques and electromagnetic transponders for localization of the prostate. Radiat Oncol 2012;7:101.
[33] Bell LJ, Eade T, Kneebone A, Hruby G, Alfieri F, Bromley R, et al. Initial experience with intra-fraction motion monitoring using Calypso guided volumetric modulated arc therapy for definitive prostate cancer treatment. J Med Radiat Sci 2017;64(1):25–34.
[34] Vanhanen A, Kapanen M. The effect of rectal retractor on intrafraction motion of the prostate. Biomed Phys Eng Express 2016;2:035021.
[35] Litzenberg DW, Willoughby TR, Balter JM, Sandler HM, Wei J, Kupelian PA, et al. Positional stability of electromagnetic transponders used for prostate localization and continuous, real-time tracking. Int J Radiat Oncol Biol Phys 2007;68:1199–206.
[36] Dearnaley D, Syndikus I, Sumo G, Bidmead M, Bloomfield D, Clark C, et al. Conventional versus hypofractionated high-dose intensity-modulated radiotherapy for prostate cancer: preliminary safety results from the CHHiP randomized controlled trial. Lancet Oncol 2012;13(1):43–54.
[37] Bland JM, Altman DG. Statistical methods for assessing agreement between two methods of clinical measurement. Lancet 1986;327(8476):307–10.
[38] Bland JM, Altman DG. Measuring agreement in method comparison studies. Stat Methods Med Res 1999;8(2):135–60.
[39] Pouliot J, Aubin M, Langen KM, Liu Y-M, Pickett B, Shinohara K, et al. (Non)-migration of radiopaque markers used for on-line localization of the prostate with an electronic portal imaging device. Int J Radiat Oncol Biol Phys 2003;56:862–6.
[40] Yoo S, Kim G-Y, Hammoud R, Elder E, Pawlicki T, Guan H, et al. A quality assurance program for the on-board imager. Med Phys 2006;33(11):4431–47.
[41] Litzenberg D, Dawson LA, Sandler H, Sanda MG, McShan DL, Ten Haken RK, et al. Daily prostate targeting using implanted radiopaque markers. Int J Radiat Oncol Biol Phys 2002;52:699–703.
[42] Poggi MM, Gant DA, Sewchand W, Warlick WB. Marker seed migration in prostate localization. Int J Radiat Oncol Biol Phys 2003;56:1248–51.
[43] Kupelian P, Willoughby TR, Meeks SL, Forbes A, Wagner T, Maach M, et al. Intraprostatic fiducials for localization of the prostate gland: monitoring intermarker distances during radiation therapy to test for marker stability. Int J Radiat Oncol Biol Phys 2005;62:1291–6.
[44] Braide K, Lindencrona U, Welinder K, Götstedt J, Ståhl I, Pettersson N, et al. Clinical feasibility and positional stability of an implanted wired transmitter in a novel electromagnetic positioning system for prostate radiotherapy. Radiother Oncol 2018;128:336–42.
[45] Kudchadker RJ, Lee AK, Yu ZH, Johnson JL, Zhang L, Zhang Y, et al. Effectiveness of using fewer implanted fiducial markers for prostate target alignment. Int J Radiat Oncol Biol Phys 2009;74:1283–9.
[46] Ghasemi A, Zahediasl S. Normality tests for statistical analysis: a guide for non-statisticians. Int J Endocrinol Metab 2012;10(2):486–9.
[47] Kim HY. Statistical notes for clinical researches: assessing normal distribution (2) using skewness and kurtosis. Restor Dent Endod 2013;38(1):52–4.

III

DOSIMETRIC EFFECT OF INTRAFRACTION MOTION AND DIFFERENT LOCALIZATION STRATEGIES IN PROSTATE SBRT

by

Vanhanen, A. & Poulsen, P. & Kapanen, M. 2020

Manuscript.

Dosimetric effect of intrafraction motion and different localization strategies in prostate SBRT

A Vanhanen[1,2], P Poulsen[3], M Kapanen[1,2]

[1]Department of Oncology, Unit of Radiotherapy, Tampere University Hospital, POB-2000, 33521 Tampere, Finland
[2]Department of Medical Physics, Medical Imaging Center, Tampere University Hospital, POB-2000, 33521 Tampere, Finland
[3]Department of Oncology and Danish Center for Particle Therapy, Aarhus University Hospital, Palle Juul-Jensens Boulevard 25, Entrance B3, 8200 Aarhus N, Denmark

E-mail: antti.vanhanen@pshp.fi

Abstract

The aim of this study was to evaluate the dosimetric effect of continuous motion monitoring based localization (Calypso, Varian Medical Systems), gating and intrafraction motion correction in prostate SBRT. Delivered doses were modelled by reconstructing motion inclusive dose distributions for different localization strategies. Actually delivered dose (strategy A) utilized initial Calypso localization, CBCT and additional pre-treatment motion correction by kV-imaging and Calypso, and gating during the irradiation. The effect of gating was investigated by simulating non-gated treatments (strategy B). Additionally, non-gated and single image-guided (CBCT) localization was simulated (strategy C). A total of 308 fractions from 22 patients were reconstructed. The dosimetric effect was evaluated by comparing motion inclusive target and risk organ dose-volume parameters to planned values. Motion induced dose deficits were seen mainly in PTV and CTV to PTV margin regions, whereas CTV dose deficits were small in all strategies: mean ± SD difference in CTVD99% was -0.3 ± 0.4%, -0.4 ± 0.6% and -0.7 ± 1.2% in strategies A, B and C, respectively. Largest dose deficits were seen in individual fractions for strategy C (maximum dose reductions were -29.0% and -7.1% for PTVD95% and CTVD99%, respectively). The benefit of gating was minor, if additional motion correction was applied immediately prior to irradiation. Continuous motion monitoring based localization and motion correction ensured the target coverage and minimized the OAR exposure for every fraction and is recommended to use in prostate SBRT. The study is part of clinical trial NCT02319239.

Keywords: Prostate, SBRT of the prostate, dose reconstruction, intrafraction motion, interfraction motion, treatment localization, kV-imaging, CBCT-imaging, continuous motion monitoring, Calypso

1. Introduction

Due to proposed high fractionation sensitivity (low α/β-ratio) of prostate cancer [1, 2] and technical advancements in radiotherapy (RT), the use of stereotactic body radiation therapy (SBRT) for treatment of localized prostate cancer has increased in recent years. Growing clinical evidence has proven the feasibility of prostate SBRT and suggests it as an appropriate treatment modality for low-risk and intermediate-risk prostate cancer [3], and also for intermediate-to-high risk prostate cancer [4]. Based on these results, the use of prostate SBRT is likely to increase further. The impact of treatment localization errors increases with higher doses per fraction and treatments comprising of only few fractions. Even a single localization error may compromise target coverage and expose organs at risk (OARs), such as rectum and bladder, to very high doses. There is also an urge to reduce the planning target volume (PTV) margins in order to reduce the high dose volumes of the OARs, which increases precision requirements even more. Image-guidance of conventionally fractionated prostate radiotherapy typically corrects for interfraction variations in the prostate position. Different imaging modalities applied in prostate RT have been discussed previously [5]. Most effective and widely available technique, and established practice in many clinics, is the daily kV or cone beam computed tomography (CBCT) imaging of implanted fiducial markers (FMs)[6]. Hypofractionated protocols, such as SBRT, have higher precision requirements, and also the intrafraction motion of the prostate needs to be considered [7]. Dedicated devices, such as Calypso (Varian Medical Systems) [8, 9] and RayPilot (Micropos Medical) [10, 11], have been developed for continuous monitoring of intrafraction prostate motion. The advantage of these methods is that they provide real-time prostate localization and they can be used for beam gating and re-alignment of the patient, if the prostate motion exceeds pre-defined tolerances. Main tradeoff of these methods are the MRI artefacts caused by the ferromagnetic intraprostatic transponders and transmitters, which reduce the utilization of MRI imaging in treatment planning and for Calypso, because of the permanent implantation of the transponders, also the follow-up. These methods also rely on additional hardware to a linear accelerator (Linac).

The current procedure for prostate SBRT at Tampere University Hospital involves initial Calypso localization with additional CBCT and kV imaging prior to treatment delivery with volumetric modulated arc therapy (VMAT), and Calypso motion monitoring and automatic beam gating during treatment to prevent geometrical target misses caused by intrafraction motion. If the use of Calypso could be avoided, then this

method could have potential for wider use worldwide and is therefore of interest to investigate. A lot of studies have looked at intrafraction motion and its dosimetric impact: Colvill et al [12] studied the dosimetric impact of prostate intrafraction motion and the use of multileaf collimator (MLC) tracking and gating as motion correction strategies in conventionally fractionated prostate RT. They found that without motion correction there can be significant decrease in target dose coverage for some fractions. Li et al [13] investigated the characteristics of intrafraction prostate motion and dosimetric consequences of the motion for different PTV margins and different motion management procedures in conventionally fractionated step-and-shoot intensity modulated RT (IMRT) of the prostate. Their findings suggest that 2 mm PTV margin would be adequate provided that the pre-fraction localization is based on Calypso, and that intrafraction realignment would enable even further margin reduction. Continuous motion monitoring and intrafraction motion correction have been shown to increase the target coverage also in prostate SBRT using IMRT [14]. Juneja et al [15] evaluated the dosimetric effect of prostate intrafraction motion using different motion metrics and found strong correlation between mean of the highest 50% of motion and PTVD95%. In CyberKnife treatments, due to their long duration, target position is monitored and controlled throughout the treatment with orthogonal kV imaging and robotic position corrections using user-defined time intervals. Van de Water et al [16] found, that the correction interval required for optimal target coverage in prostate SBRT would be between 60 and 180 seconds, when using 3 mm CTV-to-PTV margins.

While previous studies have investigated the dosimetric effect of intrafraction prostate motion in many different ways, none of them have specifically addressed the pre-treatment motion during the setup procedure. In the advent of modern treatment techniques, such as VMAT and flattening filter free (FFF) beams, which enable short treatment times, the duration of the setup period might be longer than the duration of the actual beam delivery. This increases the relevance of prostate motion during the setup period, and thus more emphasis should be put on the geometric accuracy of the initial setup. In this study, we will look specifically at this problem.

The aim of this study was to investigate the dosimetric benefit of gating and continuous motion monitoring based motion correction prior to and during the treatment delivery using the data of clinically treated patients. Of special interest was whether prostate SBRT could be implemented safely using only pre-treatment imaging with FMs without additional technical accessories such as the Calypso system. To our knowledge,

a direct dosimetric comparison between inter- and intrafraction motion correction strategies in prostate SBRT has not been previously made. The dosimetric effect of the motion in different motion control and localization strategies was evaluated by reconstructing motion inclusive dose distributions and comparing reconstructed dose volume histogram (DVH) parameters both in target and normal tissue structures to the planned values. The study is part of a clinical trial (ClinicalTrials.gov NCT02319239) which aims at developing safe extremely hypofractionated treatment protocol for prostate cancer.

2. Materials and methods

2.1. Patients and treatment technique

Twenty-two patients treated between July 2016 and January 2019 were included in the study. Patients were treated with 5 x 7 Gy (n=11) or 5 x 7.25 Gy (n=11) fractions every other day. The clinical target volume (CTV) was the prostate alone and the PTV was formed by adding 3 mm posterior margin and 5 mm elsewhere around the CTV. Prostate and prostatic urethra were delineated with the help of MRI image fused with the planning CT. The urethra was delineated as an 8 mm diameter cylindrical structure to cover the geometrical uncertainties arising from image registration and prostate deformation between imaging sets and during the treatment course. The treatment technique was VMAT using two full arcs or two partial arcs (gantry 240°-120°) and 10 MV FFF beams. The treatments were delivered with a TrueBeam STx (Varian Medical Systems) linear accelerator. Dose optimization and calculation were made with Eclipse treatment planning system (TPS) (versions 13.6 and 15.6, Varian Medical Systems). The PTV mean dose was normalized to 100% of the prescribed dose and the 95% isodose covered the whole PTV. The maximum allowed dose in PTV was 105%. For patients receiving 5 x 7.25 Gy, the urethra dose was optimized to a mean of 35 Gy, while the surrounding PTV was simultaneously optimized to mean dose of 36.25 Gy. Organ at risk (OAR) structures were bladder, rectum and femoral heads, which were optimized according to clinically approved criteria. The dose calculation algorithm was AAA, version 13.6.23 or 15.6.03.

2.2. Localization and motion tracking

Patients were positioned supine on the treatment couch by aligning setup lasers with tattooed skin marks. An in-house made knee support was used. The Calypso system was used for initial localization and subsequent motion tracking of the prostate. Technical aspects and operating principle of the system are presented in detail elsewhere [8, 9]. Described briefly, the system consists of three transponders implanted into the prostate and electromagnetic (EM) source/receiver array setup above the patient during the treatment. The system detects the locations of the transponders (and thus the prostate) responding to the EM signals sent by the array source coils. The system is calibrated to the treatment machine isocenter. Based on treatment plan information sent to the system, 3D positions of the transponders relative to the treatment isocenter are known and by detecting transponder positions, machine isocenter can be matched to the treatment isocenter. Transponder positions are read at 25 Hz (Calypso version 3.0), resulting in real-time continuous prostate motion detection. The motion is detected and reported in translational [left-right (LR), superior-inferior (SI) and anterior-posterior (AP)] directions. Reported precision and accuracy of the system is 0.4 ± 0.4 mm and 0.1 ± 0.1 mm, respectively [17] and the clinical localization accuracy of the system is comparable to FM based orthogonal kV imaging [5]. CBCT was acquired to check the filling status of the bladder and rectum and matched to planning CT using transponders as FMs. If the rectum was too filled pushing anterior rectal wall into the treatment volume, or the bladder was too empty, patient was advised to empty the rectum or drink water, after which a new CBCT was taken. When the prostate was covered by the PTV with the fiducial alignment, OAR filling status was adequate and OARs were not unreasonably exposed in the treated area, setup and treatment procedures could proceed. If the prostate had shifted between initial localization and CBCT, the displacement was corrected by couch shifts. After the CBCT, the localization was further confirmed by an orthogonal kV image pair, using transponders as FMs. The kV imaging was done in comparative purposes and is not necessary, if the Calypso is used [5]. Possible shift of the prostate after CBCT acquisition, detected by the kV imaging, was corrected by corresponding couch shifts. In addition to kV image verification and repositioning, Calypso adaptive couch repositioning was used in some fractions to correct for prostate displacement that occurred during and after the CBCT or kV imaging, prior to irradiation. The treatment was started and if the motion of the prostate exceeded tolerances (2 mm posteriorly, 3 mm elsewhere) the irradiation was gated off

automatically. If the position of the prostate did not return within the tolerances, the Calypso adaptive couch repositioning was used. Calypso motion data was exported for further analysis and dose reconstruction purposes after the treatment. The clinically implemented localization and motion correction strategy including the use of Calypso and CBCT and kV imaging is referenced as “strategy A” hereafter.

2.3. Simulation of alternative localization strategies

To evaluate the dosimetric benefit of continuous monitoring based localization and gating, two alternative localization strategies were simulated by editing Calypso motion trajectories. To simulate the motion of the prostate without intrafraction beam gating and motion correction, the motion data were corrected for gating events and Calypso based couch adjustments during the treatment delivery. This is referenced as “strategy B” hereafter.

Further, to evaluate the prostate motion and its effect on dose distribution following a localization based only on initial Calypso localization and CBCT imaging, the data were corrected for all couch adjustments other than CBCT based. This is referenced as “strategy C” hereafter. Figure 1 shows an example of real (strategy A) and simulated (strategy C) motion trajectories for the same fraction.

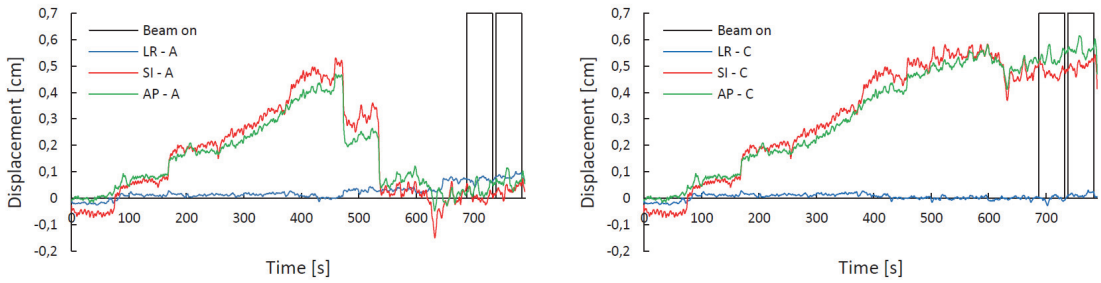

Fig. 1. Real (left) and simulated (right) prostate intrafraction motion trajectories for one fraction. At the start of the fraction, the target was already aligned to isocenter with Calypso. During CBCT acquisition and image interpretation the prostate was displaced due to intrafraction motion. Motion correction was first done by kV imaging, but due to motion during kV imaging and image matching procedure, SI and AP positions were still 2-3 mm displaced after the correction. This residual error was then corrected by Calypso adaptive couch repositioning. On simulated trajectory, couch corrections were removed. Without the additional couch correction prior the irradiation, the mean displacement during treatment would have been 4.9 mm in the

superior direction and 5.5 mm in the anterior direction. Rectangular bars represent the beam on time intervals.

2.4. Motion including dose reconstruction

Motion including dose distributions were reconstructed using an isocenter shift dose reconstruction method, which has previously been developed and validated for moving targets with dynamic treatments [18]. The method incorporates the 3D target motion trajectory during the treatment delivery into the Dicom treatment plan exported from the TPS. The motion encoded treatment plan is sent back to the TPS where it is recalculated resulting in the motion including dose distribution.

Motion encoding of the treatment plan was done by dividing the intrafraction motion trajectory, extracted from the Calypso log files, into 1 mm position bins. The motion trajectory was synchronized with the original treatment plan and for each position bin, sub-beams were constructed from the treatment plan control points to represent the part of the treatment delivery, while the target was located within each position bin. For each sub-beam the target displacement was modelled as a corresponding isocenter shift [18]. Motion encoding of the treatment plans was made with in-house MATLAB program (MATLAB R2017b, MathWorks), and all of the recalculations in TPS were made using dose calculation algorithm AAA, version 13.6.23. Motion including dose distributions were reconstructed for localization strategies A, B and C.

2.5. Data analysis, statistical tests

Intrafraction motion during the beam delivery was analyzed for each fraction. Mean displacement in 3D, LR, SI and AP directions was calculated for every fraction and over all fractions in each strategy. Mean percentage time of absolute displacements ≥ 1, 2, 3, 5 and 7 mm in LR, SI and AP directions were calculated as well. The position of the prostate was defined relative to the tracking starting point position, immediately after Calypso localization, before any imaging and treatment delivery.

To evaluate the dosimetric effect of the motion in each localization strategy, dose-volume parameters were derived from DVHs of each fraction in each strategy. Analyzed dose-volume parameters for target structures were: PTVD95%, PTV mean dose, CTVD99%, CTV mean dose, PTVsubCTVD95% (PTV shell volume around the CTV), urethra D2%, urethra D99% and urethra mean dose. For patients with 5 x 7.25 Gy fractionation, the urethra was irradiated to 7 Gy causing heterogeneous PTV and CTV dose distributions. For these patients, the urethra was excluded (with

zero-margin) from the CTV and PTV volumes to get comparable DVHs with 5 x 7 Gy fractionated patients. However, due to dose gradients within the target volume of 5 x 7.25 Gy fractionated patients, prostate motion may cause different kind of defects to the dose distribution than with 5 x 7 Gy patients with more homogenous dose distribution. Therefore, differences in target dose-volume parameters to the planned values were also calculated separately for both fractionation schemes.

For OAR structures the analyzed parameters were: V50%, V65%, V90% and V100% for the bladder and V50%, V65%, V90%, V96.2% and V100% for the rectum. V96.2% to the rectum is used as a measure of the plan quality in our clinic, and thus chosen as one of the parameters. Dose parameters in each localization strategy were compared to planned values and the comparisons were made for individual fractions, individual patients (cumulative effect of 5 fractions) and different strategies (averaged over all fractions per strategy). Running cumulative variation in PTVD95% and CTVD99% was calculated to evaluate whether the differences would average out with treatment progression.

Correlation of the motion and dosimetric changes was evaluated calculating Pearson correlation coefficients between motion metrics (mean LR, SI and AP displacements, mean of absolute LR, SI and AP displacements and mean 3D displacement) and change in dosimetric parameters relative to planned doses. For brevity, only the strongest correlations are presented. Wilcoxon signed rank test was used to test whether the motion inclusive dose-volume parameters (strategies A, B and C) were significantly different from the planned dose-volume parameters and strategies B and C were also tested against strategy A (delivered dose). Kolmogorov-Smirnov test was used to evaluate whether or not the dose-volume parameters were normally distributed.

3. Results

Due to missing motion trajectory, or fractionated treatment trajectory log files, some of the 110 fractions from the 22 patients included in the study could not be reconstructed. Thus the total number of fractions analyzed was 103 for strategies A and B and 102 for strategy C.

3.1. Prostate intrafraction motion

Mean prostate displacement and maximum and minimum values of the fraction mean displacements during treatment delivery for all patients and fractions are presented in table 1. In addition to mean values in 3D and translational directions, means of absolute values of translational displacements and range of the motion that occurs during beam-on are given. Positive values represent anterior, superior and left displacements. It is noteworthy, that there are displacement values that exceed the motion tolerances in strategy A. These appear in the motion data log just before the beam is interrupted by the gating system and are probably due to slightly inaccurate synchronization between logged position and logged beam-on status. Range between strategies B and C differ because of the differences in the pre-treatment motion correction between the strategies. The maximum cumulative time of tolerance exceeding motion in Calypso logs for single fraction was about 0.4 seconds. The bias this creates in the modelled dose is negligible and can be ignored. Most of the motion occurred in SI and AP directions, which can be seen in percentage times with absolute displacement ≥ 1, 2, 3, 5 and 7 mm within treatment delivery time, presented in table 2.

Table 1. Mean and SD of the intrafraction prostate displacement during treatment delivery, averaged over all fractions in each localization strategy. Subscript "abs" refers to absolute value. Range describes the observed maximum amplitude of the motion. Maximum and minimum of mean fraction displacements are shown as well. All values are given in mm.

Strategy		3D	LR abs	SI abs	AP abs	LR	SI	AP
A	Mean	1.0	0.4	0.5	0.5	0.0	0.0	0.1
	SD	0.4	0.3	0.4	0.4	0.5	0.7	0.7
	Min	0.3	0.0	0.0	0.0	-1.5	-1.8	-1.3
	Max	2.2	1.5	1.8	1.9	1.1	1.6	1.9
	Range					-2.7,1.8	-4.1,9.8	-2.2,3.1
B	Mean	1.1	0.4	0.5	0.6	0.0	0.0	0.1
	SD	0.6	0.3	0.5	0.6	0.5	0.7	0.8
	Min	0.3	0.0	0.0	0.0	-2.4	-1.9	-1.3
	Max	4.8	2.4	2.3	4.5	1.1	2.3	4.5
	Range					-2.8,1.8	-4.2,11.8	-2.4,9.0
C	Mean	1.7	0.6	0.9	0.9	0.1	0.1	-0.1
	SD	1.1	0.6	0.9	0.9	0.8	1.3	1.3
	Min	0.5	0.0	0.0	0.0	-2.6	-4.6	-4.0
	Max	7.4	3.4	4.9	5.5	3.4	4.9	5.5
	Range					-3.0,4.1	-6.8,12.8	-5.2,7.9

Table 2. Percentage time with absolute prostate displacements above 1, 2, 3, 5 and 7 mm within the treatment delivery time.

	Strategy A			Strategy B			Strategy C		
	LR	SI	AP	LR	SI	AP	LR	SI	AP
≥ 1 mm	5.0	15.9	15.7	5.4	17.8	16.8	14.8	32.5	37.0
≥ 2 mm	0.1	1.1	1.4	1.1	2.6	3.6	3.6	10.4	10.8
≥ 3 mm	0.0	0.0	0.0	0.0	0.3	1.3	1.0	4.8	3.2
≥ 5 mm	0.0	0.0	0.0	0.0	0.0	0.2	0.0	0.6	1.1
≥ 7 mm	0.0	0.0	0.0	0.0	0.0	0.1	0.0	0.0	0.1

3.2. Dosimetric data

3.2.1. Target structures

Mean, SD and maximum differences in dose parameters between motion inclusive and planned dose distributions are presented in table 3. Deviations in PTVD95% and PTVsubCTVD95% relative to planned values are generally small in strategies A and B but larger in strategy C. Despite the dose deficits seen in PTV and PTVsubCTV parameters, mean PTV, mean CTV and CTVD99% values over all fractions were minimally affected in any of the strategies. Dose deficits can also be seen in mean DVHs, which are presented for PTV, CTV, PTVsubCTV and urethra in figure 2. The heterogeneous dose in the prostate-urethra region of 5 x 7.25 Gy plans compared to 5 x 7 Gy plans did not have effect on differences between motion inclusive CTVD99%, mean CTV and planned doses. However, differences in mean PTV, PTVD95% and PTVsubCTVD95% values were larger especially in strategy C with 5 x 7.25 Gy fractionation (table 4).

Table 3. Mean, SD and maximum percentual differences in calculated dose parameters between motion inclusive and planned dose distributions over all patients and fractions.

	Strategy A			Strategy B			Strategy C		
	Mean	SD	Max	Mean	SD	Max	Mean	SD	Max
PTVsubCTVD95%	-1.6	1.5	-8.4	-2.0	2.2	-15.4	-5.2	7.2	-45.2
PTVD95%	-0.9	0.8	-4.3	-1.2	1.5	-10.8	-3.1	4.9	-29.0
PTV mean	-0.2	0.2	-1.2	-0.2	0.3	-2.1	-0.5	0.9	-6.4
CTVD99%	-0.3	0.4	-2.5	-0.4	0.6	-3.5	-0.7	1.2	-7.1
CTV mean	0.0	0.2	-0.5	0.0	0.2	-0.5	-0.1	0.3	-2.2
Urethra D2%	0.7	0.8	3.8	0.9	1.1	6.6	1.3	0.9	6.1
Urethra D99%	-1.3	3.4	-20.2	-1.4	3.5	-20.8	-5.7	12.4	-59.6
Urethra mean	0.1	0.3	1.2	0.1	0.4	2.1	0.1	0.8	-2.8
V100% bladder	9.5	63.9	325.4	6.6	62.6	323.0	44.5	170.6	1095.8
V90% bladder	-0.6	22.0	89.9	-1.8	23.6	88.1	8.6	59.9	347.4
V65% bladder	-0.2	13.7	43.6	-0.9	15.1	43.0	2.4	33.3	149.8
V100% rectum	55.1	159.4	913.0	81.3	265.9	2004.7	83.6	224.2	1347.9
V96.2% rectum	3.6	39.7	116.5	7.6	51.4	292.8	8.1	77.9	413.9
V65% rectum	2.2	25.5	65.5	4.6	31.7	174.5	2.5	51.3	269.3

Table 4. The effect of heterogeneous dose distribution (urethra sparing in 5 x 7.25/7 Gy fractionation) on differences between motion inclusive and planned target dose parameters. All results are relative to planned values [%].

	5 x 7 Gy			5 x 7.25/7.0 Gy		
	A	B	C	A	B	C
PTVsubCTVD95%	-1.7 ± 1.6	-1.9 ± 1.9	-3.7 ± 5.1	-1.5 ± 1.4	-2.0 ± 2.5	-6.7 ± 8.6
PTVD95%	-0.9 ± 0.8	-1.0 ± 1.0	-2.0 ± 3.3	-0.9 ± 0.8	-1.3 ± 1.9	-4.1 ± 5.9
PTV mean	-0.1 ± 0.3	-0.1 ± 0.2	-0.3 ± 0.5	-0.2 ± 0.2	-0.2 ± 0.4	-0.7 ± 1.2
CTVD99%	-0.4 ± 0.5	-0.4 ± 0.6	-0.6 ± 1.1	-0.2 ± 0.3	-0.3 ± 0.5	-0.7 ± 1.2
CTV mean	0.0 ± 0.2	0.0 ± 0.2	0.0 ± 0.2	0.0 ± 0.2	0.0 ± 0.2	-0.1 ± 0.4

For individual fractions, larger deviations were seen with maximum observed differences of -6.4% (PTV mean), -2.2% (CTV mean), -29.0% (PTVD95%) and -7.1% (CTVD99%) (Table 3). These occurred within the same fraction in localization strategy C for which the mean 3D intrafraction displacement was the largest observed, 7.4 mm. DVHs from the motion inclusive dose distribution from the corresponding fraction are compared with strategy A and the planned doses in figure 3. Shift of the dose

distribution of strategy C at this fraction can be seen in figure 4, while the delivered dose (strategy A) hit the target precisely. The maximum differences in PTV mean, CTV mean, PTVD95% and CTVD99% were -1.2%, -0.5, -4.3% and -2.5%, in strategy A and -2.1%, -0.5%, -10.8% and -3.5% in strategy B, respectively (Table 3).

Larger than 1% dose difference in CTVD99% was seen in 6 (5.8%), 7 (6.8%) and 17 (16.7%) fractions in strategies A, B and C, respectively. At least 5% dose deficit in PTVD95% was seen in 0, 2 and 11 (10.8%) fractions in strategies A, B and C, respectively. According to Wilcoxon signed rank test, all of the dose parameters, except CTV mean dose in strategies A, B and C, and urethra mean dose in strategy C differed significantly ($p < 0.05$) from planned values. However, for urethra mean dose, the differences were near the significance level in all strategies: *p* values were 0.011, 0.025 and 0.084 for strategies A, B and C, respectively. Between strategies A and B, the difference was significant ($p < 0.05$) for all other dose parameters than CTV (D99% and mean dose) and urethra (D2, D50, D99, mean dose) parameters. Between strategies A and C, the difference was significant for all other dose parameters than urethra mean dose. Based on Kolmogorov-Smirnov test, CTVD99% in strategies A and B and urethra D2% in strategy A were found to be normally distributed. Thus, the comparison results of these parameters may be uncertain.

Running cumulative variation in CTVD99% and PTVD95% as a function of treated fractions for patients with five successfully reconstructed fractions (n=16) is shown in figure 5. Larger than 1% differences in CTVD99% between cumulative doses of five summed fractions and planned doses were seen only in strategy C for 4 patients. Larger than 5% cumulative differences in PTVD95% were seen only for the same 4 patients. The maximum cumulative differences after five fractions in CTVD99% and PTVD95% were -1.9 and -12.5%, respectively, in strategy C. Mean (± SD) cumulative variations in PTVD95% after five fractions were -0.9 ± 0.5, -1.2 ± 0.7 and -3.6 ± 3.3% for strategies A, B and C, respectively. The corresponding variations in CTVD99% were -0.3 ± 0.2, -0.4 ± 0.3 and -0.7 ± 0.5%.

PTVD95%, PTVsubCTVD95% and mean PTV correlated strongly with mean absolute AP, SI and 3D displacements (r = -0.74 – -0.89). CTVD99% correlated moderately with mean 3D displacements (r = -0.67).

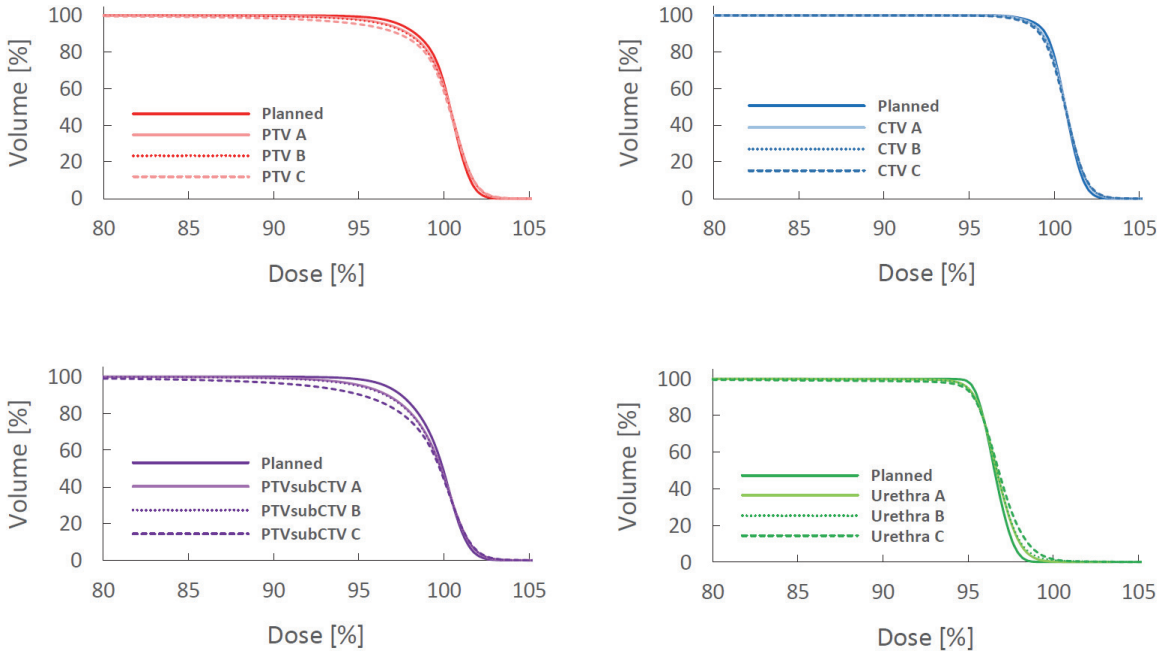

Fig. 2. Mean DVHs for PTV, CTV, PTVsubCTV and urethra for localization strategies A (light solid line), B (dotted line) and C (dashed line). Planned mean DVHs (solid line) are plotted for comparison.

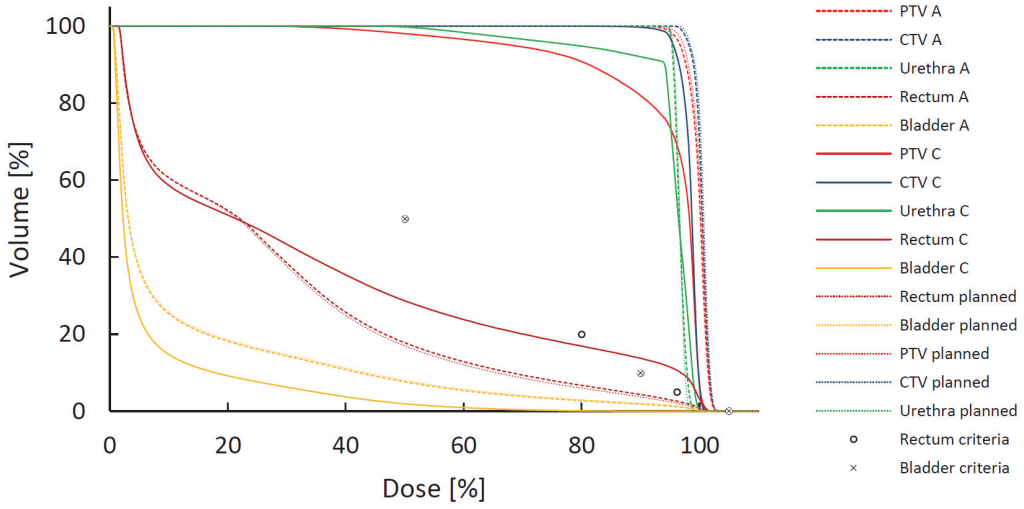

Fig. 3. DVHs from motion inclusive dose distribution (strategy C) for a fraction with largest observed differences to planned values in PTV and CTV parameters (solid line). DVHs representing delivered dose (strategy A) (dashed line) for the same fraction and planned values (dotted line) are plotted for comparison. Plan evaluation criteria for rectum (circle) and bladder (cross) are plotted as well.

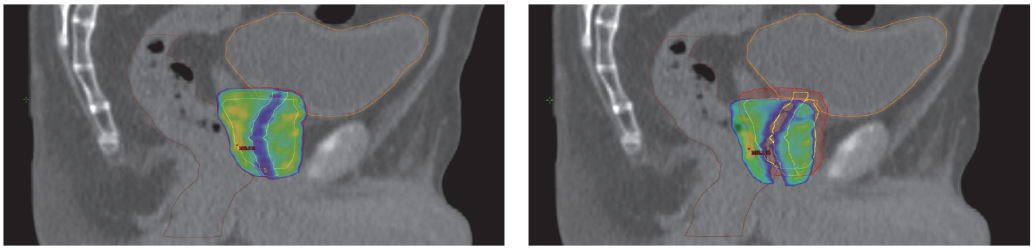

Fig. 4. Distributions of at least 95% of the prescribed dose (7.25 Gy per fraction) in localization strategies A (left) and C (right) for a fraction of largest observed motion in strategy C. Mean 3D intrafraction displacements of the prostate were 1.0 mm and 7.4 mm in strategies A and C, respectively. Colder dose area is the urethra region, which was optimized to 7 Gy.

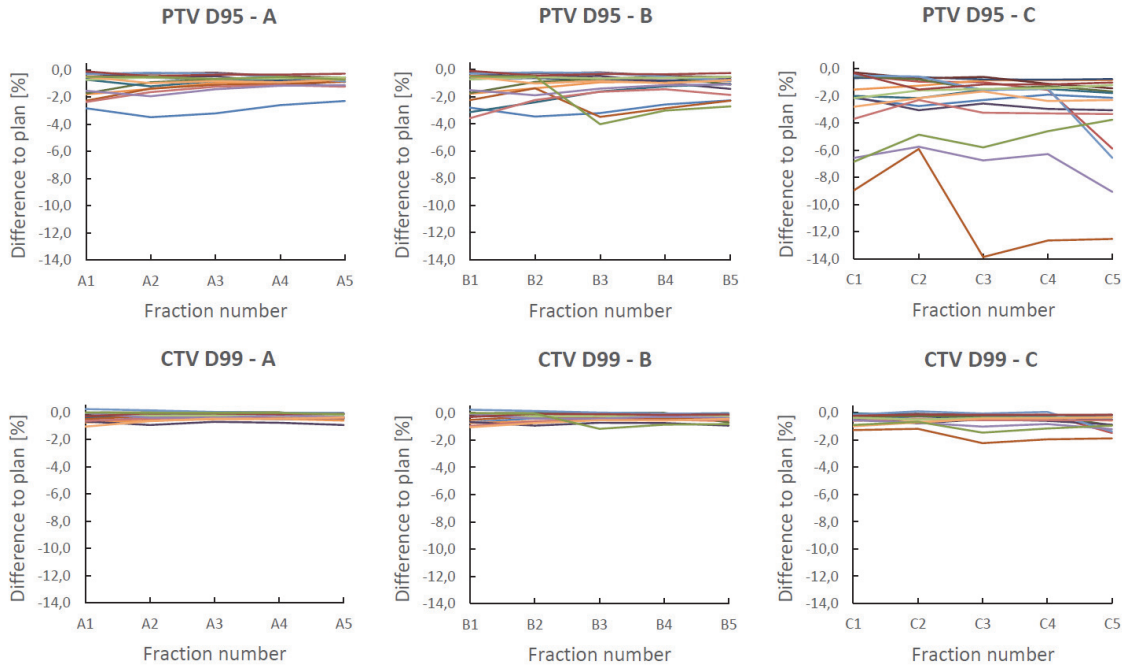

Fig. 5. Running cumulative variation from planned values in motion inclusive PTVD95% and CTVD99%. Each curve correspond to a patient. A, B and C refer to corresponding localization strategies as explained in the text.

3.2.2. Organs at risk

Table 3 shows mean, SD and maximum differences between motion inclusive and planned dose distributions for rectum and bladder, over all fractions in each localization strategy. V100% in bladder increased in each strategy but mostly in strategy C. However, mean absolute V100% values were small, 1.9 ± 1.4, 1.8 ± 1.4 and 2.0 ± 1.6 cm^3 in strategies A, B and C, respectively. Due to small planned values, the maximum percentual increase in bladder V100% was substantial although the corresponding maximum V100% in absolute volumes was small: 0.9, 0.9 and 2.6 cm^3 in strategies A, B and C, respectively. Delivered absolute V90% and V65% corresponding to maximum percentual increase were 3.2, 3.1, 7.5 cm^3 and 8.3, 8.3, 14.5 cm^3 in strategies A, B and C, respectively. Delivered maximum absolute volumes for V100%, V90% and V65% were 8.0, 8.0 and 13.1 cm^3 (strategy A), 17.5, 17.3 and 24.0 cm^3 (strategy B), 31.3, 31.1 and 46.5 cm^3 (strategy C). Compared to planned values, the lower dose volumes changed only little in each strategy but the variation was large overall. Similarly to bladder, high dose volumes to rectum (V100% and V96.2%) increased the most, whereas lower dose volumes were affected only little in each strategy. However, delivered absolute volumes of rectum V100% and V96.2% corresponding to largest percentual increase were only 0.6, 1.3 and 0.9 cm^3, and 2.9, 4.2 and 7.5 cm^3, whereas maximum absolute V100% and V96.2% values were 2.9, 2.9 and 2.3 cm^3, and 4.9, 4.9 and 7.5 cm^3 in strategies A, B and C, respectively. For rectum V90%, corresponding values were 4.0, 6.6 and 9.7 cm^3 and 6.9, 6.9 and 9.7 cm^3, and for rectum V65% they were 5.9, 14.8 and 15.3 cm^3 and 13.2, 14.8 and 15.3 cm^3 in strategies A, B and C, respectively. Absolute mean (+SD) V100% values for rectum were 0.6 ± 0.6, 0.6 ± 0.6 and 0.6 ± 0.5 cm^3 and V96.2% were 1.6 ± 0.9, 1.6 ± 1.0 and 1.6 ± 1.1 cm^3 in strategies A, B and C, respectively. Our clinical plan evaluation criterion V96.2% ≤ 5% was exceeded in 7 (6.8%), 9 (8.7%) and 11 (10.8%) fractions in strategies A, B and C, respectively, while the maximum planned V96.2% was 4.3%. Variation over all fractions was large. Maximum observed absolute rectum V96.2% [7.5 cm^3 (10.6%)] occurred in strategy C, in a fraction with largest observed mean displacement (figures 1, 3 and 4). Delivered V96.2% for the same patient and fraction was 1.8 cm^3 (2.6%).

Large deficits were seen in urethra D99% on individual fractions. These are due to craniocaudal displacement of the prostate, which leaves cranial or caudal parts of the urethra outside of the radiation field. Averaged over all fractions, urethra D2%

increased in all strategies, urethra structure being surrounded by higher prescribed dose to prostate. Urethra D99% correlated strongly with mean absolute SI displacements (r = -0.81). Bladder V100% and V90% correlated strongly with mean SI displacements (r = -0.71 and r = -0.84, respectively). Rectum V96.2% and V90% correlated strongly with mean AP displacements (r = 0.91 for both).

4. Discussion

Dosimetric effects of prostate motion were mainly seen in PTV and PTVsubCTV structures, whereas CTV dose degradation was small in all localization strategies. Larger dose degradation especially in PTVsubCTV structure emphasizes that the dosimetric effects were mainly limited to the peripheral area of the PTV. These findings reflect that the prostate motion during the treatment delivery was small and that the applied CTV to PTV margins mostly accounted for the motion induced dose deficits, even when the localization was not as accurate as possible, and gating was not used, as in strategy C. The largest changes for urethra were seen in parameter D99%, which is explained by SI motion causing dose deficits to the most superior and inferior parts of the urethra. Lower prescribed dose to the urethra, may cause underdosage to the surrounding CTV in the presence of prostate motion (figure 4), although the results of this study indicate that the effect, on average, is small.

On individual fractions, larger dose differences were seen. However, if additional motion correction prior to treatment was used, CTVD99% dose deficits were less than -2.5%, and -3.5% in strategies A and B, respectively. Without additional motion correction (strategy C), CTV dose deficits were larger. The maximum dose deficit in CTV mean and CTVD99% was -2.2% and -7.1%, respectively, which according to the dose response of prostate cancer in conventionally fractionated or moderately hypofractionated RT without androgen deprivation could lead to 5-16% decrease in tumour control probability (TCP) [19]. Figure 3 shows the DVHs for this particular fraction and also the DVHs for the actually delivered dose and planned dose distributions. The delivered fraction utilized kV imaging and Calypso based couch corrections in addition to CBCT (figure 1), to correct for the displacement induced by prostate drift between CBCT and treatment delivery. Overall, continuous motion monitoring based localization and motion correction (strategy A) ensured accurate dose delivery for each fraction, whereas single pre-fraction image-guided setup (strategy C)

was susceptible to intrafraction motion compromising target coverage and exposing OARs to higher doses for some fractions.

Motion induced dose deficits seen in the current study are similar to those in the literature. Colvill et al [12] found that motion induced dose degradation in CTVD99% and PTVD95% can be even more than -19% and -34%, respectively, from the planned values on individual fractions. If gating was used, these figures dropped to -0.7% and -2.7%, respectively. They found also that the dose degradation PTVD95% and CTVD99% was highly correlated with 3D motion (-0.97 and -0.85, respectively). In a study of 294 prostate VMAT fractions from 18 patients, Juneja et al [15] found an average drop of 6.2% in PTVD95%, if the mean of the highest 50% of 3D motion was more than 3 mm. They also found that the dosimetric impact on PTVD95% was well correlated with many motion metrics, especially with the mean of the highest 50% of motion. Averaged over 486 fractions from 15 patients treated with step-and-shoot IMRT, Langen et al [20] found mean (±SD) change of -0.2 ± 0.5% and -0.5 ± 1.1% in CTV D95% and PTVD95%, respectively, but contrary to findings of Colvill et al [12] and Juneja et al [15], they did not find correlation between motion and its dosimetric impact. Colvill et al [12], Langen et al [20] and Juneja et al [15] partly, analysed the dosimetric effect of conventionally fractionated treatments. Though the absolute dose values differ between this study and theirs, relative dose distributions in prostate RT with intensity modulated techniques are quite similar [21], and thus considered comparable between each other. In the present study, similarly to findings of Colvill et al [12] and Juneja et al [15], PTVD95% was found to have strong correlation with 3D motion whereas CTVD99% was correlated moderately. The almost negligible benefit of beam gating, that is seen in the small dosimetric differences between strategies A and B, is in contrast to findings of van de Water et al [16] on the dosimetric impact of intrafraction position corrections in CyberKnife treatments. However, the beam delivery time of a prostate SBRT treatment is significantly higher for CyberKnife than for VMAT [21], and thus the CyberKnife treatments are more susceptible to intrafraction prostate motion.

In conventional or moderately hypofractionated fractionation schemes, dose deficits tend to average out due to large number of fractions [7, 20], but in SBRT with small number of fractions, the averaging of the errors may not happen, as indicated in this study. In localization strategy A the average cumulative effect of the motion decreased in PTVD95% and remained unchanged in CTVD99%. In strategy B without gating, the

average variation in PTVD95% decreased and CTVD99% increased, but only negligible (from -0.3% to -0.4%). Without additional motion correction prior to irradiation (strategy C) the average variation in cumulative PTVD95% and CTVD99% increased as a function of treated fractions (from -2.6% to -3.6% and from -0.5% to -0.7%, respectively). It is noteworthy, that for some patients, the cumulative variation increased still at the fifth and last fraction, which indicates that additional motion correction and gating are needed throughout the treatment course to ensure the correct target coverage.

Motion tolerances used with gating ensure that the CTV lies within the high dose region throughout the treatment. However, as the total dose of a single VMAT fraction is a sum of sub fields with varying beam apertures and dose rates per gantry angle, even small intrafraction target motion may result in sub beam doses that do not cumulate onto each other as planned, which can give heterogeneities into the delivered dose distribution. This interplay effect can cause cold and hot spots within inner part of the PTV (figure 6). Dose degradation due to interplay effect in prostate VMAT is small for most patients and the effect is reduced over multiple fractions [22]. In SBRT with five fractions or less, the effect is unknown. However, more detailed investigation of the interplay effect was out of scope of this study.

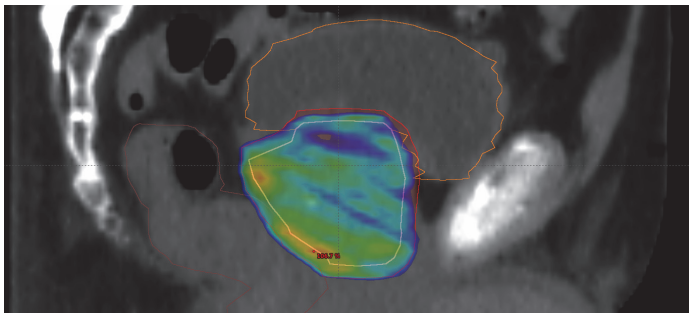

Fig. 6. Dose degradation in inner part of the target due to interplay effect between prostate motion and changing dynamic beam parameters. CTVD99% differed -2.5% from the planned value and the mean 3D displacement was 1.7 mm for this strategy A fraction. Doses of at least 95% of the prescribed dose are shown.

In addition to target structures, prostate motion affects the dose of the nearby OARs. V100% in both bladder and rectum increased in general, regardless of the localization strategy. OAR volumes within or in close vicinity to PTV are very sensitive to large

dosimetric changes due to prostate motion because of steep dose gradients and therefore even a small displacement may multiply V100%. Bladder volumes receiving 90% or 65% of the prescribed dose decreased in strategies A and B and increased in strategy C. V96.2% and V65% of the rectum increased in all strategies. It is noteworthy, that the increase in rectal volumes getting high doses (V96.2% and V100%) can be substantial (figure 3) without accurate localization prior to treatment. High rectal and bladder wall doses in prostate SBRT are associated with increased toxicity [23, 24] and thus different means of OAR dose sparing (e.g. reduced margins with continuous motion monitoring, or rectal spacers [25-27]) should be considered when planning prostate SBRT.

Though the additional localization prior to treatment seems to be sufficient for target coverage, continuous motion monitoring based localization and gating strategy is required to minimize the high dose volumes in rectum and bladder. This is consistent with findings of Zhang et al [28], who showed that with 3 mm posterior margin and 5 mm margins elsewhere, intrafraction motion would have only little effect on CTVD95%, but sparing of OARs would require relatively tight 1 mm posterior and inferior motion tolerances, especially with higher doses (42.5 Gy in five fractions). Choi et al [29] found that toxicity related to CyberKnife prostate SBRT treatment was highly sensitive to intrafractional prostate motion, although local tumor control was not affected. CyberKnife may produce higher doses to the OARs when compared to VMAT or other IMRT techniques resulting in higher normal tissue complication probability (NTCP) [21] and while the results of Choi et al [29] may not be fully applicable in assessing the risks of VMAT treatments, they provide clinical evidence supporting the role of precise motion correction in minimizing the OAR doses in prostate SBRT.

While small CTV-to-PTV margins reduce OAR doses, they increase the risk of target underdosage due to prostate motion. Tighter margins also put higher demands on correct target definition, as the plan becomes less forgiving for delineation errors. Better target coverage would have been expected, even in strategy C, if larger margins were used, but with the cost of increased OAR doses. In addition to prostate motion, optimal treatment margins depend on many clinical and technical aspects and detailed margin analysis was out of scope of this study.

Averaged over all patients, the observed prostate motion was small in the present study, even in strategy C. This is explained by the fact that only a small fraction of patients exhibit large prostate motions [30, 31], and on the other hand, short treatment times specific to VMAT-FFF treatments. This is compatible with the fact that the

likelihood of the prostate motion increases with increasing treatment time [31, 32]. Most of the motion occurred in SI and AP directions (table 2), which is consistent with findings in literature [33]. Beam gating keeps the displacement within predefined tolerances in strategy A and differences in displacements between strategies A and B originate from the prostate motion that would have happened if there was not gating in strategy A. Small difference in mean displacements between strategies A and B reflects that the motion beyond tolerances was rare if additional motion correction was used and gating had only little effect on the average displacement. It is probable that with larger dataset, large prostate displacements during the beam delivery would have been observed more often, although it is unlikely, that their frequency would have changed a lot. However, it is noteworthy, that with treatment techniques having longer beam delivery time, the probability of prostate motion during the treatment increases, and the gating may have bigger beneficial effect. Differences in motion between strategies B and C reflect the residual localization error after the CBCT based motion correction and the benefit of additional motion correction in strategy B. Thus, in contrast to previous studies that concentrated investigating the dosimetric impact of intrafraction motion [12, 15, 20], the current study evaluated also the effect of residual error in interfraction motion correction. Results suggest that prostate motion between the localization imaging and beam delivery may have larger dosimetric impact than prostate motion during the beam delivery and emphasize the importance of accurate interfraction motion correction with minimized time between the correction and treatment delivery. The findings of this study are consistent with the results of Litzenberg et al [34], who found that eliminating the delay during pre-fraction imaging and alignment procedure reduces the required margins in conventionally fractionated prostate RT. Especially, if the time between localization imaging and treatment delivery stretches, prostate may be displaced between imaging and delivery and additional motion correction is required. This is very often the case at our clinic, as the CBCT image interpretation (image matching and comparison of target and OAR structures with planned image) may take up to five minutes. At our clinic Calypso or FM based kV imaging (using Calypso transponders as fiducials) are used. The benefit of continuous motion monitoring with Calypso is to reveal sudden changes in the prostate position, like the motion shown in figure 7. In this case small prostate drift happened during the interpretation of the CBCT image and was corrected prior the irradiation. After the correction, just before the irradiation was initiated, a large prostate shift occurred. Without continuous motion

monitoring, the sudden large movement would have been unnoticed and the treatment would have been localized incorrectly. Similar findings have been reported in the literature [35].

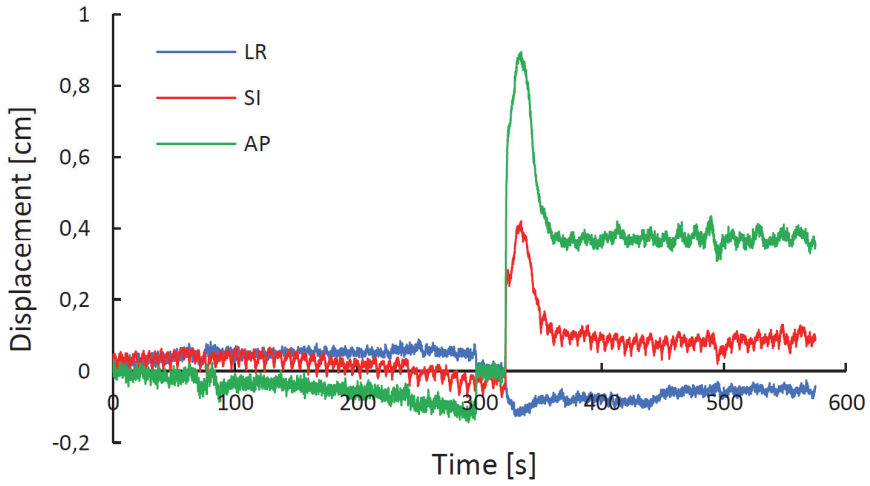

Fig. 7. The benefit of the continuous motion monitoring is to reveal sudden movements of the prostate, which might not be seen with regular imaging methods. In this example case, the prostate drifted slowly during and after the CBCT imaging (which was acquired around 50-150 s of the tracking). The drift that would not have been seen without continuous motion monitoring, or additional imaging, was corrected (at 300 s), after which the prostate shifted largely again. Without the continuous monitoring, the latter, sudden large movement would not have been detected and the treatment would have been delivered inaccurately.

One of the limitations of the study is that it is retrospective and in the simulation of initial Calypso and CBCT based localization (strategy C), there is additional delay between the localization and treatment due to additional kV imaging prior to treatment, elevating the likelihood of larger intrafraction motion. Thus, the simulation may overestimate the geometrical miss and resulting dosimetric differences. In reality, if only CBCT would be used, the delay would be shorter, but the risk of unnoticed intrafraction motion would still exist.

The dose reconstruction method used in the current study models the target shift by isocenter shifts on a rigid patient anatomy and while it takes into account changes in physical path length, it does not take into account changes in radiological path length caused by changes in tissue density and amount along the beam path [18]. It does not

take into account possible deformation of the tissues either. As the standardization of rectal and bladder volumes is difficult, the volumes and their position relative to prostate can vary during the treatment course. Therefore, modelled OAR dose parameters do not present accurately the real situation, but are more of an approximation of the motion induced dose effects in nearby OARs. The same applies to prostate, which may deform and swell during the extremely hypofractionated treatment [36], though the changes in prostate volume are rather small when compared to possible changes in bladder or rectum volumes. The current study focuses on comparison of dosimetric changes due to observed prostate motion in different localization strategies and in this context the accuracy of the dose modelling can be deemed sufficient. More accurate dose modelling would require consideration of daily anatomy deformations, which provides basis for the future investigations. Prostate rotations were not analyzed in the present study. The study of Wolf et al [37] suggests, that if the translational prostate motion is corrected, and 3-5 mm PTV margins are used, inter- and intrafraction prostate rotations would not affect the CTV dose coverage in VMAT SBRT of the prostate. However, their study did not account for interplay effects between intrafraction prostate rotations and treatment machine motion, which can have substantial effect on CTV dose in VMAT prostate treatments, as is shown in the recent study of Muurholm et al [38]. Rotation corrections has been shown to increase the target coverage also in CyberKnife prostate SBRT [16].

5. Conclusions

Results of the current study indicate, that due to intrafraction motion of the prostate, and the time that CBCT image acquisition and interpretation take, CBCT-guided pre-treatment motion correction without further correction may result in clinically relevant dose deficits in prostate SBRT for patients exhibiting large prostate motion. Additional position correction prior to treatment delivery, based on kV imaging using FMs or continuous motion monitoring (e.g. Calypso), increases the accuracy and is adequate for most of the fractions and patients. However, only continuous motion monitoring based position correction strategy prior to and during the treatment ensures the target dose coverage and minimizes the OAR exposure for every fraction and patient, and is thus the recommended treatment localization method in prostate SBRT.

Acknowledgements

This study was supported by the Seppo Nieminen funding, grant number 15012, Tampere University Hospital. Medical physicists Eeva Boman and Tomppa Pakarinen are acknowledged for help with data processing.

References

[1] Vogelius IR, Bentzen SM. Dose response and fractionation sensitivity of prostate cancer after external beam radiation therapy: a meta-analysis of randomized trials. Int J Radiat Oncol Biol Phys 2018;100:858–65.

[2] Dasu A, Toma-Dasu I. Prostate alpha/beta revisited - an analysis of clinical results from 14 168 patients. Acta Oncol 2012;51:963–74.

[3] Kishan AU, Dang A, Katz AJ, Mantz CA, Collins SP, Aghdam N, et al. Long-term outcomes of stereotactic body radiotherapy for low-risk and intermediate-risk prostate cancer. JAMA Netw Open 2019;2(2):e188006.

[4] Widmark A, Gunnlaugsson A, Beckman K, Thellenberg-Karlsson, C, Hoyer M, Lagerlund M, et al. Ultra-hypofractionated versus conventionally fractionated radiotherapy for prostate cancer: 5-year outcomes of the HYPO-RT-PC randomized, non-inferiority, phase 3 trial. Lancet 2019;394:385–95.

[5] VanhanenA, Syrén H, Kapanen M. Localization accuracy of two electromagnetic tracking systems in prostate cancer radiotherapy: a comparison with fiducial marker based kilovoltage imaging. Phys Med 2018;56:10–8.

[6] O'Neill AG, Jain S, Hounsell AR, O'Sullivan JM. Fiducial marker guided prostate radiotherapy: a review. Br J Radiol 2016;89(1068):20160296.

[7] Adamson J, Wu Q, Yan D. Dosimetric effect of intrafraction motion and residual setup error for hypofractionated prostate intensity-modulated radiotherapy with online cone beam computed tomography image guidance. Int J Radiat Oncol Biol Phys 2011;80:453–61.

[8] Mate TP, Krag D, Wright JN, Dimmer S. A new system to perform continuous target tracking for radiation and surgery using non-ionizing alternating current electromagnetics. Int J Comput Assisted Radiol Surg 2004;1268:425–30. (CARS 2004—Proc. of the 18th Int. Congress and Exhibition (Chicago, USA, 23–26 June 2004)).

[9] Balter JM, Wright JN, Newell LJ, Friemel B, Dimmer S, Cheng Y, et al. Accuracy of a wireless localization system for radiotherapy. Int J Radiat Oncol Biol Phys 2005;61:933–7.

[10] Kindblom J, Ekelund-Olvenmark A, Syren H, Iustin R, Braide K, Frank-Lissbrant I, et al. High precision transponder localization using a novel electromagnetic positioning system in patients with localized prostate cancer. Radiother Oncol 2009;90:307–11.

[11] Vanhanen A, Kapanen M. The effect of rectal retractor on intrafraction motion of the prostate. Biomed Phys Eng Express 2016;2:035021.

[12] Colvill E, Poulsen PR, Booth JT, O'Brien RT, Ng JA, Keall PJ. DMLC tracking and gating can improve dose coverage for prostate VMAT. Med Phys 2014;41:091705.

[13] Li HS, Chetty IJ, Enke CA, Foster RD, Willoughby TR, Kupelian PA, et al. Dosimetric consequences of intrafraction prostate motion. Int J Radiat Oncol Biol Phys 2008;71:801–12.

[14] Lovelock MD, Messineo AP, Cox BW, Kollmeier MA, Zelefsky MJ. Continuous monitoring and intrafraction target position correction during treatment improves target coverage for patients undergoing SBRT prostate therapy. Int J Radiat Oncol Biol Phys 2015;91:588–94.

[15] Juneja P, Colvill E, Kneebone A, Eade T, Ng JA, Thwaites DI, Keall P, Kaur R, Poulsen P, Booth JT. Quantification of intrafraction prostate motion and its dosimetric effect on VMAT. Australas Phys Eng Sci Med 2017;40:317–324.

[16] van de Water S, Valli L, Aluwini S, Lanconelli N, Heijmen B, Hoogeman M. Intrafraction prostate translations and rotations during hypofractionated robotic radiation surgery: dosimetric impact of correction strategies and margins. Int J Radiat Oncol Biol Phys 2014;88:1154–60.

[17] Franz AM, Schmitt D, Seitel A, Chatrasingh M, Echner G, Oelfke U, et al. Standardized accuracy assessment of the calypso wireless transponder tracking system. Phys Med Biol 2014;59:6797–810.

[18] Poulsen PR, Schmidt ML, Keall P, Worm ES, Fledelius W, Hoffman L. A method of dose reconstruction for moving targets compatible with dynamic treatments. Med Phys 2012;39(10):6237–46.

[19] Tamponi M, Gabriele D, Maggio A, Stasi M, Meloni GB, Conti M, et al.Prostate cancer dose-response, fractionation sensitivity and repopulation parameters evaluation from 25 international radiotherapy outcome data sets. Br J Radiol 2019;92(1098):20180823.

[20] Langen KM, Chauhan B, Siebers JV, Moore J, Kupelian PA. The dosimetric effect of intrafraction prostate motion on step-and-shoot intensity-modulated radiation therapy plans: magnitude, correlation with motion parameters, and comparison with helical tomotherapy plans. Int J Radiat Oncol Biol Phys 2011;84:1220–5.

[21] Scobioala S, Kittel C, Elsayad K, Kroeger K, Oertel M, Samhouri L, Haverkamp U, Eich HT. A treatment planning study comparing IMRT techniques and cyber knife for stereotactic body radiotherapy of low-risk prostate carcinoma. Radiat Oncol 2019;14:143.

[22] Azcona JD, Xing L, Chen X, Bush K, Li R. Assessing the dosimetric impact of real-time prostate motion during volumetric modulated arc therapy. Int J Radiat Oncol Biol Phys 2013;88:1167–74.

[23] Wang K, Chen RC, Kane BL, Medbery CA, Underhill KJ, Gray JR, Peddada AV, Fuller DB. Patient and dosimetric predictors of genitourinary and bowel quality of life after prostate SBRT: secondary analysis of a multi-institutional trial. Int J Radiat Oncol Biol Phys 2018;102:1430–7.

[24] Repka MC, Kole TP, Lee J, Wu B, Lei S, Yung T, Collins BT, Suy S, Dritschilo A, Lynch JH, Collins SP. Predictors of acute urinary symptom flare following stereotactic body

radiation therapy (SBRT) in the definitive treatment of localized prostate cancer. Acta Oncol 2017;56(8):1136–8.

[25] Karsh LI, Gross ET, Pieczonka CM, Aliotta PJ, Skomra CJ, Ponsky LE, Nieh PT, Han M, Hamstra DA, Shore ND. Absorbable hydrogel spacer use in prostate radiotherapy: a comprehensive review of phase 3 clinical trial published data. Urology 2017;115:39–44.

[26] Whalley D, Hruby G, Alfieri F, Kneebone A, Eade T. SpaceOAR hydrogel in dose-escalated prostate cancer radiotherapy: rectal dosimetry and late toxicity. Clin Oncol 2016;28:e148–e154.

[27] Hwang ME, Mayeda M, Liz M, Goode-Marshall B, Gonzalez L, Elliston CD, et al. Stereotactic body radiotherapy with periprostatic hydrogel spacer for localized prostate cancer: toxicity profile and early oncologic outcomes. Radiat Oncol 2019;14:136.

[28] Zhang P, Mah D, Happersett L, Cox B, Hunt M, Mageras G. Determination of action thresholds for electromagnetic tracking system-guided hypofractionated prostate radiotherapy using volumetric arc therapy. Med Phys 2011;38(7):4001–8.

[29] Choi HS, Kang KM, Jeong BK, Song JH, Lee Y H, Ha IB, et al. Analysis of motion-dependent clinical outcome of tumor tracking stereotactic body radiotherapy for prostate cancer. J Korean Med Sci 2018;33:e107.

[30] Kupelian P, Willoughby T, Mahadevan A, Djemil T, Weinstein G, Jani S, et al. Multi-institutional clinical experience with the Calypso system in localization and continuous, real-time monitoring of the prostate gland during external radiotherapy. Int J Radiat Oncol Biol Phys 2007;67:1088–98.

[31] Tong X, Chen X, Li J, Xu Q, Lin M, Chen L, et al. Intrafractional prostate motion during external beam radiotherapy monitored by a real-time target localization system. J Appl Clin Med Phys 2015;16(2):51–61.

[32] Li JS, Lin M, Buyyounouski MK, Horwitz EM, Ma C. Reduction of prostate intrafractional motion from shortening the treatment time. Phys Med Biol 2013;58:4921–32.

[33] Lin Y, Liu T, Yang W, Yang X, Khan MK. The non-Gaussian nature of prostate motion based on real-time intrafraction tracking. Int J Radiat Oncol Biol Phys 2013;87:363–9.

[34] Litzenberg DW, Balter JM, Hadley SW, Sandler HM, Willoughby TR, Kupelian PA, Levine L. Influence of intrafraction motion on margins for prostate radiotherapy. Int J Radiat Oncol Biol Phys 2006;65:548–53.

[35] Bell LJ, Eade T, Kneebone A, Hruby G, Alfieri F, Bromley R, et al. Initial experience with intra-fraction motion monitoring using Calypso guided volumetric modulated arc therapy for definitive prostate cancer treatment. J Med Radiat Sci 2017;64(1):25–34.

[36] Gunnlaugsson A, Kjellén E, Hagberg O, Thellenberg-Karlsson C, Widmark A, Nilsson P. Change in prostate volume during extreme hypo-fractionation analysed with MRI. Radiat Oncol 2014;9:22.

[37] Wolf J, Nicholls J, Hunter P, Nguyen DT, Keall P, Martin J. Dosimetric impact of intrafraction rotations in stereotactic prostate radiotherapy: a subset analysis of the TROG 15.01 SPARK trial. Radiother Oncol 2019;136:143–7.

[38] Muurholm CG, Ravkilde T, Skouboe S, Eade T, Nguyen DT, Booth J, et al. Dose reconstruction including dynamic six-degree of freedom motion during prostate radiotherapy. J Phys: Conf Ser 2019;1305:012053